

IITRI Project No. M272 (Phase III)
(Final Report)

STUDIES OF LUNAR SOIL MECHANICS

National Aeronautics and Space Administration
Washington, D. C. 20546

Contract No. NASr-65(02)

May, 1966

IIT RESEARCH INSTITUTE
Technology Center
Chicago, Illinois 60616

IITRI Project No. M272 (Phase III)
(Final Report)

STUDIES OF LUNAR SOIL MECHANICS

Contract No. NASr-65(02)

by

E. Vey and J. D. Nelson

National Aeronautics and Space Administration
Structures and Operations Problem Group
Space Vehicles Division
Washington, D. C.

May, 1966

PREFACE

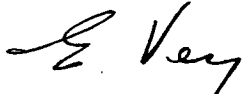
This report represents the final report on Phase III of IIT Research Institute Project No. M272, sponsored by the National Aeronautics and Space Administration under Contract No. NASr-65(02). Final reports on Phases I and II were published previously and are listed in the bibliography.^{1,2}

The research reported herein was performed during the period December 15, 1964 to March 1, 1966. Persons who contributed materially to this work are W. J. Courtney, D. Franson, W. E. Jamison, A. Kirch, J. D. Nelson, R. D. Nelson, R. D. Rowe, E. Vey and R. A. Wetzel.

Respectfully submitted,
IIT RESEARCH INSTITUTE


John D. Nelson
Research Engineer

APPROVED:



E. Vey, Assistant Director
Mechanics Research Division

JDN:is

ABSTRACT

27244

An experimental program was conducted to investigate the effect of ultra-high vacuum on the properties of simulated lunar soils. The materials used consisted of fine grained powders (approximately 2 to 40 μ) of quartz, obsidian, enstatite and olivine. Fine grained enstatite sand was also used for a limited number of experiments.

The results of direct shear tests and measurements of the resistance to dynamic penetration showed an increase in the soil strength under vacuum due to increases in both the stiffness and shear strength parameters. The magnitude of the increase, however, was dependent upon mineralogical composition because of variations in the amounts of initially adsorbed and/or absorbed gas.

Static penetrometer experiments were also performed and the results correlated with the amount of gas desorbed from the soil prior to measuring the penetration resistance. The strength of the soil was observed to vary exponentially with the relative cleanliness and extrapolation of the results to atomically clean surfaces yielded values of penetration resistance substantially less than that of the same material sintered at high temperatures.

Dynamic penetration experiments were also performed in simulated Martian soils, (fine grained limonite) and indicated an increase in interparticle forces even at low vacuum levels (3 to 15 torr).

CONTENTS

<u>Section</u>	<u>Page</u>
I. INTRODUCTION	1
II. SELECTION AND DESCRIPTION OF SOIL	3
III. DETERMINATION OF SHEAR STRENGTH PARAMETERS	12
A. Results of Direct Shear Tests on Quartz Powder	17
B. Results of Direct Shear Tests on Olivine Powder	21
C. Results of Direct Shear Tests on Obsidian Powder	24
D. Results of Direct Shear Tests on Enstatite Powder	28
E. Results of Direct Shear Tests on Enstatite Sand	31
F. Summary	35
IV. PENETRATION RESISTANCE UNDER DYNAMIC LOADING	36
A. Results of Experiments in Powder Samples	41
B. Results of Experiments in Sand	59
C. Summary	62
V. COMPOSITION OF ADSORBED GAS	67
A. Results of Experiments on Quartz Powder	69
B. Results of Experiments on Olivine Powder	70
C. Results of Experiments on Obsidian and Enstatite	72
D. Gas Species Desorbed	72
VI. GENERATION OF CLEAN PARTICLE SURFACES	99
VII. EFFECT OF SURFACE CLEANLINESS ON SHEAR STRENGTH	114
VIII. STUDIES OF SIMULATED MARTIAN SOILS	134
IX. DISCUSSION OF RESULTS	140
A. Simulated Lunar Soils	140
B. Simulated Martian Soils	146
X. CONCLUSIONS	146
BIBLIOGRAPHY	149

LIST OF ILLUSTRATIONS

<u>Figure</u>		<u>Page</u>
1	Grain Size Distribution of Powder Samples	8
2	Grain Size Distribution of Sand Samples	9
3	Grain Size Distribution of Limonite	11
4	Direct Shear Apparatus	13
5	Direct Shear Apparatus in Vacuum Chamber	15
6	Shear Stress vs Displacement for Quartz Powder	18
7	Mohr's Rupture Diagram for Quartz Powder	20
8	Shear Stress vs Displacement for Olivine Powder	22
9	Mohr's Rupture Diagram for Olivine Powder	23
10	Shear Stress vs Displacement for Obsidian Powder	25
11	Mohr's Rupture Diagram for Obsidian Powder	27
12	Shear Stress vs Displacement for Enstatite Powder	29
13	Mohr's Rupture Diagram for Enstatite Powder	30
14	Mohr's Rupture Diagram for Quartz Sand	32
15	Shear Stress vs Displacement for Enstatite Sand	33
16	Mohr's Rupture Diagram for Enstatite Sand	34
17	Dynamic Penetration Apparatus	38
18	Schematic of Dynamic Penetrometer	39
19	Typical Signatures in Quartz Powder	42
20	Typical Signatures in Olivine Powder	43

LIST OF ILLUSTRATIONS (Contd.)

<u>Figure</u>		<u>Page</u>
21	Typical Signatures in Obsidian Powder	44
22	Typical Signatures in Enstatite Powder	45
23	Resistance as a Function of Penetration in Quartz Powder	49
24	Resistance as a Function of Penetration in Olivine Powder	50
25	Resistance as a Function of Penetration in Obsidian Powder	51
26	Resistance as a Function of Penetration in Enstatite Powder	52
27	Penetration at 0.3 in.-lb Work vs Porosity for Quartz Powder	55
28	Penetration at 0.3 in.-lb Work vs Porosity for Olivine Powder	56
29	Penetration vs Porosity at 0.3 in.-lb Work for Obsidian Powder	57
30	Penetration at 0.3 in.-lb Work vs Porosity for Enstatite Powder	58
31	Typical Signatures in Loose Quartz Sand	60
32	Typical Signatures in Loose Enstatite Sand	61
33	Resistance as a Function of Penetration in Quartz Sand	63
34	Resistance as a Function of Penetration in Enstatite Sand	64
35	Effect of Vacuum on Penetration at 0.3 in.-lb Work in Enstatite Sand	65
36	Desorption Apparatus	68
37	Background Residual Gas Spectrum	74

LIST OF ILLUSTRATIONS (Contd.)

<u>Figure</u>		<u>Page</u>
38	Background Residual Gas Spectrum	75
39	Desorbed Gas Spectrum for Quartz Powder	76
40	Desorbed Gas Spectrum for Quartz Powder	77
41	Desorbed Gas Spectrum for Quartz Powder	78
42	Desorbed Gas Spectrum for Quartz Powder	79
43	Desorbed Gas Spectrum for Quartz Powder	80
44	Desorbed Gas Spectrum for Quartz Powder	81
45	Desorbed Gas Spectrum for Quartz Powder	82
46	Desorbed Gas Spectrum for Olivine Powder	83
47	Desorbed Gas Spectrum for Olivine Powder	84
48	Desorbed Gas Spectrum for Olivine Powder	85
49	Desorbed Gas Spectrum for Olivine Powder	86
50	Desorbed Gas Spectrum for Olivine A	87
51	Desorbed Gas Spectrum for Olivine A	88
52	Desorbed Gas Spectrum for Olivine A	89
53	Desorbed Gas Spectrum for Obsidian Powder	90
54	Desorbed Gas Spectrum for Obsidian Powder	91
55	Desorbed Gas Spectrum for Obsidian Powder	92
56	Desorbed Gas Spectrum for Enstatite Powder	93
57	Desorbed Gas Spectrum for Enstatite Powder	94
58	Desorbed Gas Spectrum for Enstatite Powder	95
59	Desorbed Gas Spectrum for Enstatite Sand	96

LIST OF ILLUSTRATIONS (Contd.)

<u>Figure</u>		<u>Page</u>
60	Desorbed Gas Spectrum for Enstatite Sand	97
61	Desorbed Gas Spectrum for Enstatite Sand	98
62	Pumpdown Curve for Quartz Powder	100
63	Pumpdown Curve for Quartz Powder	101
64	Pumpdown Curves for Oven Dry and Air Dry Quartz	103
65	Pumpdown Curve for Olivine Powder	107
66	Pumpdown Curve for Olivine A	108
67	Pumpdown Curves for Obsidian Powder	109
68	Pumpdown Curves for Enstatite Powder	110
69	Pumpdown Curves for Enstatite Sand (105 to 149 μ)	111
70	Penetration Resistance for Various Edge Distances	115
71	Penetration Resistance for Various Edge Distances	116
72	Penetration Resistance for Various Edge Distances	117
73	Penetration Resistance for Various Soil Depths	119
74	Penetration Resistance for Various Soil Depths	120
75	Penetration Resistance for Various Soil Depths	121
76	Static Penetration Apparatus	122
77	Throughput as a Function of Time for Penetration Experiments	124
78	Throughput as a Function of Time for Penetration Experiments	126
79	Penetration Resistance for Various Degrees of Outgassing	127

LIST OF ILLUSTRATIONS (Contd.)

<u>Figure</u>		<u>Page</u>
80	Penetration Resistance for Various Degrees of Outgassing	128
81	Effect of Relative Cleanliness on Strength Ratio	130
82	Penetration Resistance of Sintered Quartz Powder	132
83	Effect of Relative Cleanliness on Penetration Resistance	133
84	Typical Signatures in Limonite Powder	135
85	Resistance as a Function of Penetration for Loose Limonite	137
86	Resistance as a Function of Penetration for Dense Limonite	138
87	Penetration at 0.3 in.-lb Work vs Porosity for Limonite	139

IIT Research Institute Project No. M272

Final Report

STUDIES OF LUNAR SOIL MECHANICS

I. INTRODUCTION

The success of the future missions in space is highly dependent upon the properties of the surface material in the regions where spacecraft land. However, because of the paucity of knowledge regarding even the type of material existing on the surfaces of extraterrestrial bodies, the prediction of the material properties is extremely difficult and uncertain. Hence, the correct interpretation of data obtained in earlier space flights is essential in order to ascertain the actual surface conditions that exist.

The correct interpretation of observations and in-situ measurements however, requires a comprehensive knowledge and understanding of the mechanics of materials on which measurements are taken. The purpose of the research reported herein was to investigate the properties of probable lunar and Martian surface materials and the manner and degree of influence of the prevailing environmental conditions on these properties.

This research is a continuation of previous work^{1,2*} and consists primarily of investigating the shear strength and resistance to penetration of a variety of minerals and soil types and the degree to which these properties are affected by ultra-high vacuum. Since the vacuum effects are due primarily to a reduction in the amount of adsorbed gas on the particle surfaces the composition and amount of gas on the particles of the different minerals were also investigated in order to explain the dependency of these effects on mineralogical composition.

* Superscript numbers refer to references listed in the bibliography.

After an understanding had been developed of the manner in which the composition of the material influenced the change in properties in vacuum, experiments were performed to determine the relationship between soil strength and cleanliness of the individual particles. In addition, preliminary experiments were performed to study the penetration resistance of simulated Martian soils under simulated Martian environmental conditions.

Although the research program has been largely an experimental investigation of specific properties of selected soils under prescribed environmental conditions it was not the intent to provide actual values of the lunar and Martian surface properties. Rather the purpose was to develop an understanding of the behavior of these materials under various environmental conditions. It is believed that in this way, the optimum use can be made of these results to indicate true lunar and Martian soil behavior when a more accurate definition of the actual surface conditions becomes known.

II. SELECTION AND DESCRIPTION OF SOIL

The materials used in Phases I and II were quartz and olivine and the basis for selection of these two minerals is discussed fully in the final report on Phase I.¹ Since it was observed that the effect of ultra-high vacuum on the soil properties was different for these two materials, two additional materials were included in this phase in order to further study the dependence of vacuum effects on mineralogical composition.

The selection of minerals for this investigation was based on indirect measurements and what is known qualitatively about the environmental conditions and soil producing processes active on the moon. It is generally agreed that in some areas the lunar material is derived from the comminution of lunar rocks consisting of silicates or siliceous material somewhat similar to terrestrial igneous rocks. Indications of the composition of these rocks would then provide insight into the probable composition of the lunar soil.

On the basis of lunar emission temperatures, Tolbert and Coats³ hypothesize a lunar model consisting of a low density pumice to a depth of approximately 90 cm overlying a more dense material such as basalt. Strom⁴ considered the probable strength of materials in the vicinity of the lunar Straight Wall and concluded that the mare material in this vicinity does not possess a strength comparable to dense terrestrial rocks and would probably consist of extremely vesicular lava flows and/or tuffaceous deposits having depths of 200 to 300 meters. In addition the recent Luna 9 photographs indicate that in the area where it landed, the surface is covered by a material similar to a vesicular lava with a fairly high strength.

Thus, in some areas on the moon it appears that there has been some volcanic activity which suggests that the surface material has the same composition as the moon's interior. Strom

points out that the existence of porous materials is supported by radiometric, photometric and polarimetric data, but it has been shown² that a fine grained material derived from the surface rock may exhibit properties compatible with those determined by Strom and would not impose the limitation of the surface material having the same composition as the lunar interior. Consequently, it is not believed that the lunar surface consists solely of lava flows or deposits of granular material formed by meteoritic impact or other possible erosional processes. It appears more reasonable to expect different areas on the moon to be covered by one or both of the aforementioned surface materials.

Strom also points out that the existence of porous materials is supported by radiometric, photometric and polarimetric data. Although it has not been possible to closely match the brightness and color of the lunar surface with any natural terrestrial materials,⁵ Rosenberg and Wehner⁶ measured the albedo and reflection characteristics of various materials which had been bombarded by simulated solar wind and found that the reflectance curve of basalt powder after bombardment closely matched that of the lunar surface. This is in accord with conclusions by Sytinskaya⁵ who considers that meteoritic material may be darkened by heat due to the decomposition of ferromagnesium silicates to form iron and magnesium oxides. Hapke⁷ also has attributed the darkening of the lunar surface to the action of solar wind on ferrosilicates.

In support of the existence of a basic material, Kopal and Rackham^{8,9} observed a red glow in the Kepler region of the moon. Prior to this, Derham and Geake¹⁰ had observed the luminescence spectra of stony meteorites and found that most luminesced negligibly or weakly while three samples, all of which were enstatite achondrites, luminesced strongly with a main peak in the red. In a discussion of these results Anand, Oster and Soria¹¹ suggest that this may be caused by the

presence of meteoritic material in impact craters. Another explanation for the luminescence of lunar rocks has been offered by Beskrovnyy¹² who observed that under UV radiation, luminescence of rocks originated in thin cracks enriched with petroleum bitumena. He suggests that in zones of deep crevasses, the lunar rocks may contain petroleum bitumena and/or rare earth materials. However, this would require the existence of organic material at some time in the past.

The above discussion points to the existence of basic igneous rocks on the lunar surface with strong indications of the existence of ferromagnesium silicates and in particular enstatite. On the other hand, Runcorn¹³ considered the shape of the moon and hydrostatic theory and concluded that a sialic composition would not be unreasonable for the lunar highlands. By considering the density of the moon and meteorites, Urey¹⁴ concluded that the moon is more like the sun than the meteorites in composition and contains a small fraction of the heavier elements. He states that the amount of iron on the moon is probably below that found in chondritic meteorites. Lowman¹⁵ also presents a brief discussion pointing to the existence of acidic or siliceous material on the moon.

It may not, therefore, be assumed that the lunar material is solely basic or acidic and it would be reasonable to expect both types of materials to occur either individually or together. Baldwin¹⁶ considered the moon as being at one time molten and concluded that chemical differentiation may have occurred to produce acidic highlands. Miyamoto¹⁷ presents a geological interpretation of the moon and considers the maria as being composed of basaltic matter and the highlands as being siliceous.

Although no definite minerals have been proposed as making up the acidic lunar rocks, arguments have been presented to show that tektites originated on the lunar surface. Lowman¹⁵ shows that tektites are probably altered igneous rocks and

proposes that they were thrown outward from the moon as the result of meteoritic impact into silicic igneous rocks covering large areas on the visible face of the moon. An interesting implication of his conclusions is that the maria are silicic and the highlands chondritic which is "the reverse of the generally accepted concept of silicic terrae and basaltic maria." O'Keefe¹⁸ also presents an argument that, because the chemistry of tektites is almost exactly like that of granite, the moon must be derived from the same original materials as the earth.

Since tektites are a glass this could imply that the material from which they were formed was also a glass. Melting of the parent rock during impact of a meteorite and rapid cooling could also cause the glassy composition of the tektites, but it has been shown that melting of igneous rocks in vacuum¹⁹ results in a highly vesicular material. In addition, Van Diggelen²⁰ found that the radiance of glass beads matched that of the crater floors fairly closely. Although these beads were transparent and did not have the dark color which tektites exhibit on earth it is possible that tektites may not have the same dark color on the moon. Also, the dark color could serve to bring the results obtained in the laboratory into closer agreement with the lunar properties.

The quartz and olivine which were used previously represent the extremes of acidic and basic minerals. In selecting two additional materials for investigation it was considered to be desirable to choose both acidic and basic materials again. Because of the observed luminescence of enstatite this mineral was chosen to represent a basic rock. For a material to represent an acidic rock a material similar to tektites was chosen. In this way an amorphous material was included in the investigation in addition to crystalline material. Actual tektites, however, are quite rare and rather expensive, and for this reason a commonly occurring silicic obsidian was selected.

All materials were used in a powder form (silt) having the grain size distributions shown in Fig. 1. Some experiments were also performed on quartz and enstatite sand having the grain sizes shown in Fig. 2.

The quartz samples are commercially available and were obtained in the gradations shown. The powder form is commonly referred to as silica flour and the sand is called Ottawa sand. These samples are hydraulically mined from St. Peters sandstone deposits near Ottawa, Illinois, after which the material is washed and dried before screening into separate grades. The powder is obtained by grinding the sand in silex lined tube mills using either flint pebbles or high density alumina balls.

The other three materials (olivine, enstatite, and obsidian) were obtained in rock form from a commercial supplier. The olivine and enstatite were mined in North Carolina and the obsidian was a black obsidian rock from Oregon. The materials were first broken down into pieces with dimensions of 2 to 3 in. After this it was further reduced in grain size by means of a jaw crusher until it all passed a No. 4 sieve. The olivine was then ground in a ball mill in the laboratory and that portion which was retained on a No. 200 sieve was further ground in a rubber-lined fluid energy mill to provide the gradations shown in Fig. 1.

The enstatite and obsidian material which passed the No. 4 sieve was ground directly in a stainless steel-lined fluid energy mill using air that had been dried by means of an after cooler and filtered. In this process the obsidian attained the grain size distribution shown in Fig. 1. The enstatite, however, was much coarser and consequently, it was screened to provide the powder sample (Fig. 1) and the two sand samples shown in Fig. 2.

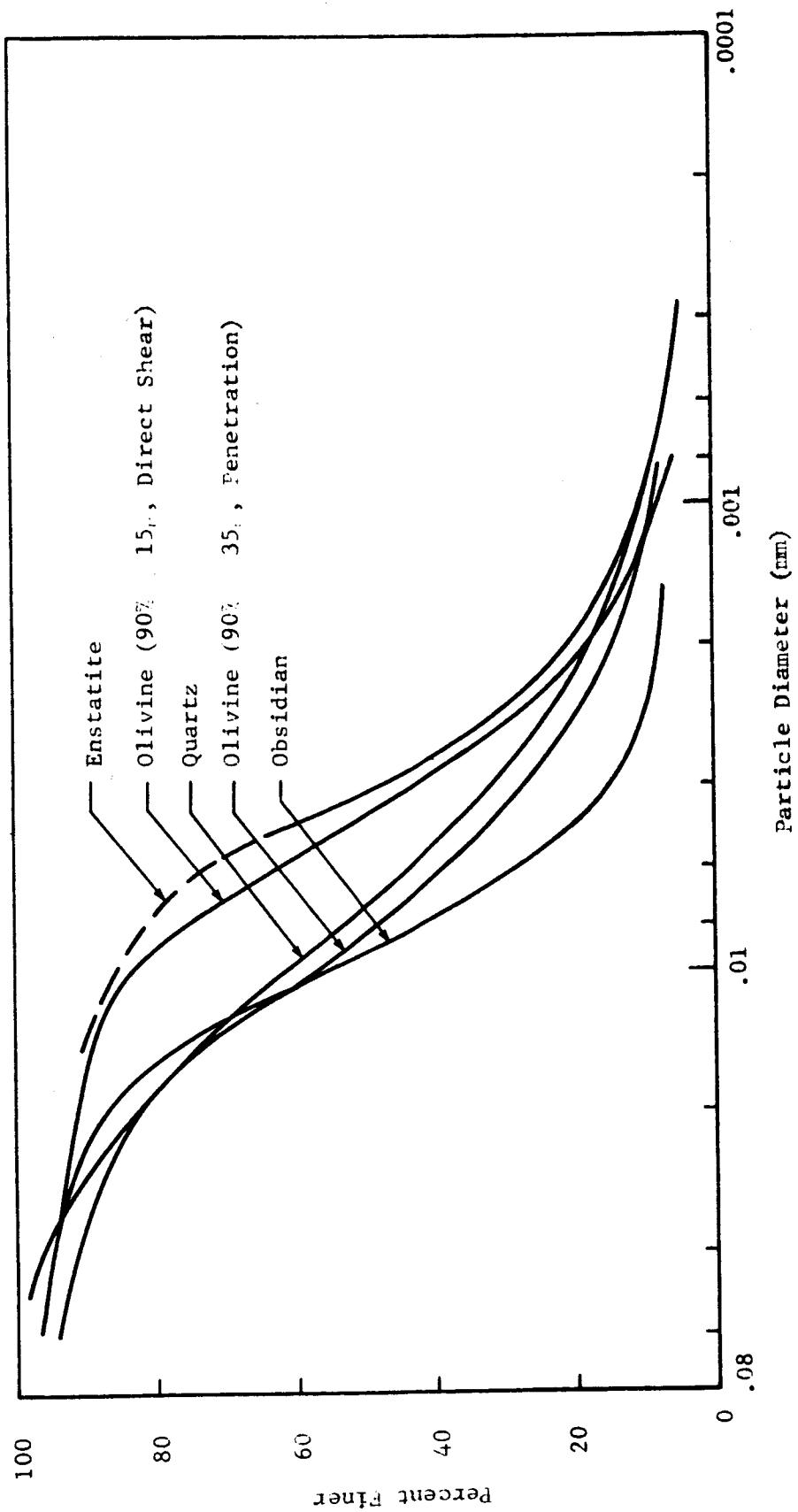


Fig. 1 GRAIN SIZE DISTRIBUTION OF POWDER SAMPLES

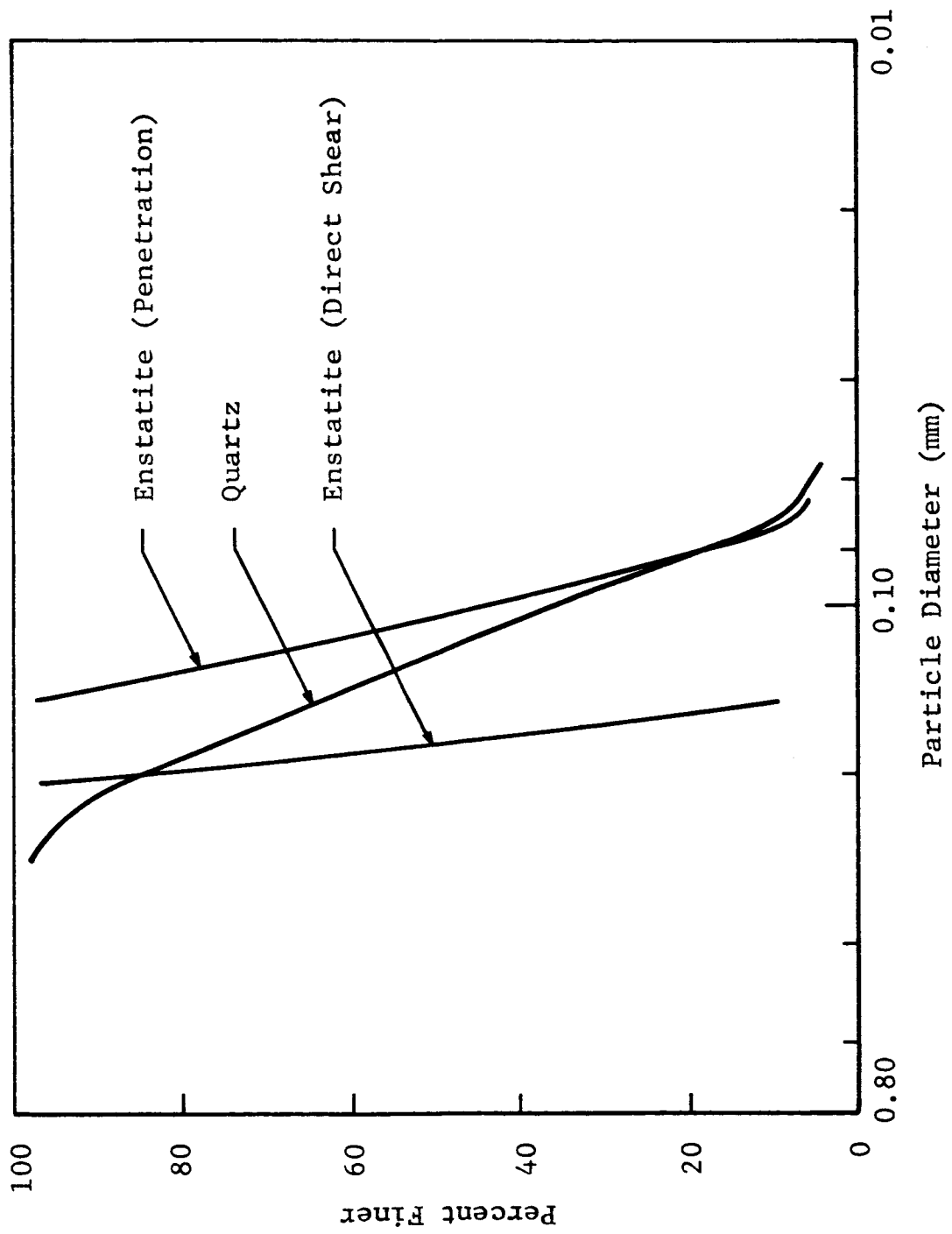


Fig. 2 GRAIN SIZE DISTRIBUTION OF SAND SAMPLES

The olivine and enstatite are ferromagnesium silicates with absolute specific gravities of 3.27 and 3.21 respectively. The quartz is almost pure silicon dioxide (SiO_2) and has a specific gravity of 2.64. The mineralogical composition of the obsidian is not as clearly defined but it is a volcanic glass consisting primarily of amorphous silica and has a specific gravity of 2.35.

The nature of the Martian surface is less well defined than the moon's. Seasonal and daily temperature changes give rise to winds similar to the terrestrial trade winds, which in addition to variations in temperature are believed to cause the surface to be highly weathered indicating a high probability of deposits of earth-like soils.²¹ The mineral constituents of the Martian soil are believed to be primarily fine grained limonite with possibly some feldspar.²²

Consequently, the material selected to simulate the Martian soil was limonite. This material was purchased in a powder form having the grain size distribution shown in Fig. 3. It is a hydrated iron oxide having a specific gravity of 3.44.

In selecting these materials to represent the lunar and Martian soil there is a reasonable degree of certainty that their major constituents would be found on the lunar and Martian surface. It is expected that they are only representative soils but within the confines of what is known categorically of these surfaces, it was deemed unwise to base the study on a more precise definition of the actual soil types.

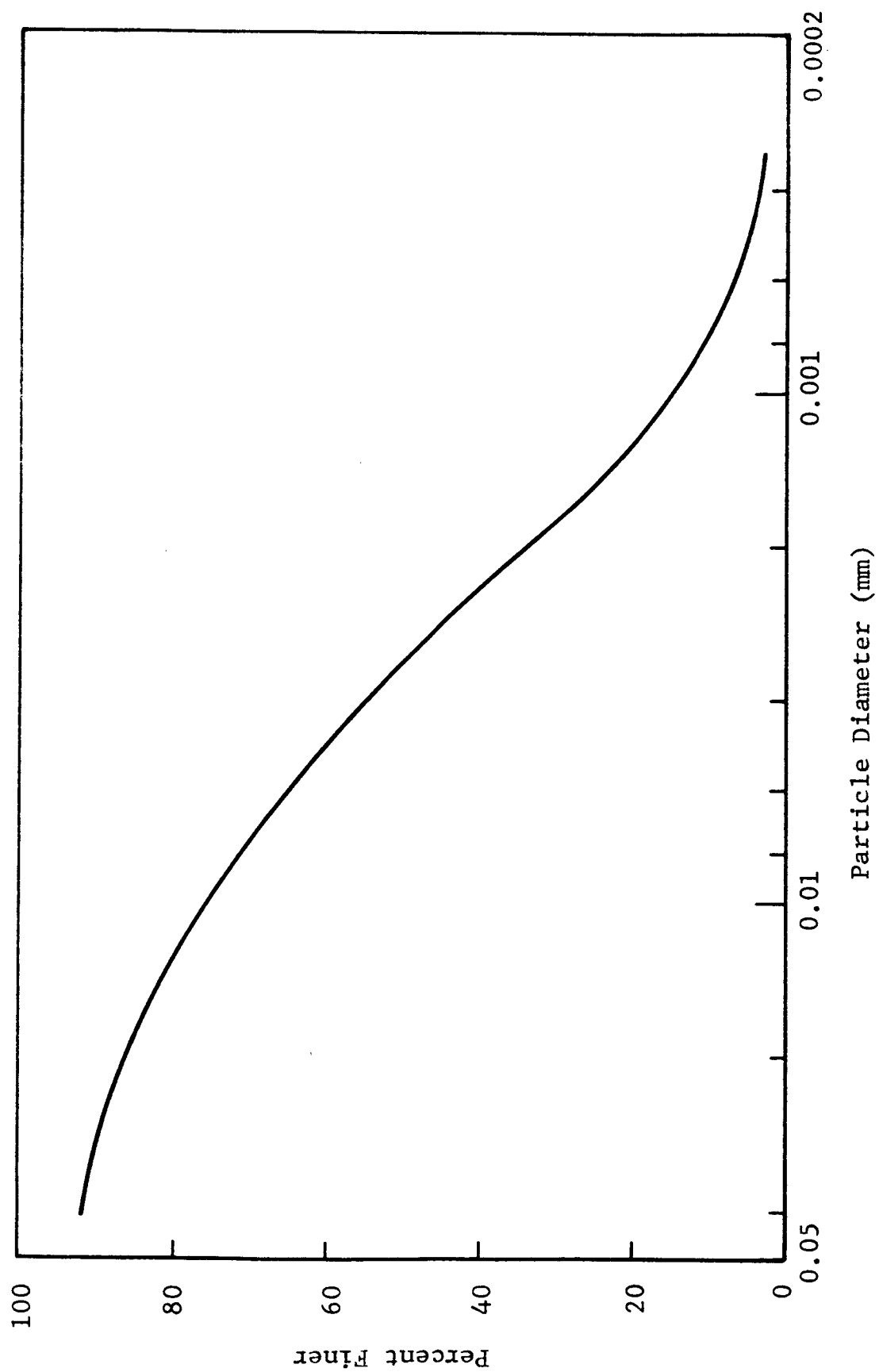


Fig. 3 GRAIN SIZE DISTRIBUTION OF LIMONITE

III. DETERMINATION OF SHEAR STRENGTH PARAMETERS

Experiments of this type were used throughout the first two phases of this program and are discussed in some detail in the preceding final reports.^{1,2} In the interest of completeness, a brief description of the apparatus and discussion of shear strength will be repeated here. For a more complete discussion of this type of measurement the reader is referred to the aforementioned reports.

The shear strength of a soil may be considered as the maximum shear stress which the soil is capable of resisting, and for most soils may be expressed by the linear relationship

$$\tau = c + \sigma \tan \phi \quad (1)$$

where

- τ is the shear stress at failure
- σ is the normal stress on the failure plane
- c is the cohesion*
- ϕ is the angle of internal friction.

Equation (1) defines a line which is termed Mohr's rupture diagram, the intercept on the τ axis defining c and the slope defining ϕ . The most direct means of measuring these parameters is by the triaxial test or direct shear test. Because of limitations imposed by the outgassing of membranes and possible contamination of the soil by this outgassing, only direct shear tests were used in these investigations.

The direct shear test consists of applying a normal stress to a prescribed failure plane and measuring the maximum shear stress that can then be applied on this plane. The apparatus used in this investigation is shown schematically in Fig. 4. To minimize outgassing the entire apparatus except for some shielding and the force transducers were made of stainless steel.

* In granular soils, this term is generally referred to as apparent cohesion to differentiate it from the cohesion exhibited by colloidal soils which is believed to be caused by somewhat different factors.

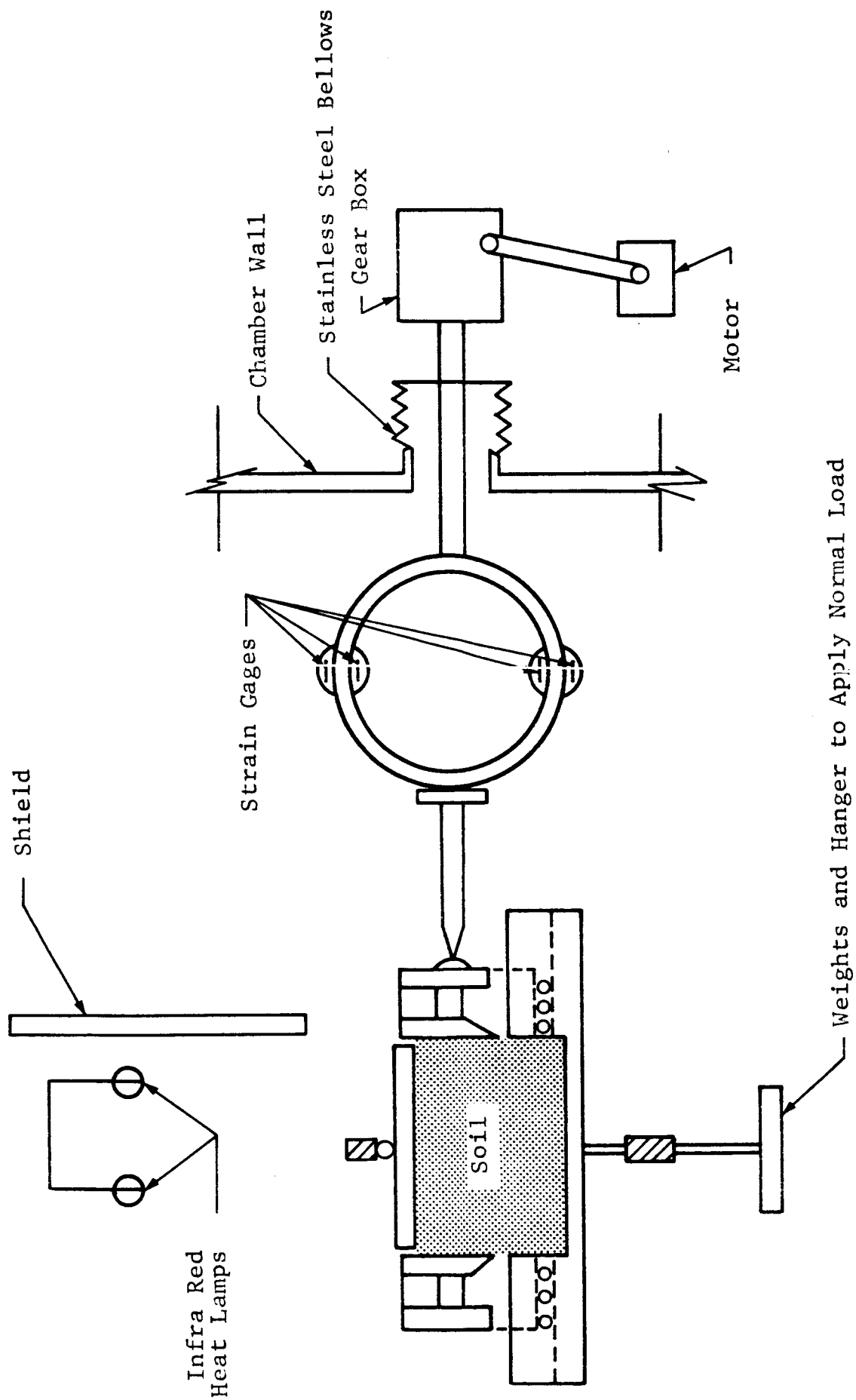


Fig. 4 DIRECT SHEAR APPARATUS

Friction in the apparatus was eliminated by supporting the upper half of the mold on ball bearings with a maximum clearance between the two parts of 0.005 inch. As discussed in the previous final report, this was quite effective in eliminating friction even at ultra-high vacuum.

Two pieces of apparatus were fabricated and mounted in a diffusion pumped vacuum chamber as shown in Fig. 5. Two shear boxes were considered to be necessary because of the long pump-down periods and had the advantage that they enabled two tests to be performed simultaneously under identical environmental conditions. Care was also taken to duplicate the pumpdown periods for all experiments as closely as possible in order that the environmental conditions be the same for all experiments. To aid in outgassing the sample, the top plates and bottoms of the shear boxes were perforated and the sample was baked during pumpdown.

Experiments were performed using quartz, obsidian, enstatite, and olivine powders and enstatite sand. The porosity of the powder samples was controlled by depositing the soil in the shear box by means of a sieve and then consolidating the sample under a normal stress equal to the greatest used in any experiment. This technique resulted in fairly uniform porosities as shown in Table 1.

The sand samples were prepared by pouring the sand into the shear box through a tube with a slotted end piece which ensured that the velocities of the sand grains were close to zero as they left the tube. The porosity was controlled by maintaining the bottom of the tube at a constant height above the surface of the deposited soil (in this case approximately 0.25 in.) and then preconsolidating the sample by the same procedure used for the powder. The resulting porosities are also shown in Table 1.

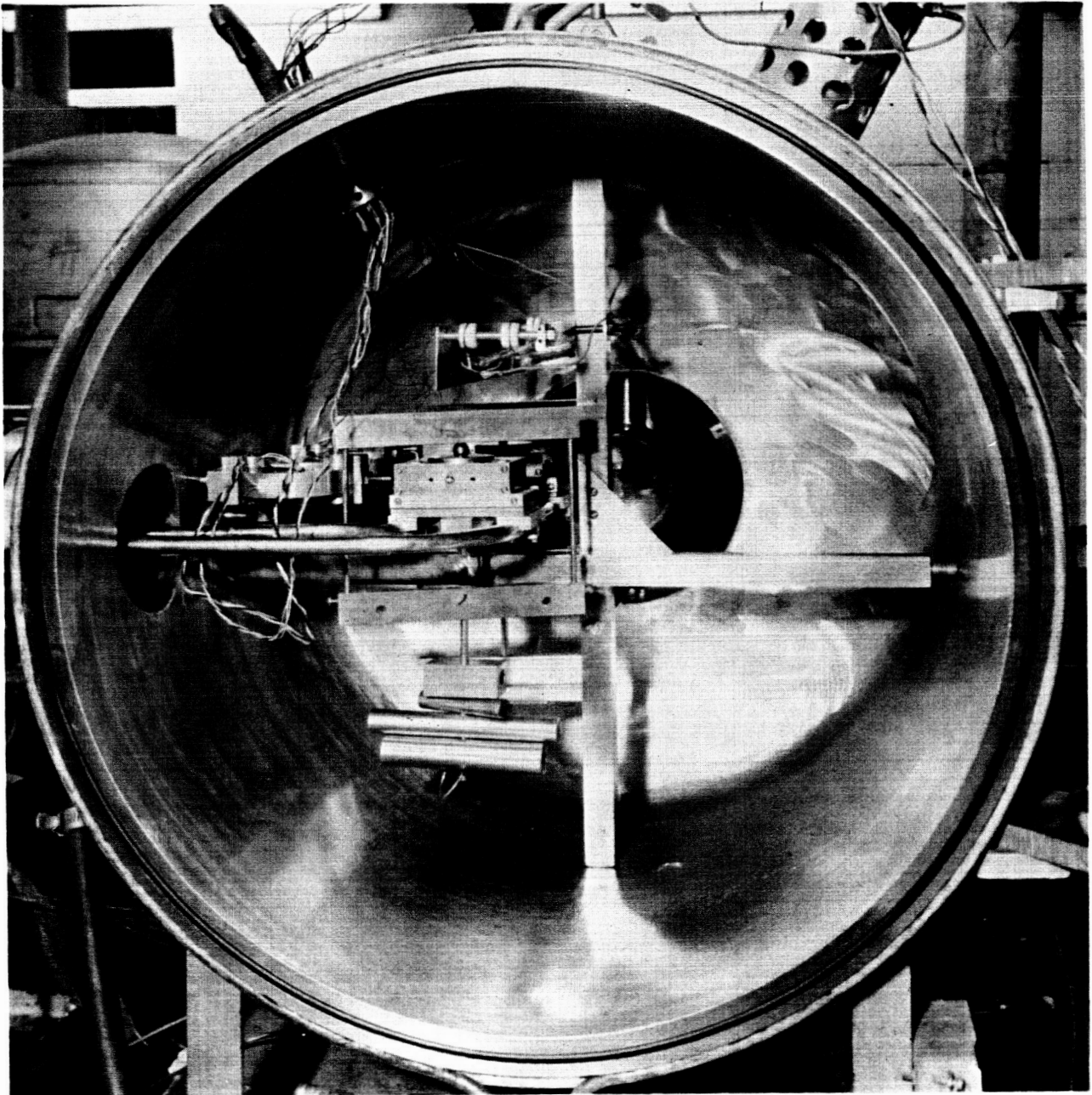


Fig. 5 DIRECT SHEAR APPARATUS IN VACUUM CHAMBER

Table 1
POROSITIES OF DIRECT SHEAR SAMPLES

Material	Porosity			No. of Experiments
	Min.	Max.	Avg.	
<u>Powder</u>				
Quartz	0.536	0.575	0.556	34
Obsidian	0.569	0.604	0.580	29
Enstatite	0.538	0.550	0.544	14
Olivine	0.618	0.640	0.631	35
<u>Sand</u>				
Quartz	0.410	0.422	0.415	6
Enstatite	0.475	0.497	0.491	8

The primary purpose of these experiments was to investigate the influence of mineralogical composition on the degree to which vacuum affects the shear strength. In the previous two phases of this program experiments were performed over a range of vacuum levels, and it was observed that only at ultra-high vacuum levels did it have an effect on the strength of either the quartz or olivine. Consequently, in this program experiments were confined to ultra-high vacuum and atmospheric conditions. Experiments were performed at temperatures of approximately 250°F and at ambient temperature. For the experiments at elevated temperatures the load cells were shielded from the heat lamps so as to maintain their temperature below that at which it would affect their calibration factors.

The samples were pumped down over a period of approximately four days. The chamber was first pumped to a rough vacuum by a mechanical pump after which the diffusion pump was started and a mild bakeout (approximately 275°F) begun. The bakeout was turned off after 48 hours and the chamber entrance-port flange and liquid nitrogen cold trap were cooled. The

vacuum level in the chamber was in the low 10^{-9} torr range at the time that the experiments were then performed.

A. RESULTS OF DIRECT SHEAR TESTS ON QUARTZ POWDER

While direct shear tests were performed on the quartz and olivine powders in Phases I and II, a limited number of experiments were performed on these materials in this program to more firmly establish indicated relationships where necessary.

Typical curves of the shear stress as a function of displacement in the quartz powder are shown in Fig. 6. In the interest of clarity the results of experiments at elevated temperature are shown for different values of normal stress than those at ambient temperatures. It is seen that all curves have nearly the same slope for the initial, almost linear, portion of the curve. However, in vacuum the stress at which the slope of the curve begins to change is considerably higher than in atmosphere and the maximum shear stress occurs at a smaller value of displacement. This indicates a substantial increase in stiffness of the soil caused by the ultra-high vacuum.

Although not demonstrated conclusively by Fig. 6 alone, it was shown in the final report on Phase II that the elevated temperature had little if any affect on the shape of the stress-displacement curve in atmosphere but resulted in a further but smaller increase in stiffness in ultra-high vacuum.

An interesting point to note is the peak shear stress attained at the small values of displacement in the experiments at the lower normal stresses. It is seen that beyond this peak, the shear stress then increased again to another maximum value at displacements more compatible with those at which the maximum stress was reached in the other experiments. It is believed that this peak was caused by the development of fairly strong interparticle bonds which were broken at small values of displacement after which the frictional component of shear stress caused another buildup of stress to the second observed maximum.

IIT RESEARCH INSTITUTE

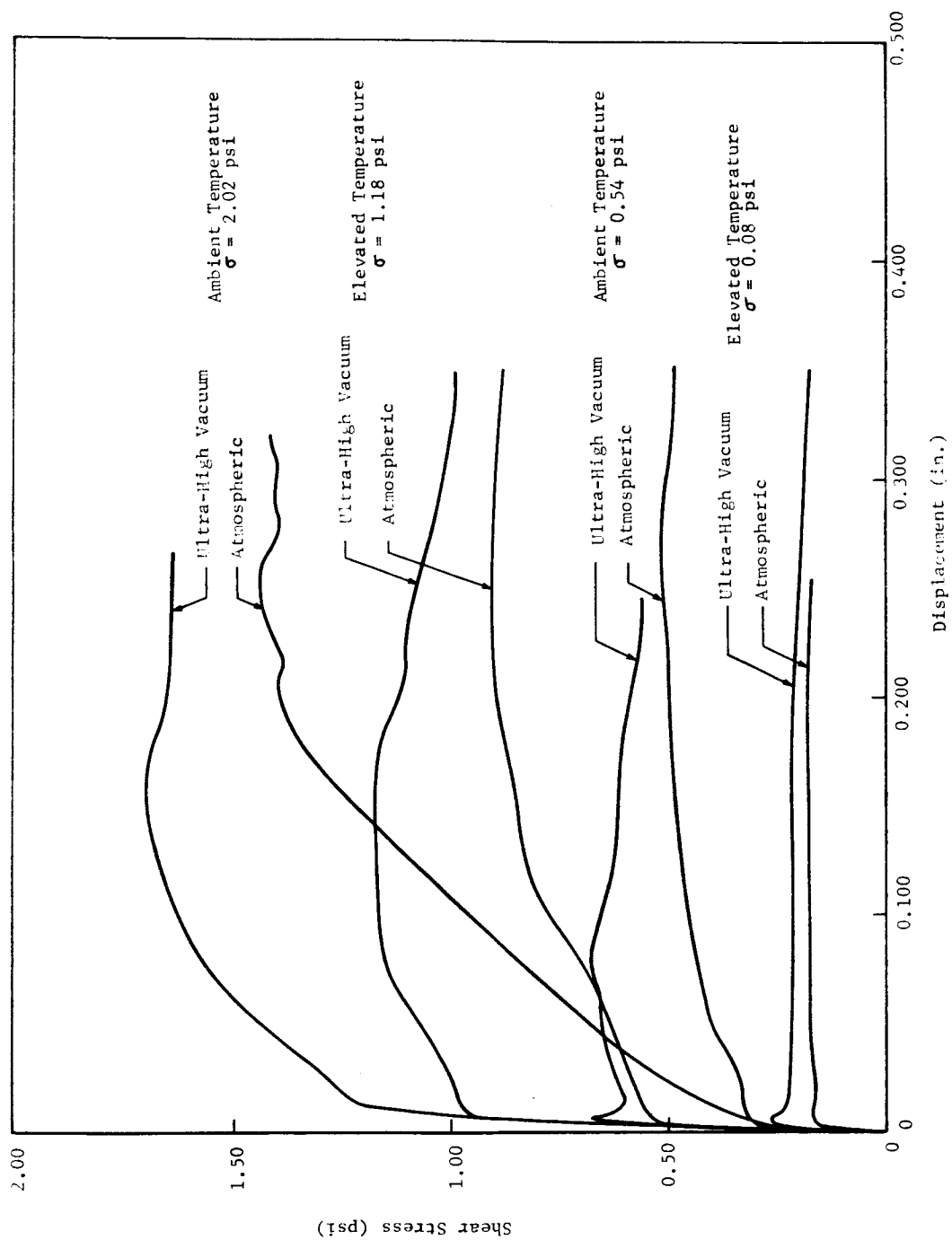


Fig. 6 SHEAR STRESS VS DISPLACEMENT FOR QUARTZ POWDER

The maximum shear stress for each particular value of normal stress was plotted as a function of the thickness of the soil sample to establish to what extent, if any, arching in the shear box affected the measured shear strength. It was observed that arching had a very small effect on the results and, in addition, this served to clarify extremely high or low values and indicated the weighted mean of the strengths measured. These mean values were plotted in Fig. 7 to obtain the Mohr's rupture diagrams for atmospheric and vacuum conditions. From this figure it is evident that in atmosphere the shear strength is essentially the same at both ambient and elevated temperatures. This would indicate that the apparent cohesion is not due to surface tensions in the hygroscopic moisture and is most likely caused by interlocking of particles and/or interparticle forces as a result of the large specific surface.

It is also evident that in ultra-high vacuum a very definite increase in shear strength over that in atmosphere is indicated. Furthermore, the increase in strength is seen to be due to an increase in both the apparent cohesion and angle of internal friction. While sufficient spread in the data still exists to make it difficult to separate the exact values of the strength increase into its frictional and cohesive components it is seen that the apparent cohesion increased by approximately 50 percent in vacuum while $\tan \phi$ increased by approximately 15 percent. Also a further increase in strength is indicated in vacuum due to the elevated temperature but the magnitude of this increase is so small as to make it inconclusive. Such an increase would be consistent, however, with the observed increase in stiffness at the elevated temperatures.

In summary, the effect of ultra-high vacuum on quartz was to cause an increase in the stiffness and shear strength. Elevated temperatures caused a small, if any, further increase in these parameters in vacuum.

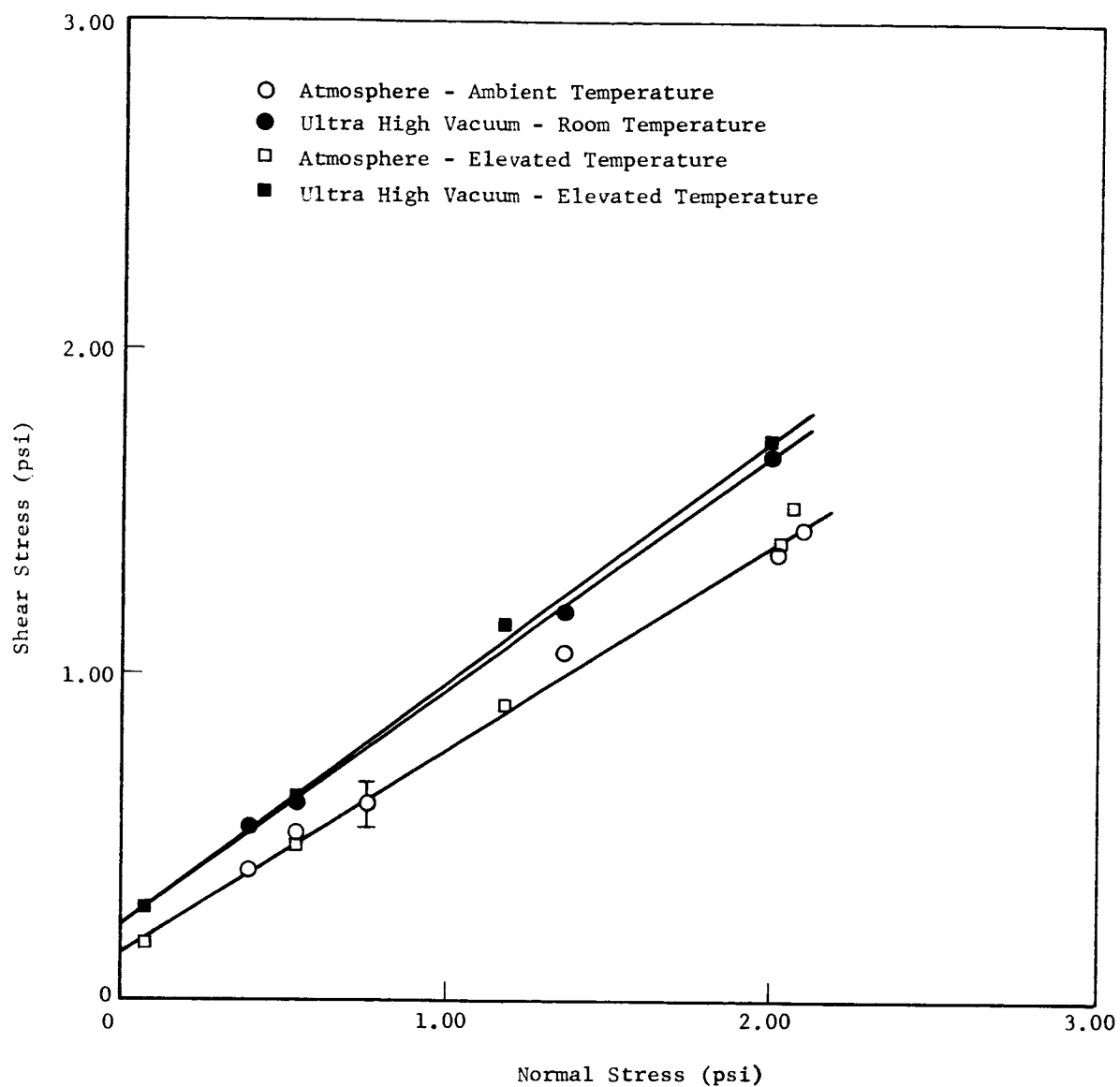


Fig. 7 MOHR'S RUPTURE DIAGRAM FOR QUARTZ POWDER

B. RESULTS OF DIRECT SHEAR TESTS ON OLIVINE POWDER

Representative stress-displacement curves for the olivine powder are shown in Fig. 8. In the final report on Phase II it was shown that in atmosphere, elevated temperatures caused an increase in the stiffness of the soil. For the higher normal stress (2.03 psi) this increase was quite small and ultra-high vacuum at ambient temperatures resulted in an additional small increase. For the lower normal stress (0.55 psi) the stiffness in vacuum at ambient temperatures was approximately the same as for elevated temperatures in atmosphere.

Thus, while in Fig. 8 it appears that the stiffness of the soil was greater in vacuum than in atmosphere it is not clear how much of this increase is due to the bakeout of the sample during the pumpdown period. It is evident, however, that in vacuum the elevated temperature caused a fairly substantial increase in the stiffness particularly for the higher normal stress.

Also, at the lower normal stress an initial peak shear stress was observed in the vacuum as was true for the quartz powder. While this peak was not formed under ambient conditions it was also observed in atmosphere at elevated temperatures.

It should also be noted that in vacuum at both ambient and elevated temperatures the maximum shear stress was reached at displacements much less than those at which it was reached in atmosphere. It was seen in Phase II² that the elevated temperature in atmosphere also decreased this displacement.

The maximum measured shear stress in the olivine was plotted as for the quartz to determine the mean values of shear strength and the Mohr's rupture diagram determined therefrom are shown in Fig. 9. It is seen that for atmospheric conditions at both temperatures and for ultra-high vacuum at ambient temperatures the shear strength shows no change. However, in

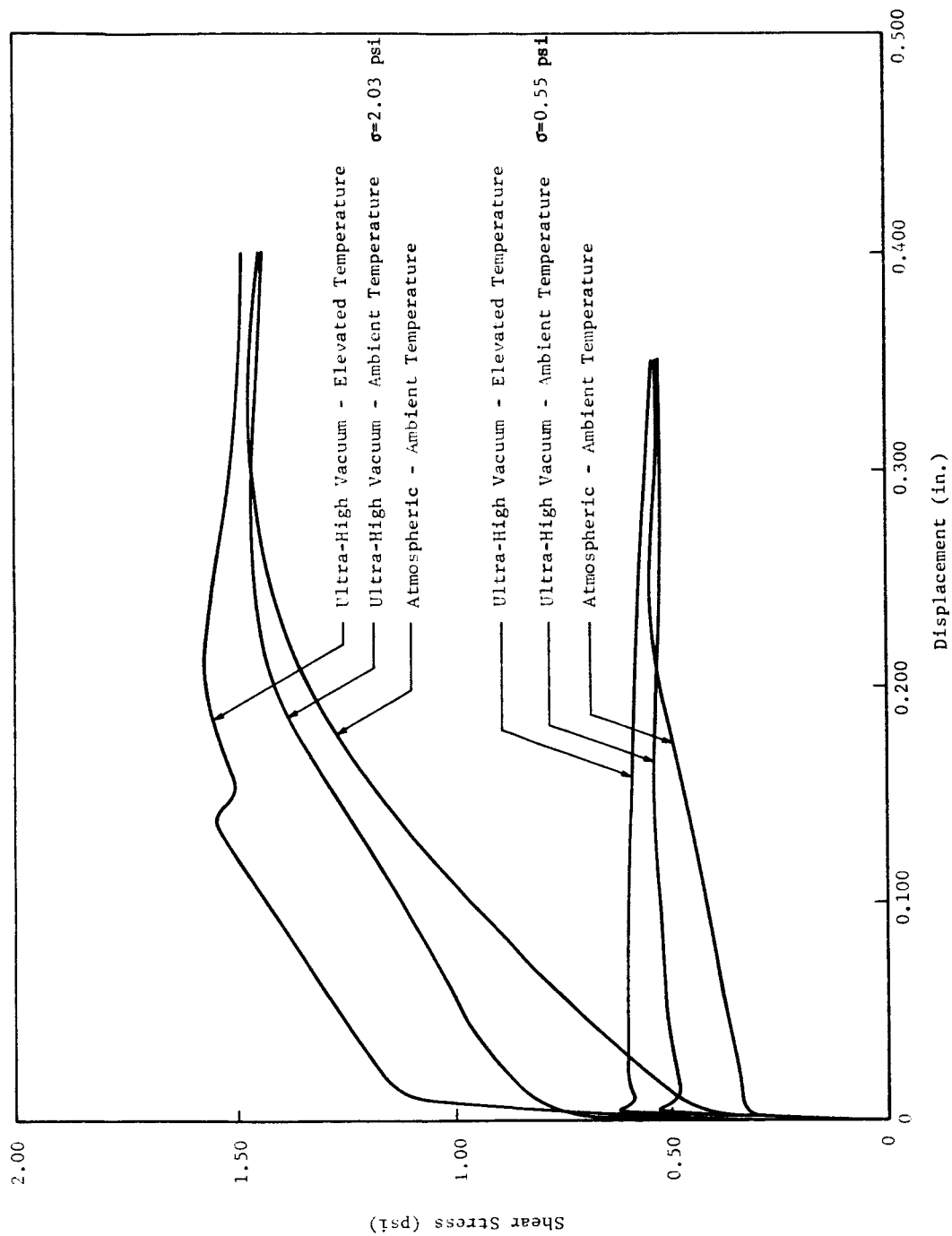


Fig. 8 SHEAR STRESS VS DISPLACEMENT FOR OLIVINE POWDER

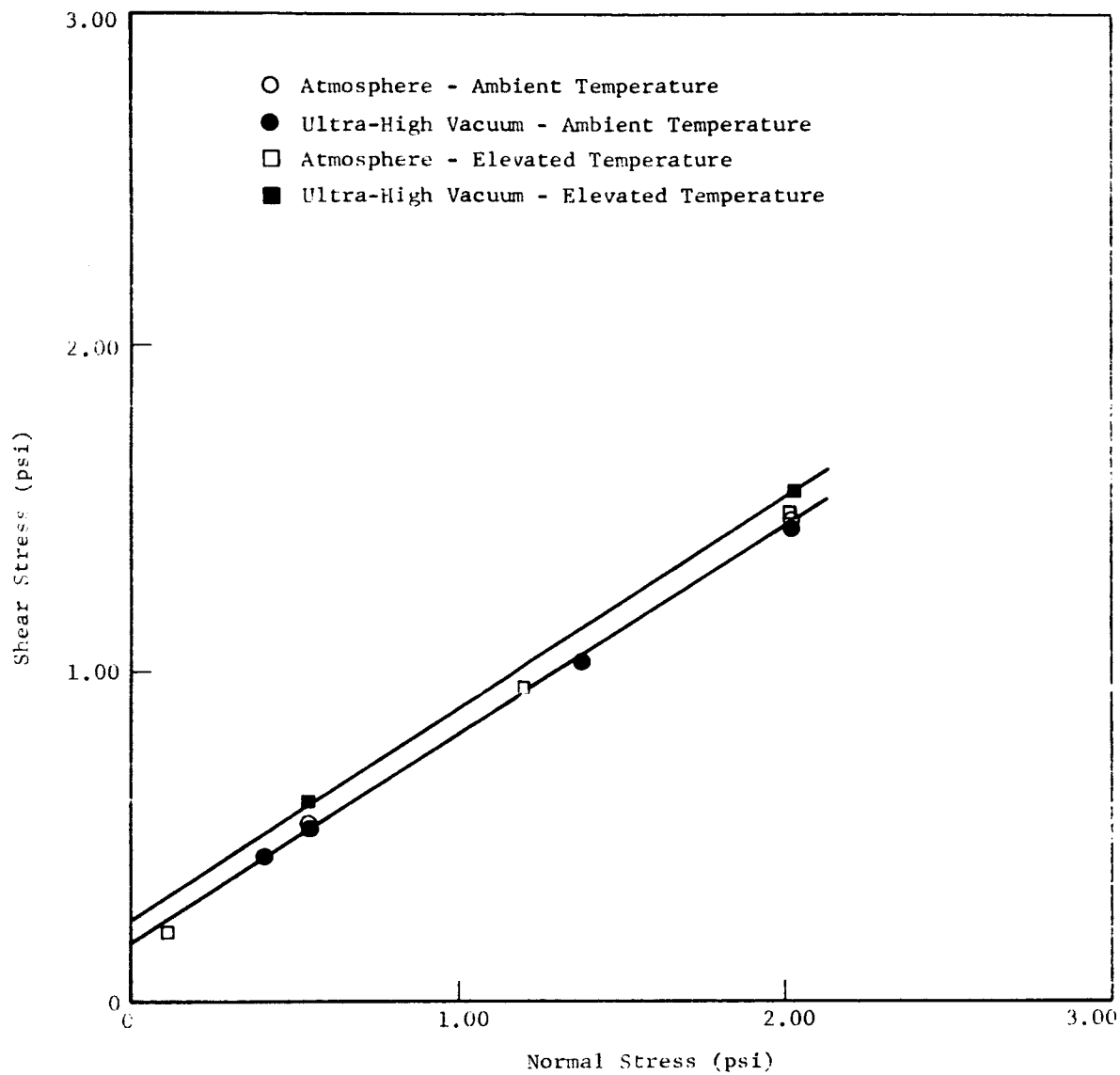


Fig. 9 MOHR'S RUPTURE DIAGRAM FOR OLIVINE POWDER

vacuum the elevated temperature resulted in a rather definite increase in shear strength due almost entirely to an increase in apparent cohesion of approximately 30 percent. The angle of internal friction, appears to have not changed by any definite amount.

Thus, it is seen that while the vacuum and temperature have an effect on the stiffness and shear strength of the olivine the nature of this effect is somewhat different for the quartz. Elevated temperatures alone appear to cause an increase in stiffness in atmosphere. Also ultra-high vacuum at room temperature causes the stiffness to increase with an additional increase at elevated temperature in vacuum. However, the shear strength parameters, ϕ and c , appear to be unaffected except at elevated temperatures in vacuum in which case the apparent cohesion increases with little or no change in the angle of internal friction.

C. RESULTS OF DIRECT SHEAR TESTS ON OBSIDIAN POWDER

The obsidian is not actually a pure mineral. It is composed primarily of amorphous silica and is more similar to the quartz than the olivine in mineralogical composition. The experimental procedure was the same as for the quartz and olivine except that more care was taken to assure a constant thickness of the sample than was done previously. The pumpdown procedures were the same as for the preceding two materials and care was taken to reproduce the pumpdown period for each experiment.

Typical stress-displacement curves for this material are shown in Fig. 10. The shapes of the curves are almost identical to those for the quartz and it can be seen that the stiffness of the soil in vacuum is considerably greater than in atmosphere. Also, the displacement at which the maximum shear stress is reached is less in the vacuum.

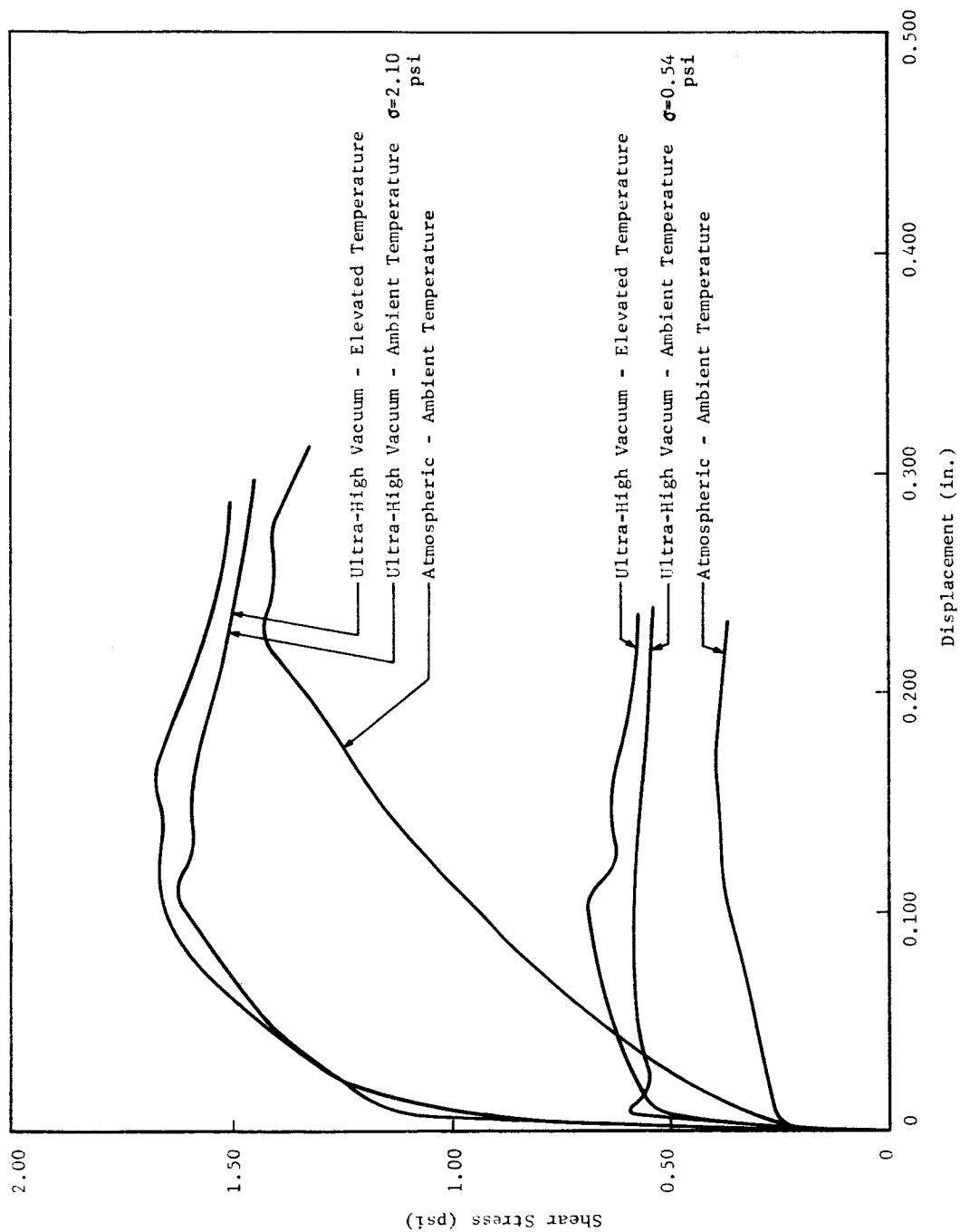


Fig. 10 SHEAR STRESS VS DISPLACEMENT FOR OBSIDIAN POWDER

The elevated temperatures, however, appear to have a very small effect on the stress-displacement relationships except possibly at the lower normal stress. A sharp initial peak shear stress was observed in ultra-high vacuum at ambient temperature but this peak was absent at elevated temperatures. While this observation is based on only one experiment at this normal stress, the experiments at normal stresses of 1.03 and 1.53 psi also showed the absence of an initial peak or leveling off at elevated temperature as opposed to its existence at ambient temperatures.

Mohr's rupture diagram for the obsidian is shown in Fig. 11. The points shown represent the average of either three or four points at each normal stress except for the individual points shown for vacuum at elevated temperature and for the intermediate stresses in vacuum at ambient temperature. The rupture diagram in atmosphere was drawn through the two points as shown because these points exhibited considerably less experimental scatter than the other two.

It is seen that ultra-high vacuum caused a rather substantial increase in both shear strength parameters, ϕ and c . The apparent cohesion increased by approximately 100 percent while $\tan \phi$ increased by approximately 30 percent. At elevated temperature, however, the shear strength appears to have been essentially the same as at ambient temperature.

The effect of ultra-high vacuum on the stiffness and shear strength of the obsidian was, therefore, essentially the same as for the quartz. The relative magnitude of the increase in ϕ and c , however, appears to be somewhat greater for the obsidian but the difference in value between the two is not great.

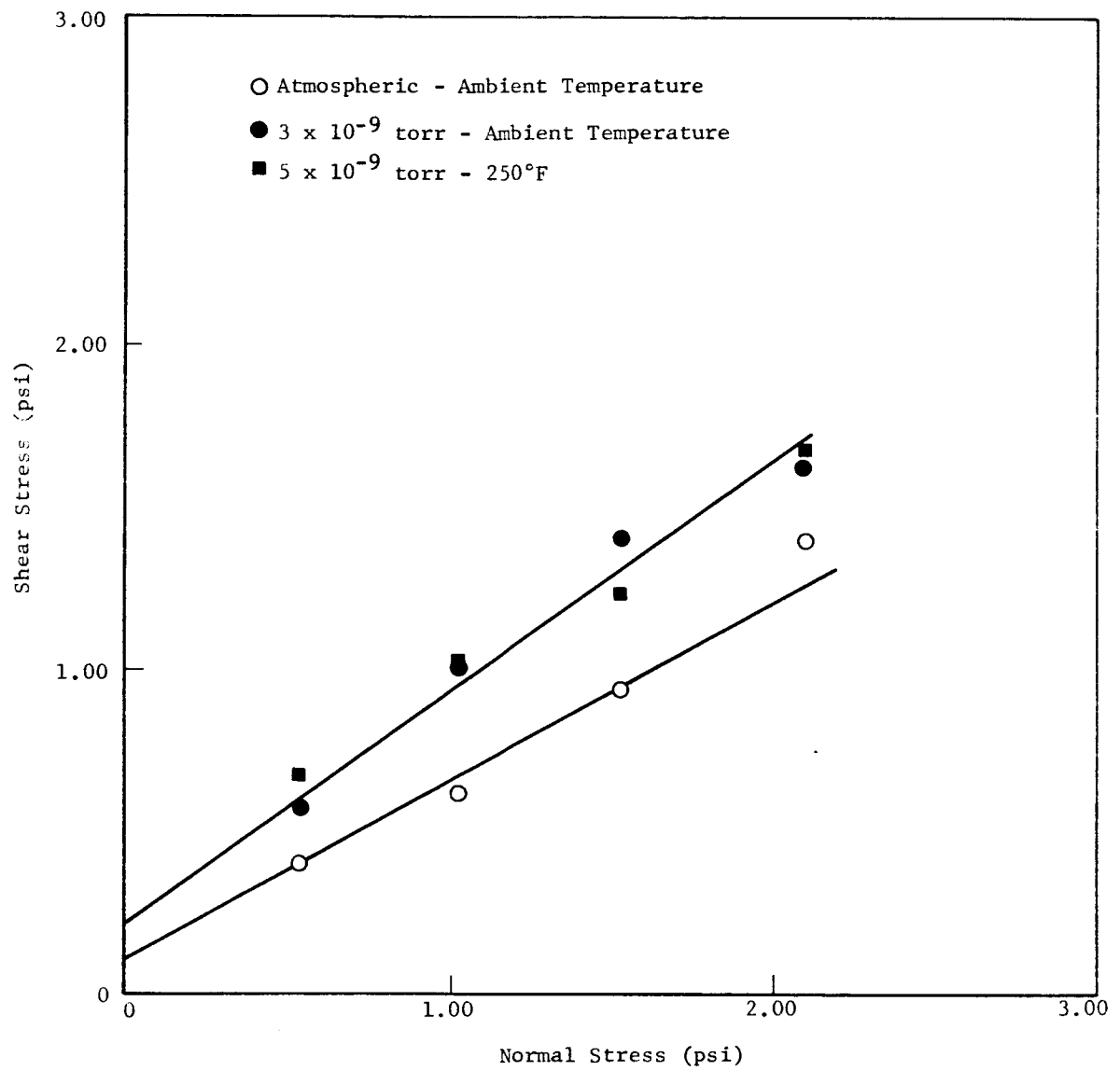


Fig. 11 MOHR'S RUPTURE DIAGRAM FOR OBSIDIAN POWDER

D. RESULTS OF DIRECT SHEAR TESTS ON ENSTATITE POWDER

The fourth material on which direct shear tests were performed was enstatite. This is a ferromagnesium silicate and is a basic mineral very similar in mineralogical composition to the olivine.

Figure 12 shows typical stress-displacement relationships for this material in atmosphere and ultra-high vacuum. While experiments were not performed on this material at elevated temperature it is seen that ultra-high vacuum alone had a rather pronounced effect on the stiffness of the soil. As was true for the quartz and obsidian the stiffness of the soil was considerably greater in vacuum than in atmosphere but the displacement at which the maximum shear stress was reached was not reduced substantially in vacuum.

At the lower normal stress it should be noted that while no sharp initial peak shear stress was formed in vacuum, a maximum was reached at a displacement of approximately 0.060 in., after which another maximum was reached at a displacement approximately equal to that for atmosphere. The first maximum would seem to be analogous to the initial peak observed in the previously discussed materials except that it occurred at larger displacements.

Figure 13 shows the Mohr's rupture diagram for the enstatite powder. The points shown represent the average of two values except for the points at the intermediate normal stresses in vacuum which are individual results. It can be seen from Fig. 13 that the shear strength parameters ϕ and c both increase in vacuum even at ambient temperature. Thus, although the mineralogical composition of the enstatite is more similar to the olivine than the quartz, the effect of vacuum on its shear strength is more similar to that of the quartz.

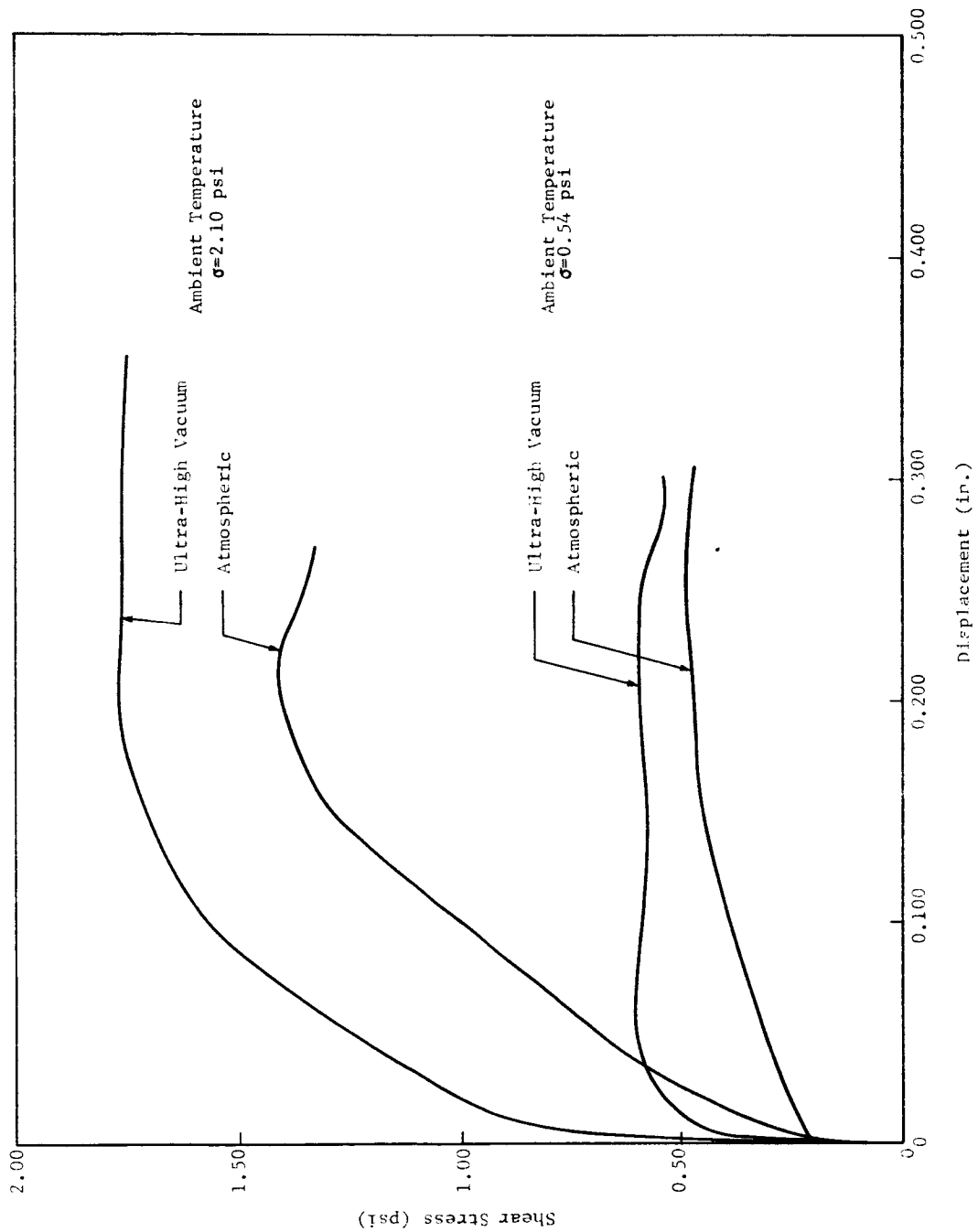


Fig. 12 SHEAR STRESS VS DISPLACEMENT FOR ENSTATITE POWDER

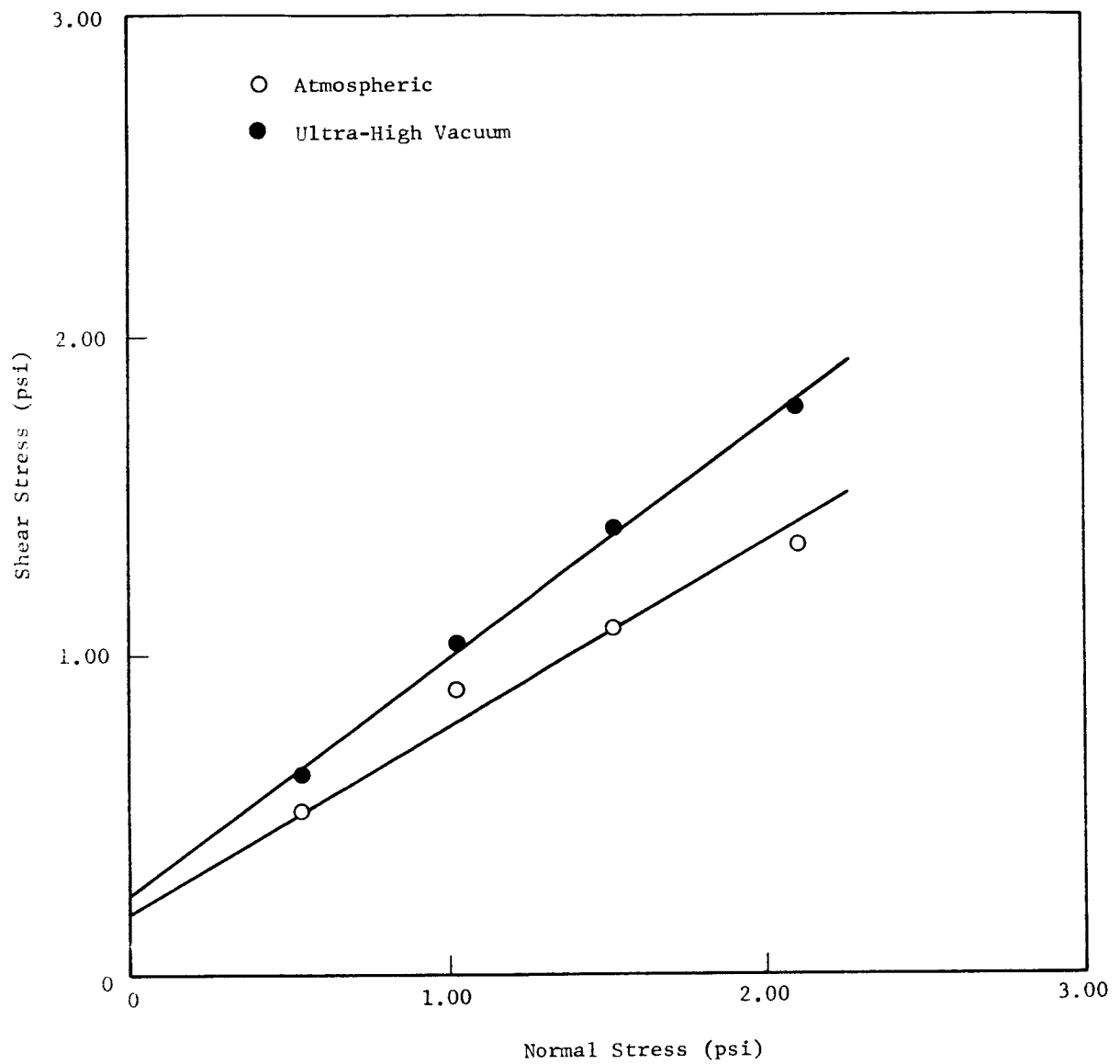


Fig. 13 MOHR'S RUPTURE DIAGRAM FOR ENSTATITE POWDER

It is interesting to note, however, that the two values of apparent cohesion are essentially the same for the enstatite as for the olivine whereas the major difference in the change in shear strength is the substantial increase in the angle of internal friction of the enstatite (approximately 25 percent).

E. RESULTS OF DIRECT SHEAR TESTS ON ENSTATITE SAND

In Phase II of this program, experiments were performed on fine grained quartz sand having the grain size shown in Fig. 2. It was observed that in ultra-high vacuum at elevated temperatures the stiffness of the sand was greater than in atmosphere. Also, the shear strength of the sand was greater in the vacuum than atmosphere (Fig. 14) but this was due to an increase in the angle of internal friction with very little, if any, change in the apparent cohesion.

A limited number of experiments were performed using fine grained enstatite sand (Fig. 2). Typical stress-displacement curves are shown in Fig. 15 in which it is evident that the soil is considerably stiffer in vacuum than in atmosphere. The rupture diagrams of the sand are shown in Fig. 16. As the points shown are for individual experiments, the data are somewhat limited but it is apparent that a rather definite increase in shear strength was observed in vacuum. While a straight line could be drawn connecting the three points in vacuum at the largest normal stresses, the point shown at $\sigma = 1.05$ psi is not considered reliable because of possible binding in the shear box in that experiment. Also the value of apparent cohesion so obtained would be unreasonably large. Because of this and in order to be consistent with the previously discussed data it is believed that the rupture diagram in vacuum should be more like that shown by the solid line than the broken line.

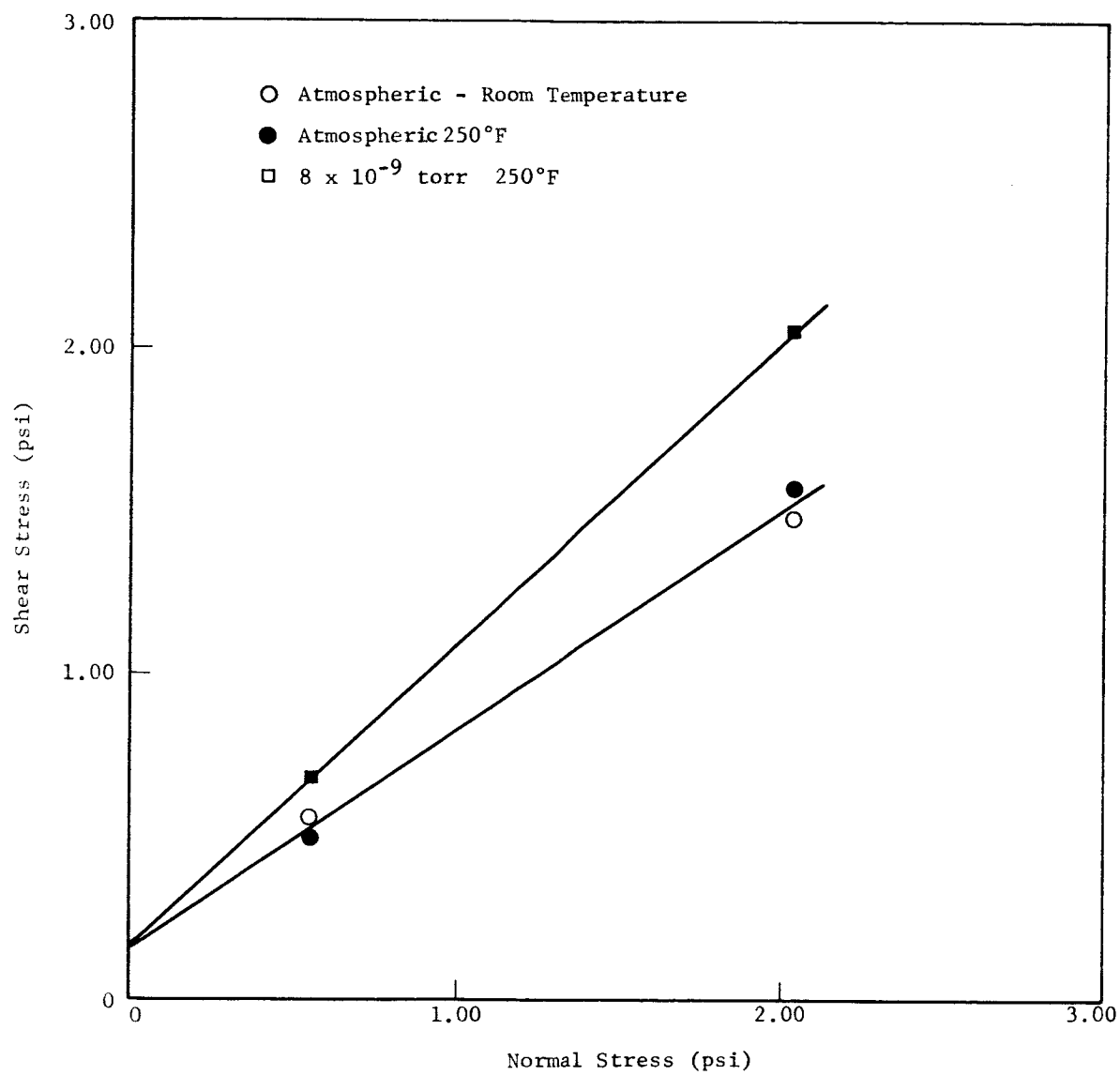


Fig. 14 MOHR'S RUPTURE DIAGRAM FOR QUARTZ SAND

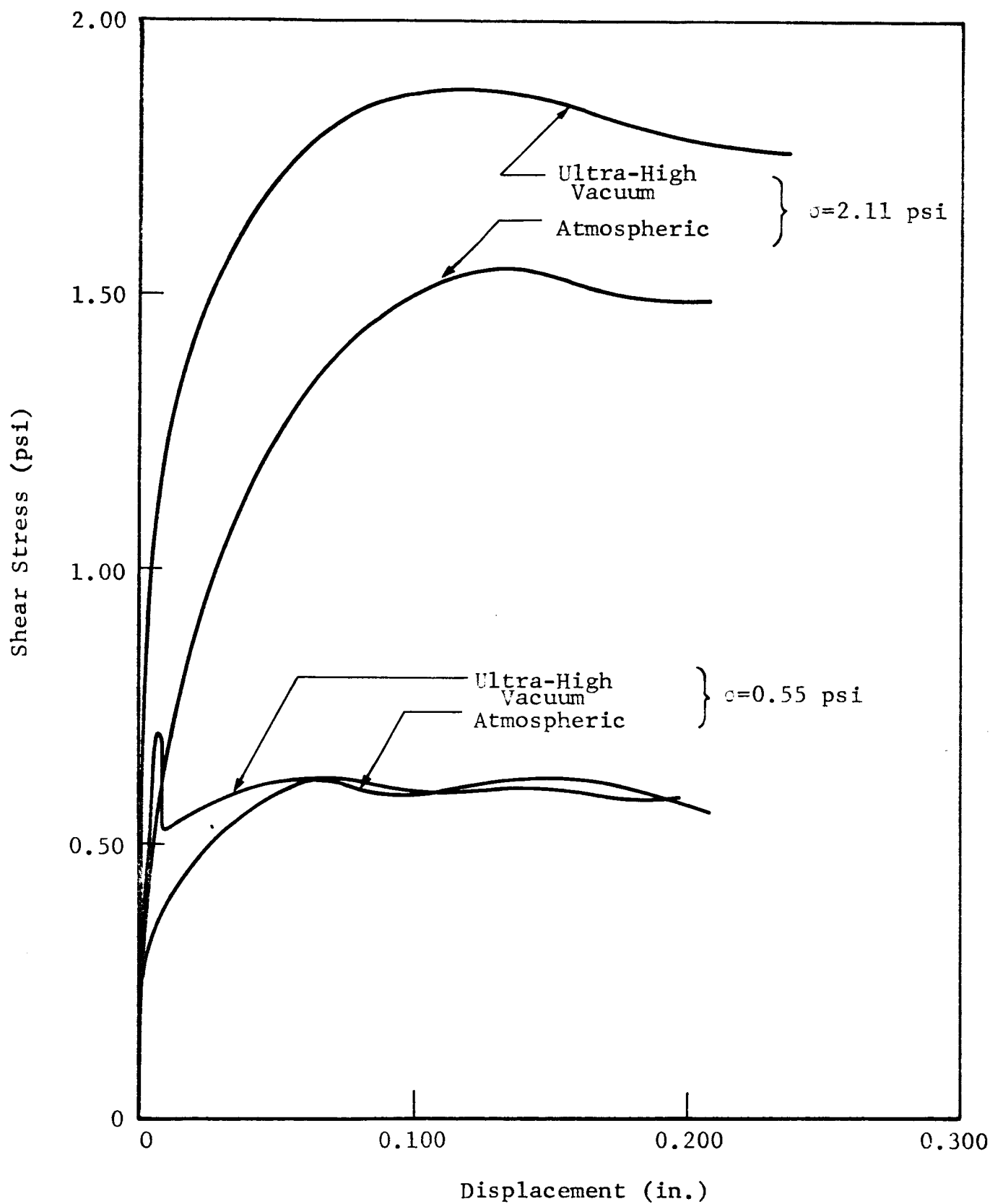


Fig. 15 SHEAR STRESS VS DISPLACEMENT FOR ENSTATITE SAND

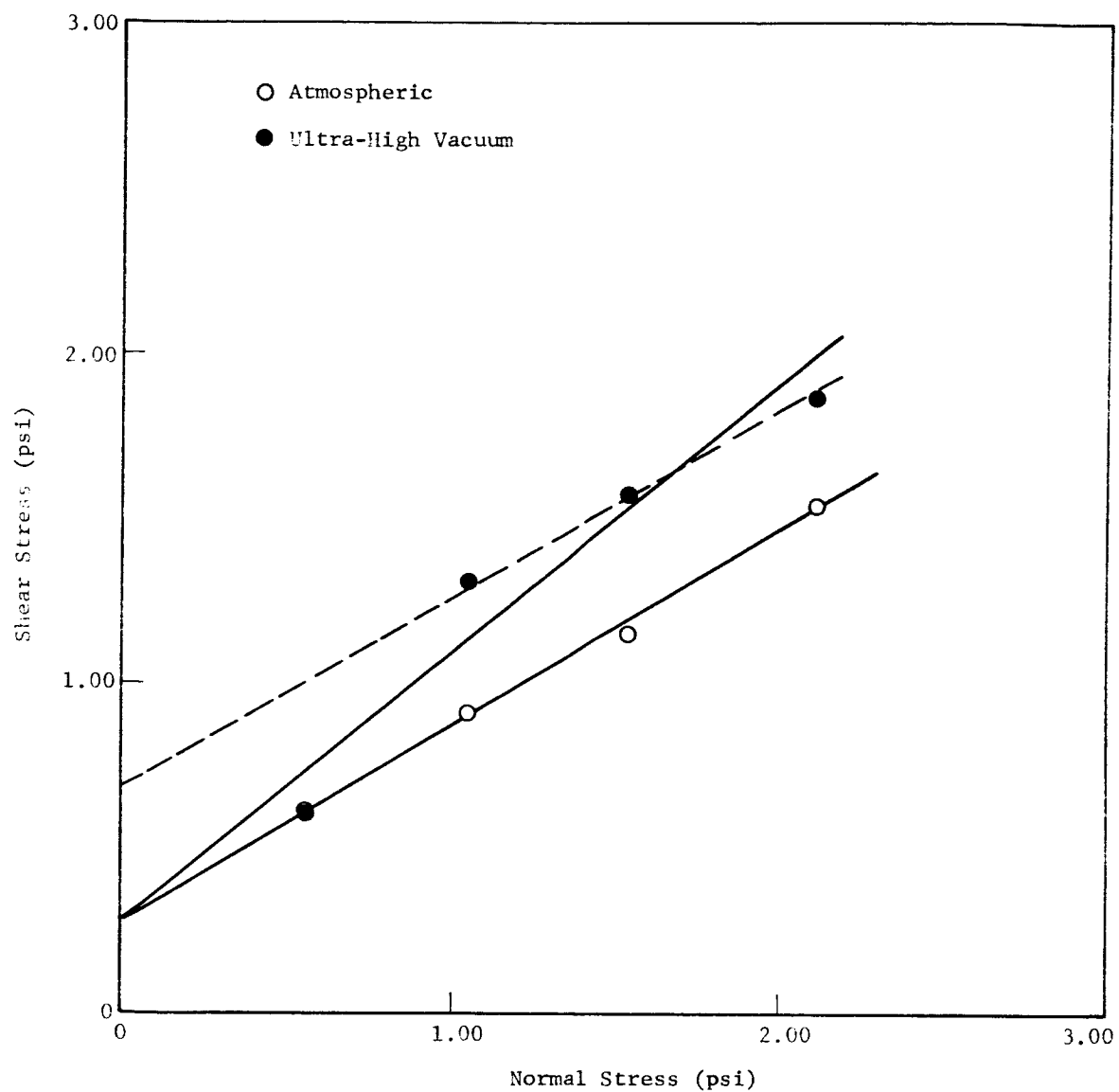


Fig. 16 MOHR'S RUPTURE DIAGRAM FOR ENSTATITE SAND

F. SUMMARY

It is quite evident, therefore, that in the powders, the ultra-high vacuum resulted in the development of bonds at the asperities and an increase in the magnitude of interparticle forces causing an increase in the shear strength (primarily in c) and stiffness. However, the magnitude of the increase and the degree of outgassing required to produce any change depended highly on the mineralogical composition. In the acidic materials (quartz and obsidian) even relatively small amounts of outgassing produced a significant change in the properties but in the basic minerals (olivine and enstatite) the effect was smaller. In fact, no effect was observed in ϕ and c of the olivine except at ultra-high vacuum at elevated temperatures.

The effect of vacuum on the properties of the sand was similar to that for the powders except that the increase in shear strength is believed to have been due primarily to a change in ϕ with little or no change in c .

IV. PENETRATION RESISTANCE UNDER DYNAMIC LOADING

The resistance of soil to penetration by dynamic loading was investigated by monitoring the deceleration of a projectile during penetration of the soil. This type of experiment may be considered as being applicable for the determination of soil properties by correlating the different features of the deceleration-time history or signature with the properties of the soil being penetrated.^{23,24,25} In this program, however, the primary purpose of these experiments was to obtain a measure of changes in soil properties caused by outgassing of the soil in vacuum rather than to determine specific values of the various properties themselves.

The dynamic penetration resistance has long been used in terrestrial soil mechanics as a measure of static bearing capacity. It has never, however, given as reliable results as static penetration tests, although the data when used in conjunction with additional knowledge of the character of the natural deposits has been most useful as a relative measure of in place soil density or stiffness.

The penetration of a projectile into soil is a very complex phenomenon which does not lend itself well to analysis by rigorous mathematical treatment. There are two ways in which the soil may fail under the projectile. One is by compression of the soil which is basically a reduction in the void ratio by rearrangement of the grain structure. The other is by shear which consists of deformation of the soil mass and may or may not be accompanied by a change in the void ratio. If a change in void ratio accompanies shear it may be either a reduction or an increase depending upon whether the soil is looser or denser, respectively, than that corresponding to the critical void ratio.

Either or both of these methods of failure may occur during penetration. For a loose material a conical zone of soil directly below the penetrometer will be compressed and accelerated initially. Depending on the energy of the penetrometer, progressive failure will then occur by compression of the soil below this region accompanied by shear failure where discontinuities in the displacement field occur. In a dense material very little compression will occur and failure will take place primarily by lateral displacement of soil along shear planes. The amount of energy required to cause penetration therefore, will be highly dependent on the constitutive relationships of the soil and its ultimate shear strength as well as its peak strength. Consequently, the resistance of soil to dynamic penetration gives a measure of the soil stiffness and shear strength combined.

The experiments described herein consisted basically of measuring the deceleration of penetrometers as a function of time during penetration. The apparatus is shown in Fig. 17 and consisted of a cylindrical soil container 10 in. in diameter and 8 in. deep on top of which fixtures were mounted to hold the penetrometers. The container dimensions were based on the results of experiments performed in the previous program² using containers of various sizes to determine the minimum dimensions that could be used with negligible boundary effects. Quartz tubular infrared lamps were mounted on the container as shown to enable the sample to be baked out during pumpdown.

The penetrometers and fixtures are shown schematically in Fig. 18. Molded teflon tubes were used as the guides in order to minimize frictional forces on the penetrometers. Several different materials were tried for the guides including polished aluminum and teflon lined aluminum but were found to cause excessive noise in the acceleration record. The penetrometers were hollow aluminum right cylinders inside of which the accelerometers were mounted. They could be used with

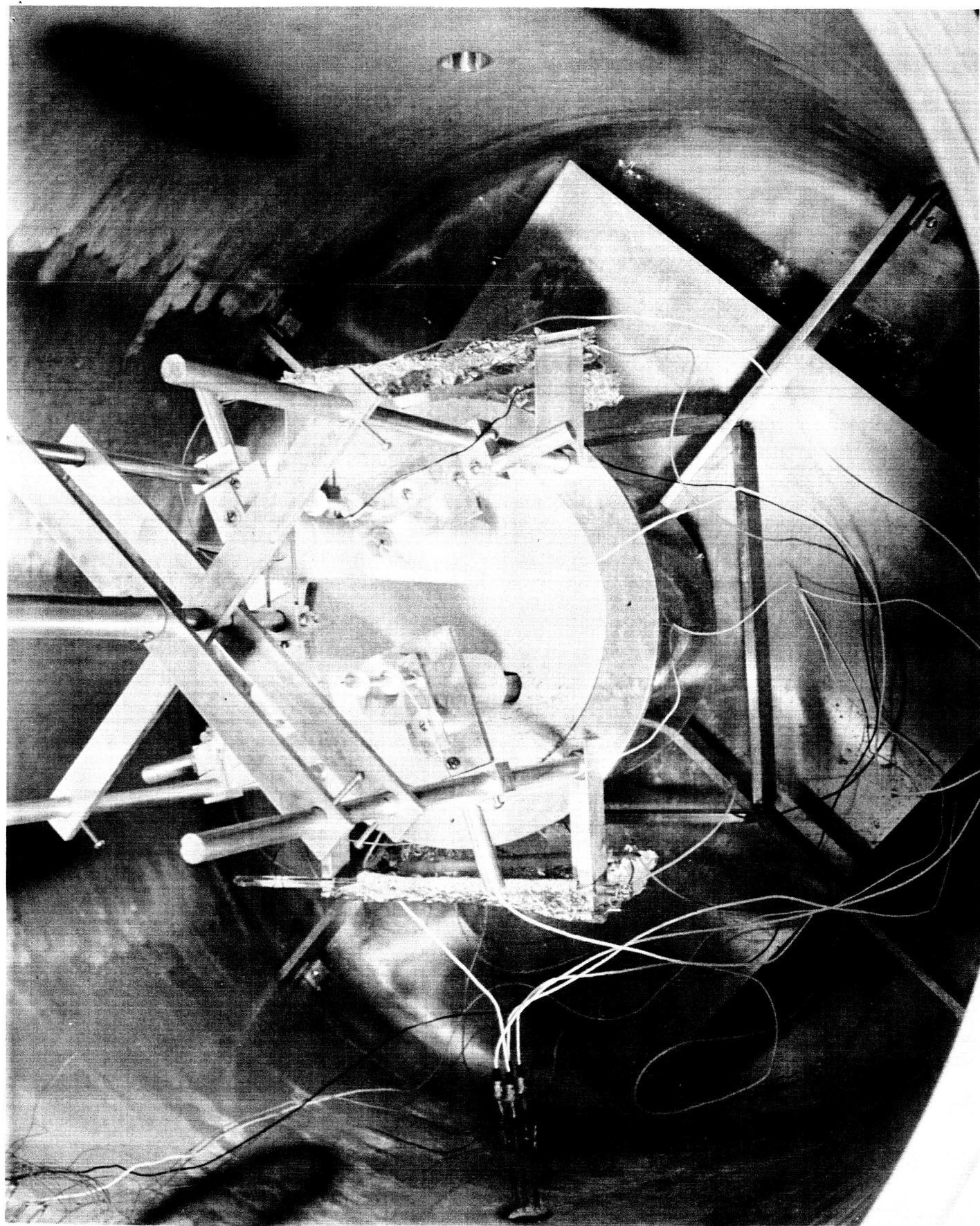


Fig. 17 DYNAMIC PENETRATION APPARATUS

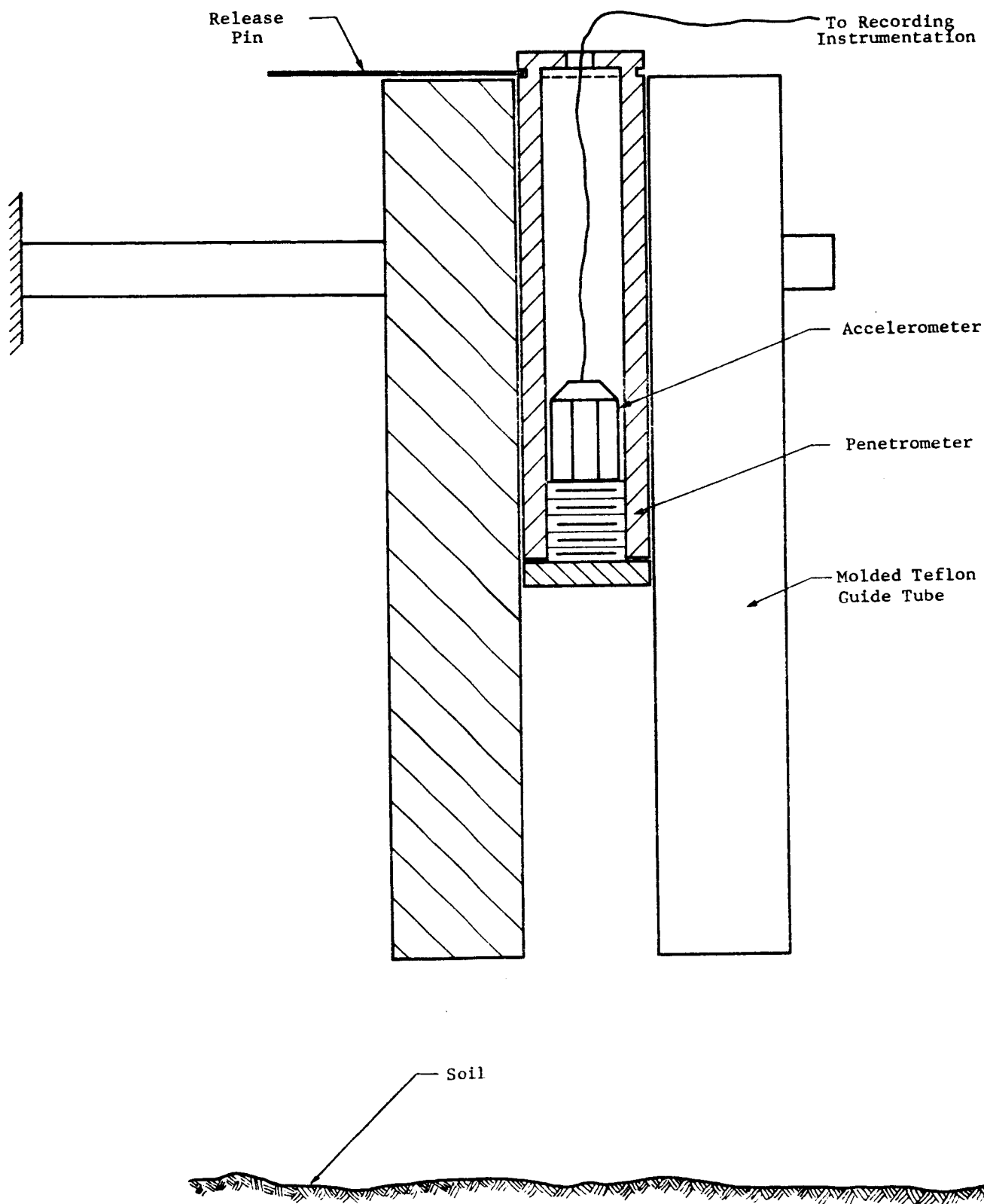


Fig. 18 SCHEMATIC OF DYNAMIC PENETROMETER

interchangeable tips of various configurations but in this program only flat tips were used. Quartz piezoelectric accelerometers were selected for use because of the wide range of temperatures in which they were operable and their desirable frequency response characteristics.

The penetrometers were accelerated prior to impact by free fall from a prescribed height above the soil surface. The drop height was maintained at 3.0 in. above the top of the soil container, but because of different amounts of settlement of the soil surface and a small amount of nonreproducible friction in the guide tubes, some variation in impact velocities was present. For each particular soil type, however, this range of variation was less than approximately 0.5 ft/sec and the impact velocities were approximately 3.75 ft/sec. It was seen in the previous program that within this range, variations in impact velocity had a very small effect on the results.

The signal from the accelerometers was recorded by two oscilloscopes one of which recorded the acceleration portion of the record in order to determine the impact velocity and the second one recorded only the deceleration. In this way maximum sensitivity could be attained for each part of the record.

Experiments were performed on all four materials (quartz, obsidian, enstatite and olivine) in the powder form (Fig. 1) and on the enstatite sand (Fig. 2). For the loose porosities, the powder samples were prepared by depositing the soil into the container through a small sieve on which an electrical vibrator was mounted. The denser samples were prepared by compacting the soil in layers under a surcharge that was varied to obtain the different porosities. The sand samples were prepared by deposition through a funnel with a slotted end as described for the direct shear tests.

For the experiments in high and ultra-high vacuum the sample was baked in atmosphere at a temperature of approximately 250°F over night and placed in the vacuum chamber while it was

hot. It was maintained at this temperature by the quartz lamps during the bakeout period. The chamber was roughed down over a period of approximately three hours after which the diffusion pumps were started. The bakeout period was continued for 48 hours after which the lamps were turned off and the soil was allowed to cool for an additional 24 hours. At this point the vacuum level in the chamber was in the low 10^{-7} torr range. In the experiments on enstatite the liquid nitrogen was added to the cold trap at the very beginning of the pumpdown period and was found to reduce the pressure to the 10^{-8} torr range. One experiment was performed and pumping was continued for an additional 72 hours during which liquid nitrogen was added to the cold trap in the throat of the chamber. At the end of this period the vacuum level was in the low 10^{-9} torr range and the remaining three experiments were performed.

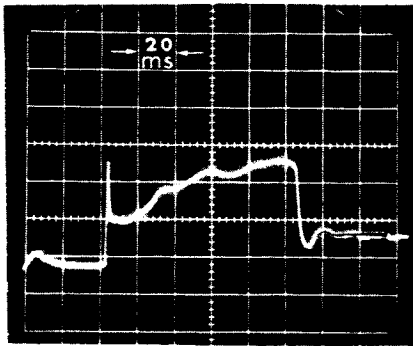
A. RESULTS OF EXPERIMENTS IN POWDER SAMPLES

In addition to the experiments in the obsidian and enstatite, experiments were also performed on the quartz and olivine to supplement the data obtained in the previous phase of the program. Therefore, some of the previously obtained results will also be presented here where it is considered desirable.

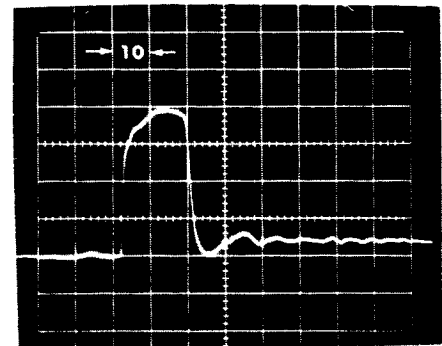
Typical deceleration-time histories or signatures for each of the four materials are presented in Fig. 19 through 22. The numbers shown on each record indicate the horizontal scale of the record in milliseconds. The vertical scale for each signature may be determined by noting that the difference in acceleration prior to impact and after the penetrometer had come to rest is approximately $1g$.

In almost all signatures of the loose samples an initial very sharp peak deceleration was observed. Although the "spike" did not occur at ultra-high vacuum in the quartz and obsidian, a very definite point of bifurcation was observed for these cases in the initial portion of the signature. This

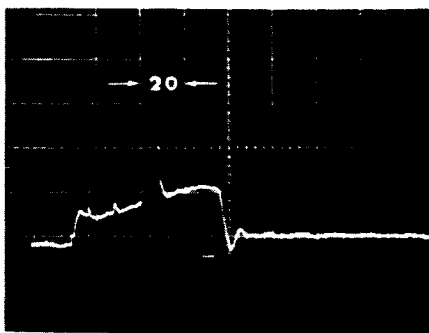
IIT RESEARCH INSTITUTE



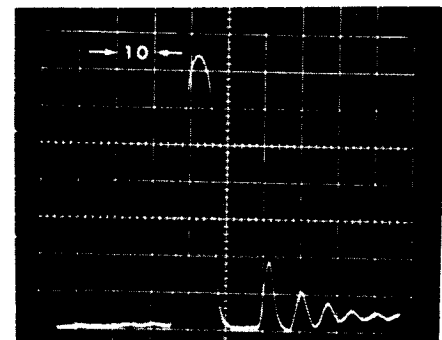
a) Atmosphere, $n = 0.639$



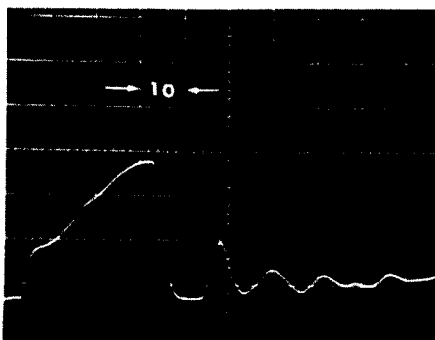
d) Atmosphere, $n = 0.574$



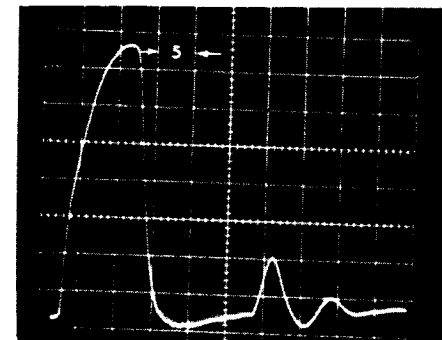
b) Rough Vacuum, $n = 0.646$



e) Rough Vacuum, $n = 0.564$



c) Ultra-High Vacuum, $n = 0.639$

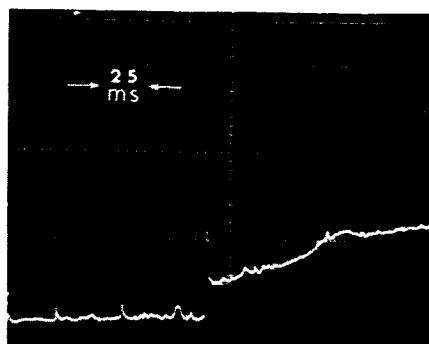


f) Ultra-High Vacuum, $n = 0.584$

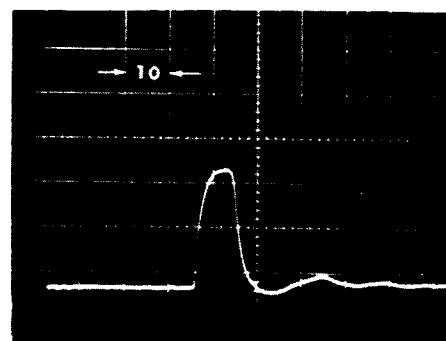
Loose

Dense

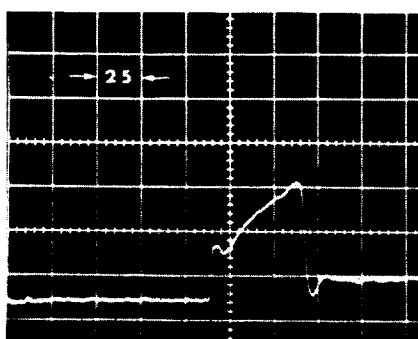
Fig. 19 TYPICAL SIGNATURES IN QUARTZ POWDER



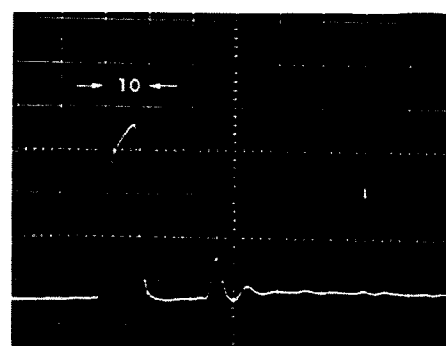
a) Atmosphere, $n = 0.676$



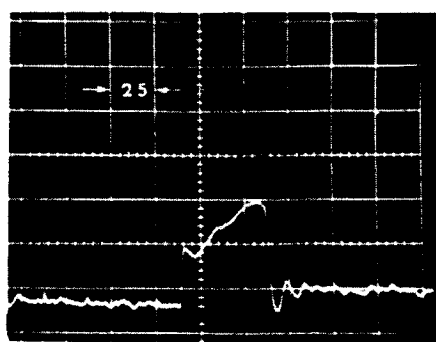
d) Atmosphere, $n = 0.584$



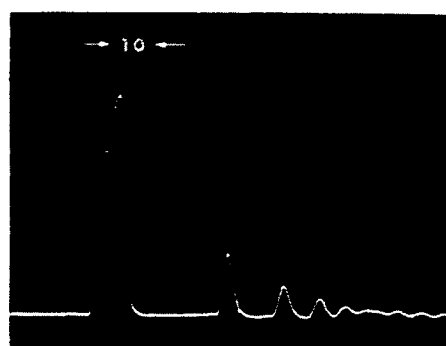
b) Rough Vacuum, $n = 0.682$



e) Rough Vacuum, $n = 0.589$



c) Ultra-High Vacuum, $n = 0.682$

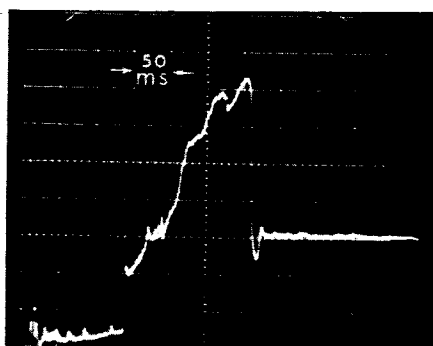


f) Ultra-High Vacuum, $n = 0.593$

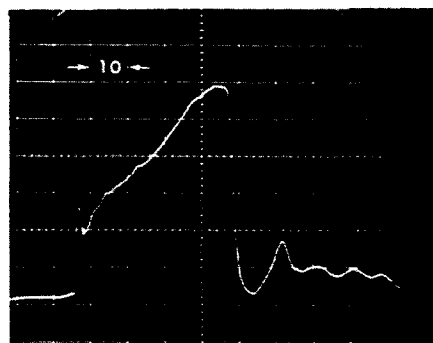
Loose

Dense

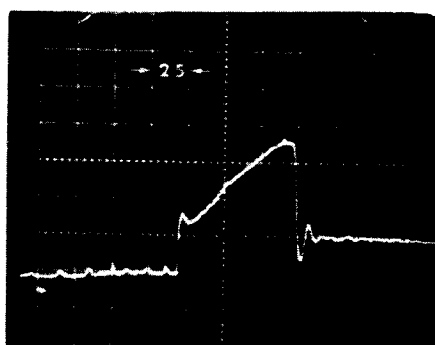
Fig. 20 TYPICAL SIGNATURES IN OLIVINE POWDER



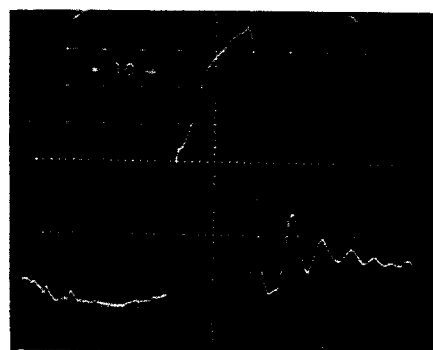
a) Atmosphere, $n = 0.652$



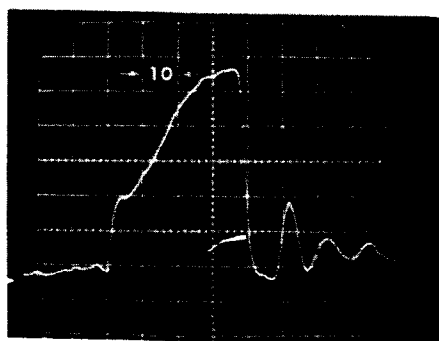
d) Atmosphere, $n = 0.578$



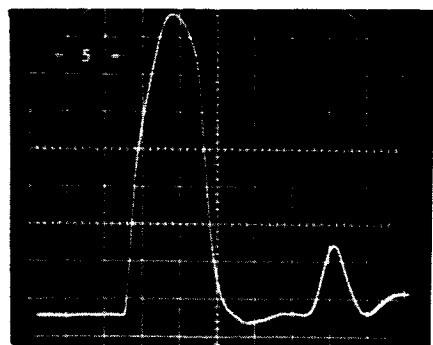
b) Rough Vacuum, $n = 0.647$



e) Rough Vacuum, $n = 0.588$



c) Ultra-High Vacuum, $n = 0.647$

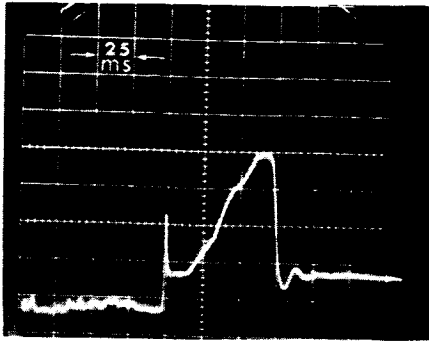


f) Ultra-High Vacuum, $n = 0.586$

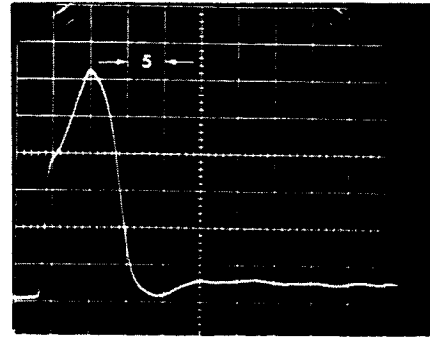
Loose

Dense

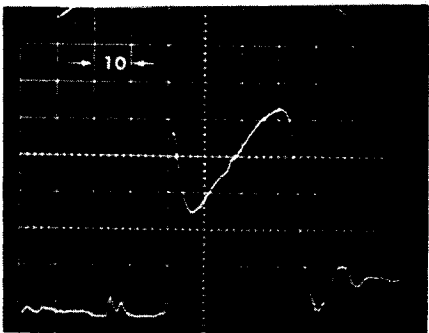
Fig. 21 TYPICAL SIGNATURES IN OBSIDIAN POWDER



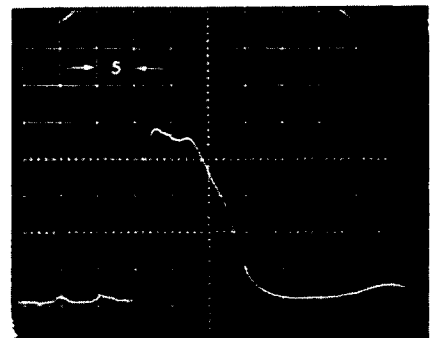
a) Atmosphere, $n = 0.542$



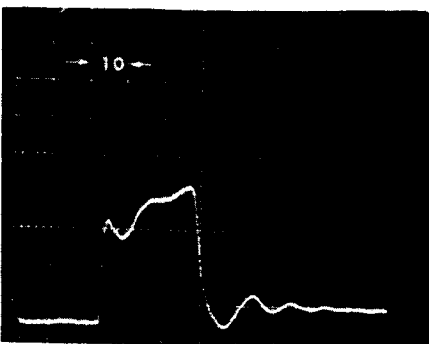
d) Atmosphere, $n = 0.482$



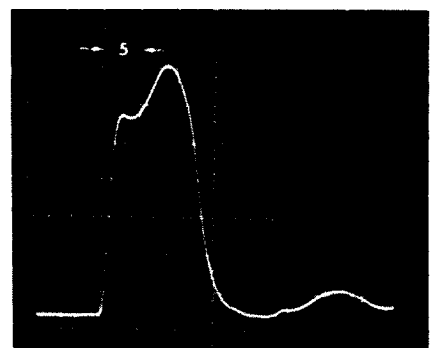
b) Rough Vacuum, $n = 0.533$



e) Rough Vacuum, $n = 0.481$



c) Ultra-High Vacuum, $n = 0.552$



f) Ultra-High Vacuum, $n = 0.507$

Loose

Dense

Fig. 22 TYPICAL SIGNATURES IN ENSTATITE POWDER

point is the same as the spike in that it represents a rapid initial deceleration except that it does not decrease rapidly after it has been reached. Subsequent to the spike the deceleration increased more slowly until all the energy of the penetrometer had been expended.

The signatures, thus, illustrate the aforementioned two mechanisms by which the energy of the penetrometer was absorbed by the soil. The initial spike was caused by the forces required to impart an acceleration to a particular zone of soil and the second portion represents the forces required to cause progressive shear failure of the remaining soil. The increase in deceleration with time was due to the fact that the force required for penetration increased with depth.

If the energy of the penetrometer was too small (or the strength of the soil too high) shear failure did not occur. In this case the energy of the penetrometer was absorbed entirely during acceleration and/or compression of the initial zone of influence. This can be seen in Fig. 19e and f, 20f and 21f in which the deceleration rose rapidly until the energy of the penetrometer had been dissipated and it had come to rest.

Another factor which should be noted for the loose material is the large decrease of the total pulse time and the increase in the deceleration in rough vacuum over those in atmosphere. This apparent increase in strength in vacuum is, in actuality, a decrease in the shear strength in atmosphere as the result of the build up of pore air pressures. The shear strength as defined by Eq. (1) can be seen to be composed of two parts one of which is dependent upon the normal effective stress on the plane of failure. The total normal stress on any plane is the sum of the neutral pressure (the pressure in the pore fluid) and the effective stress which is, therefore, the stress transmitted through the soil skeleton.

In the loose soils, the volume of the voids decreased during shear which caused an increase in the pore air pressure in atmosphere. Thus, the effective stress and the shear strength decreased. Under vacuum conditions, however, the amount of air present in the void spaces was negligible and no reduction in the effective stress resulted during failure.

In a similar manner the generation of pore pressures resulted in an increase in the shear strength of dense soils. When the void ratio was less than the critical void ratio of the particular soil, an increase in the volume of the voids accompanied shear failure. In those samples the pore air pressures were negative causing an increase in the effective stress and the shear strength in atmosphere.

It should be noted that in atmosphere some shear failure occurred in all four materials in the dense state also. For all but enstatite the rough vacuum caused an increase in the strength and in the quartz and olivine the increase was sufficient so that shear did not even occur. The void ratio of these three samples was therefore, above the critical void ratio even in the dense state.

The rough vacuum had a different effect on the signature of the dense enstatite. In atmosphere, shear occurred and the deceleration continued to increase after the initial point of bifurcation. In the rough vacuum, however, the deceleration decreased after the initial peak had been reached and the total pulse time increased over that in atmosphere. This then illustrates an increase in the shear strength in atmosphere which was undoubtedly due to the void ratio being less than the critical void ratio and the pore pressures which developed were negative.

A further increase in shear strength in ultra-high vacuum can also be seen from inspection of the signatures. While this additional increase is quite large for the quartz, obsidian

and enstatite in both the loose and dense states, it is quite small for the olivine. The increase above that caused by the rough vacuum reflects an increase in the shear strength parameters ϕ and c and/or an increase in the stiffness of the soil (i.e. a change in the stress strain relationships).

Another interesting characteristic is the oscillation of the signature about the axis of zero acceleration. It is clear that the penetrometer experienced some rebound after it had reached the maximum penetration. While this might be expected it can be seen that for all materials in ultra-high vacuum except loose olivine, and for the dense samples in rough vacuum also, the penetrometer reached an acceleration of $1g$ indicating that it had bounced back off the soil surface. In some instances it bounced off more than once and in dense olivine it left the surface three times. This shows a very substantial increase in the stiffness and "elasticity" particularly for the loose materials in which very little rebound at all was observed in atmosphere.

A number of quantitative measurements can be obtained from the signatures. By integrating the deceleration twice with respect to time the penetration can be obtained as a function of time. Also the force on the penetrometer or the resistance of the soil is directly proportional to the deceleration and can be obtained from the equation

$$R = m (g-a) \quad (2)$$

where

R is the resistance

m is the mass of the penetrometer

a is the acceleration of the penetrometer

g is the acceleration due to gravity.

Typical resistance-penetration curves for the four materials in the loose state are shown in Fig. 23 through 26. Their similarity to the signatures can be seen.

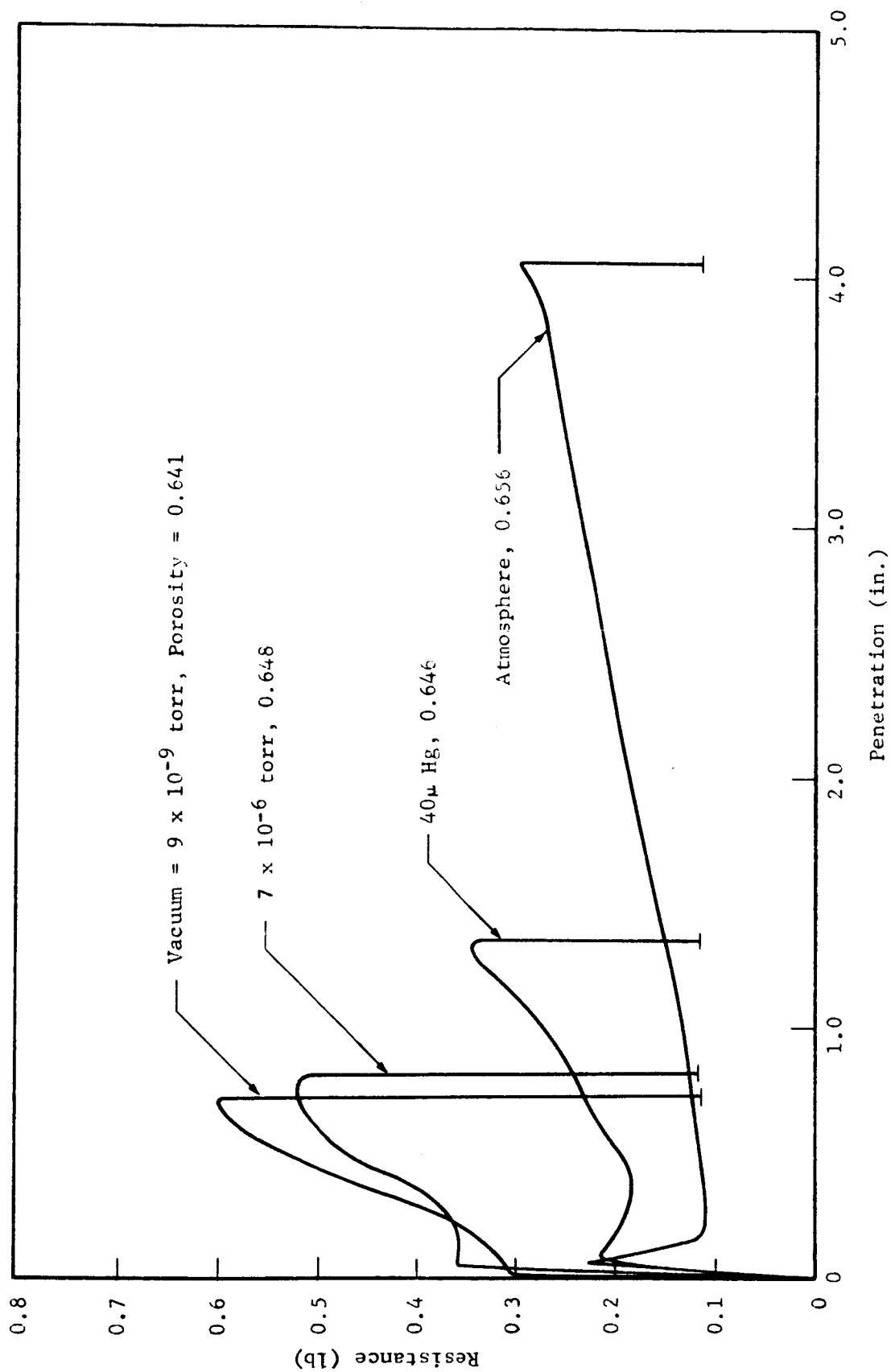


Fig. 23 RESISTANCE AS A FUNCTION OF PENETRATION IN QUARTZ POWDER

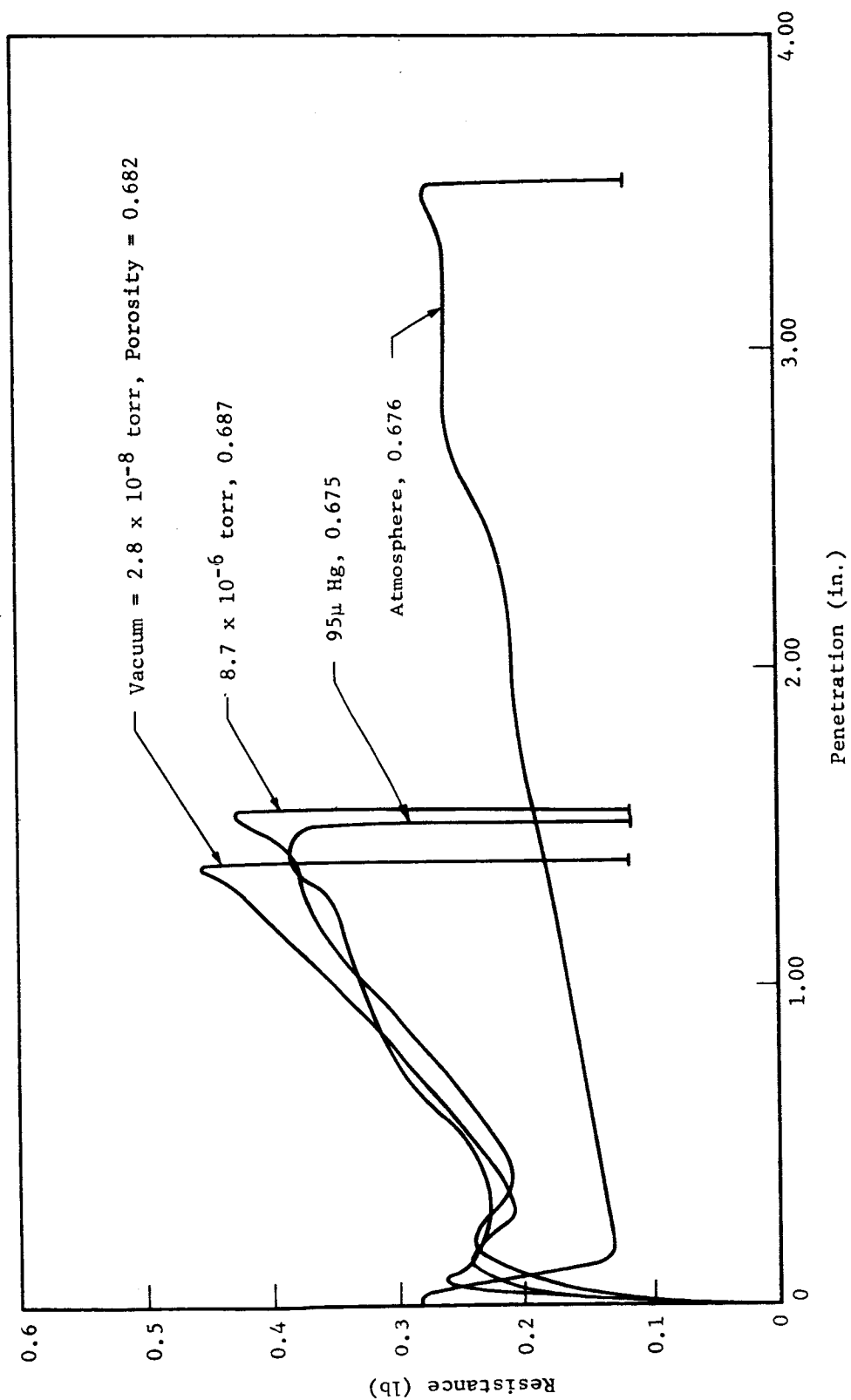


Fig. 24 RESISTANCE AS A FUNCTION OF PENETRATION IN OLIVINE POWDER

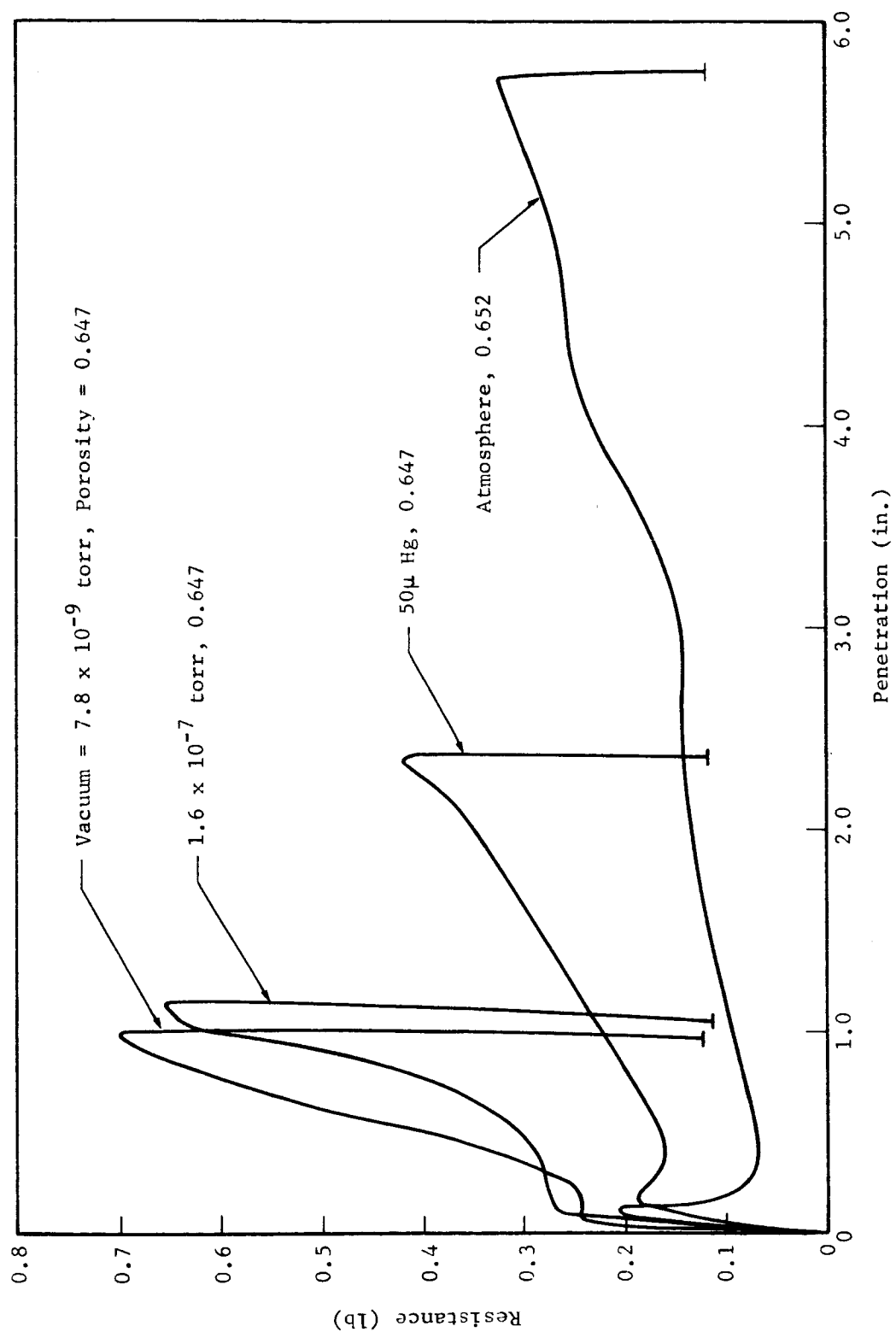


Fig. 25 RESISTANCE AS A FUNCTION OF PENETRATION IN OBSIDIAN POWDER

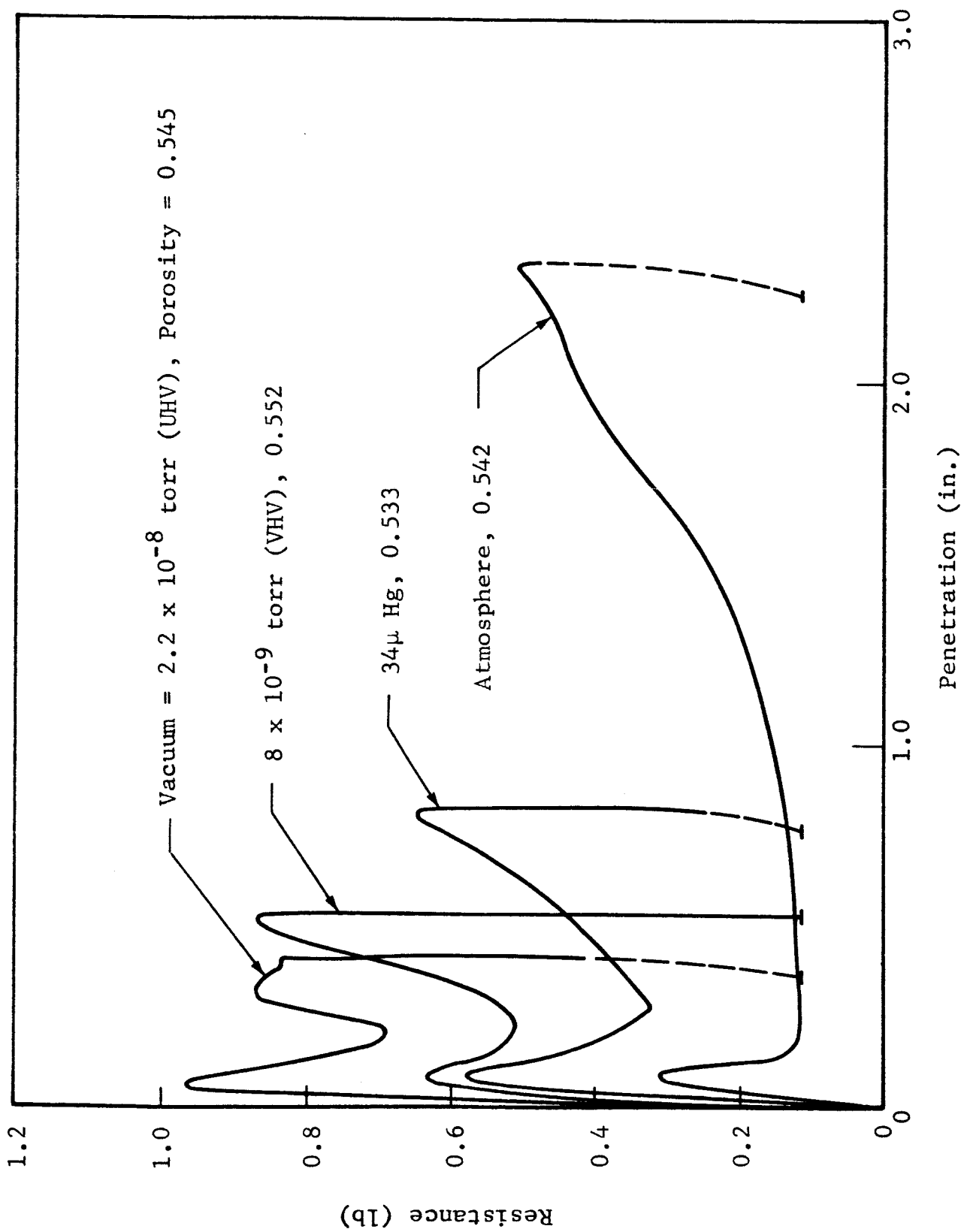


Fig. 26 RESISTANCE AS A FUNCTION OF PENETRATION IN ENSTATITE POWDER

In the preceding final report² it was shown that the resistance-penetration curve for static penetration in the quartz was very nearly the same as that for the dynamic penetration in rough vacuum. In addition to indicating a very low strain rate sensitivity this emphasized the reduction in soil strength due to the development of pore air pressures in atmosphere.

Comparison of the curves obtained in ultra-high vacuum with those obtained in rough vacuum demonstrates quite clearly a further increase in soil strength under ultra-high vacuum except in the olivine in which only a slight, if any, increase in strength was observed. For the quartz and obsidian even low vacuum levels in the 10^{-6} and 10^{-7} torr range caused a substantial increase in the resistance but higher vacuum levels caused only a small additional increase. For the enstatite the results appear to be somewhat anomalous in that a higher resistance is indicated in the 10^{-8} torr range than the 10^{-9} torr range but this is believed to be due to differences in porosity and experimental scatter.

The initial spike can also be seen in Figs. 23 through 26. For the quartz and obsidian the magnitudes of this peak are approximately equal and the effects of high and ultra-high vacuum on this peak and the shape of the curves are very similar for both materials. The increase in magnitude of the initial spike may be attributed to the fact that the soil was stiffer in vacuum and, hence, a larger zone of soil was influenced initially. It may also be due in part to inter-particle bonding similar to that which caused the initial peak shear stress in the direct shear tests.

The larger magnitude of this spike in the enstatite and olivine reflects the greater specific gravity of these two materials. It is interesting to note that the magnitudes of the peaks for the lighter materials are in approximately the same proportion to those of the heavier materials as their

specific gravities. This is in accord with the hypothesis that this spike was caused by an initial acceleration of a particular zone of soil.

It should be noted that the magnitude of the spike in the olivine appears to be relatively unaffected by even ultra-high vacuum but in the enstatite, even rough vacuum appears to have caused an appreciable increase.

A quantitative measure of the combined effects of vacuum on the shear strength and the stress-strain relationships can be obtained by integrating the resistance-penetration curve and comparing the penetration caused by a particular amount of work done for the different conditions. Since the resistance is a function of the stress-strain and strength characteristics of the soil this integral represents indirectly an integration of the shear stress as a function of displacement. It therefore, reflects not only changes in the soil stiffness and strength but it also emphasizes changes in the displacement at which the peak shear strength was developed.

The penetration caused by 0.30 in.-lb of work was determined for the various experiments and is shown as a function of the porosity in Figs. 27 through 30. The particular value of 0.30 in.-lb was chosen in these experiments because this was approximately equal to the maximum amount of energy the penetrometer was capable of imparting to the soil at the lowest impact velocities.

While the curves shown in Figs. 29 and 30 are based on only a limited number of points, they were drawn in to conform with those established more definitely in Fig. 27 and 28. Consequently, the curves shown in Figs. 29 and 30 are not intended to represent with extreme accuracy the exact relationships but rather to indicate their general shape.

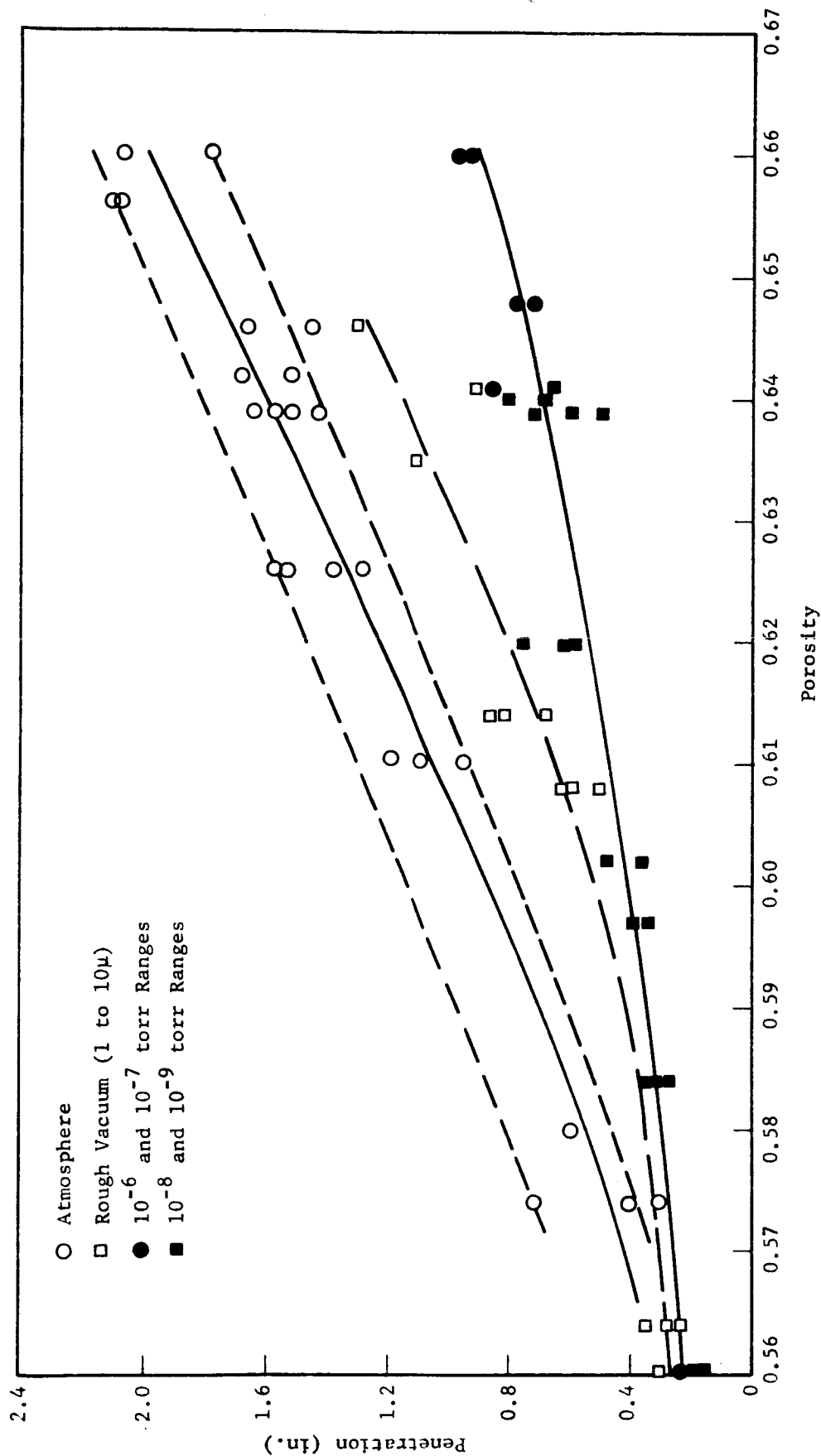


Fig. 27 PENETRATION AT 0.3 IN.- LB WORK VS POROSITY FOR QUARTZ POWDER

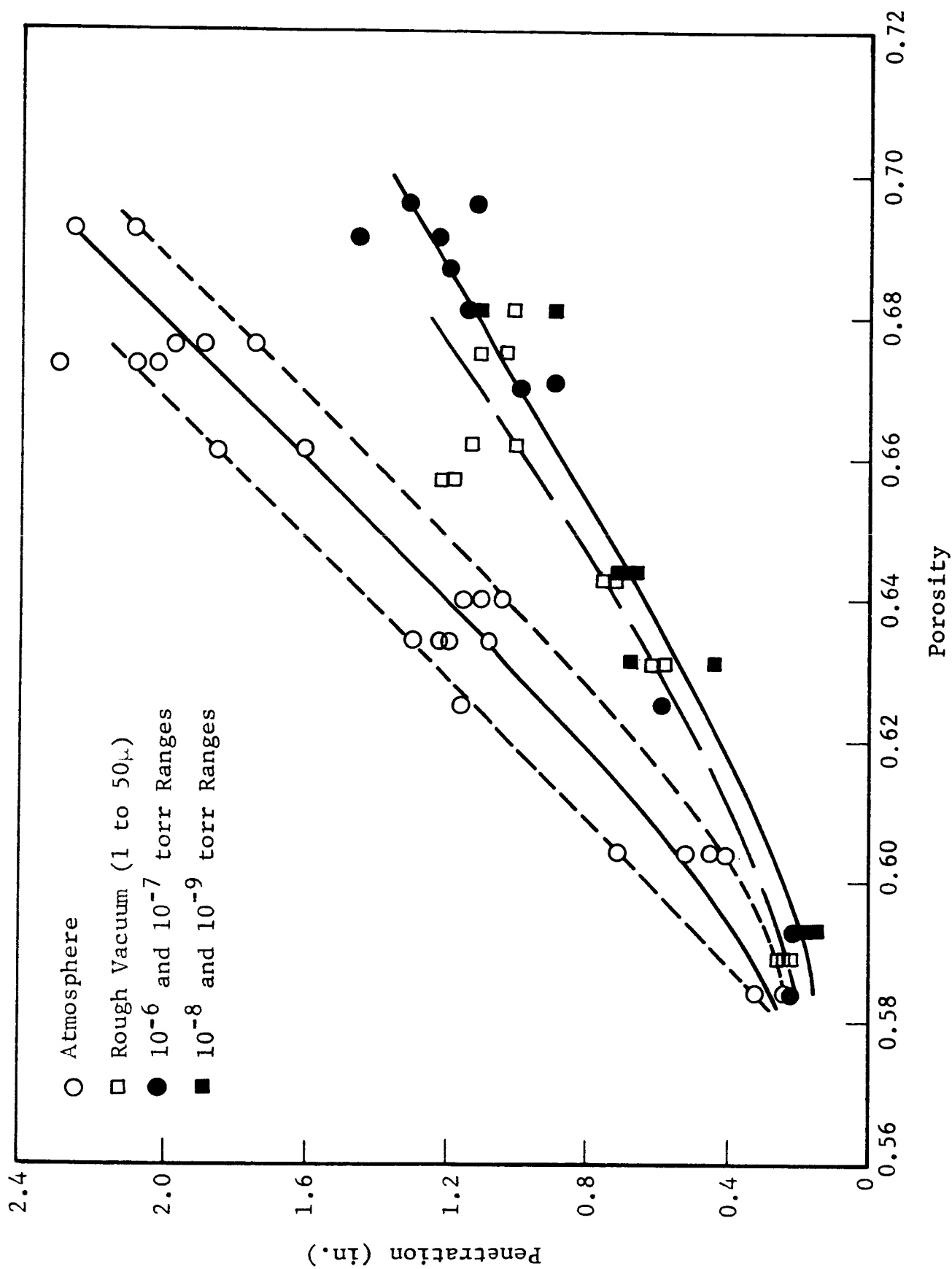


Fig. 28 PENETRATION AT 0.3 IN.-LB WORK VS POROSITY FOR OLIVINE POWDER

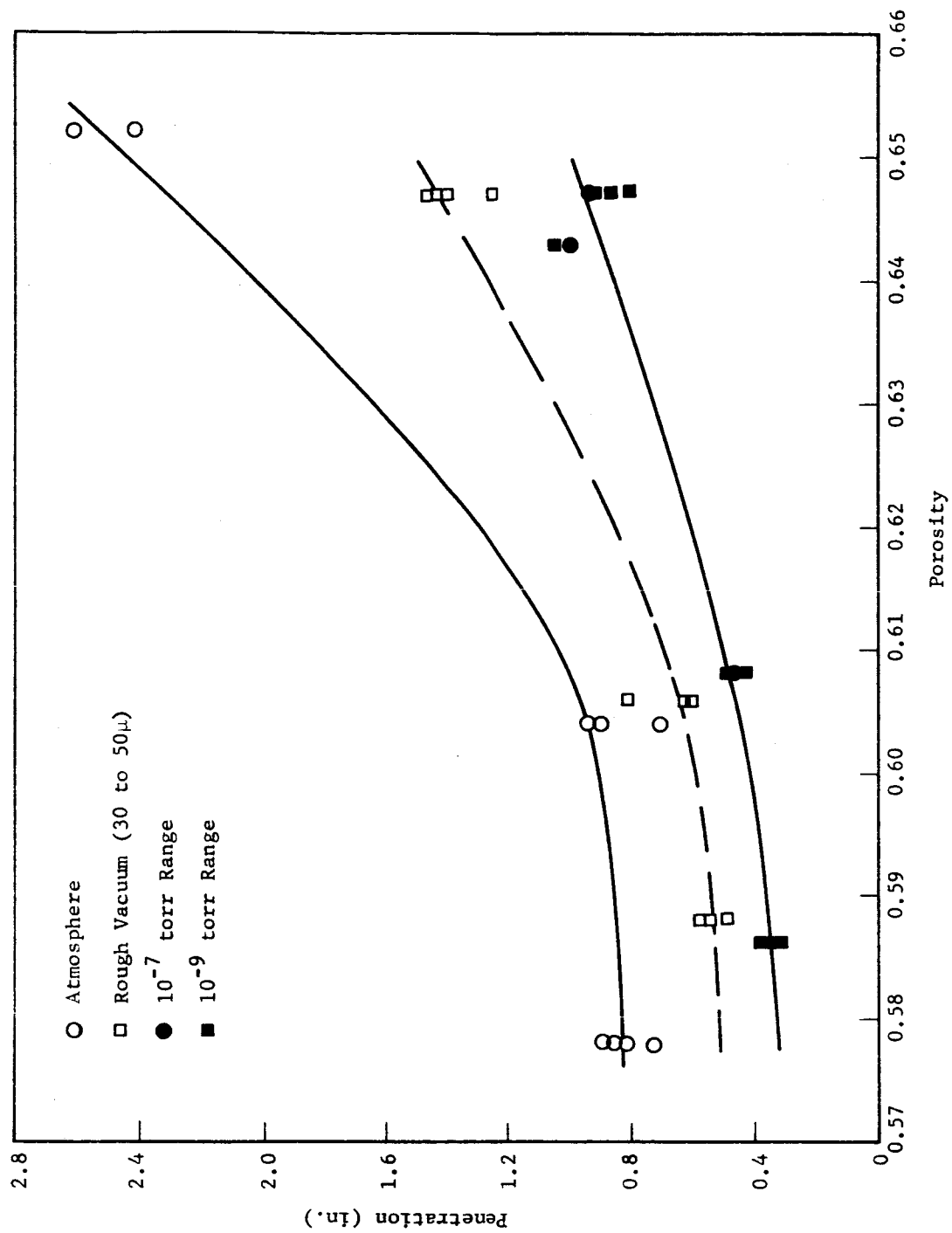


Fig. 29 PENETRATION VS POROSITY AT 0.3 IN.-LB WORK FOR OBSIDIAN POWDER

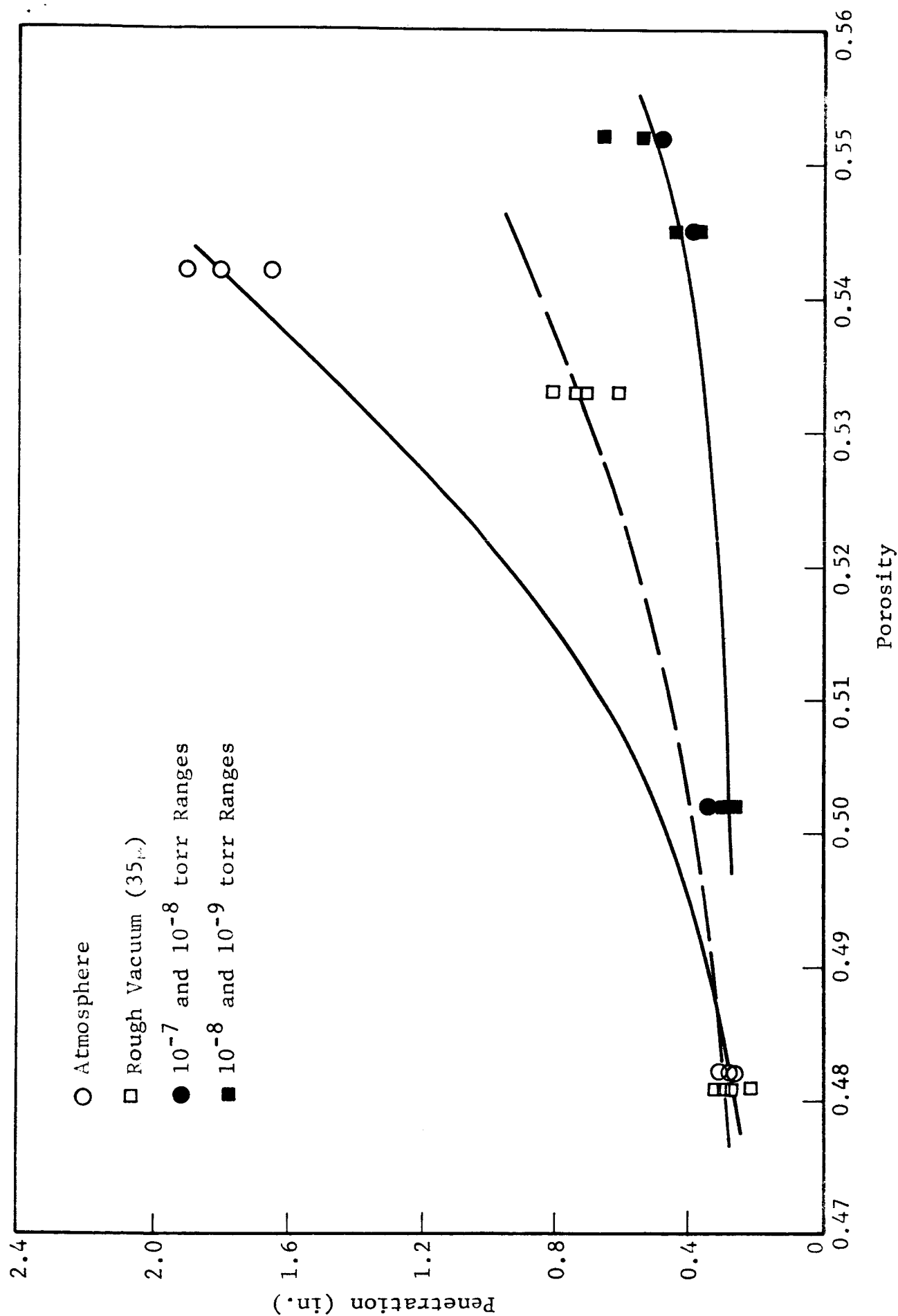


Fig. 30 PENETRATION AT 0.3 IN.-LB WORK VS POROSITY FOR ENSTATITE POWDER

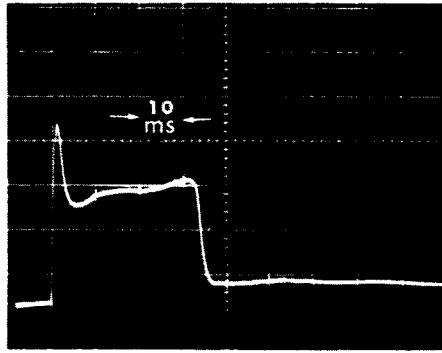
The effect of pore air pressures on the penetration resistance is very clearly demonstrated for all four materials. It can be seen that a considerable difference exists between the curves for atmosphere and rough vacuum at the higher porosities, but these curves tend to converge at the lower porosities. For a soil at its critical void ratio there is no dilatation during shear and, hence, the two curves should intersect at the porosity corresponding to the critical void ratio. Thus, while the curves in Figs. 27, 28 and 29 do not intersect they do in Fig. 30 for the enstatite which is in agreement with the previous discussion of the signatures shown in Fig. 22d and e.

A further increase in penetration resistance in ultra-high vacuum of approximately the same magnitude as that caused by the rough vacuum is also seen for all materials but olivine. It should be noted, however, that the points for experiments at ultra-high vacuum do not differ much from those for experiments in the 10^{-6} and 10^{-7} torr range. It is evident, therefore, that either the additional pumpdown from high to ultra-high vacuum had a small effect on the outgassing of the soil or else further outgassing had a negligible effect on the soil properties.

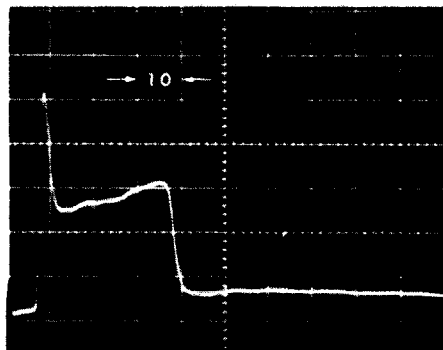
B. RESULTS OF EXPERIMENTS IN SAND

A limited number of experiments were also performed on enstatite sand and the results were compared with those obtained for quartz sand in the previous phase of this program.² Typical signatures for the quartz and enstatite are shown in Figs. 31 and 32. The horizontal and vertical scales can be determined for each as described previously for Figs. 19 through 22. It can be seen that the general shape is the same for both materials but the initial spike is considerably higher for the enstatite reflecting the difference in specific gravity and possibly a different grain size and shape of the two materials.

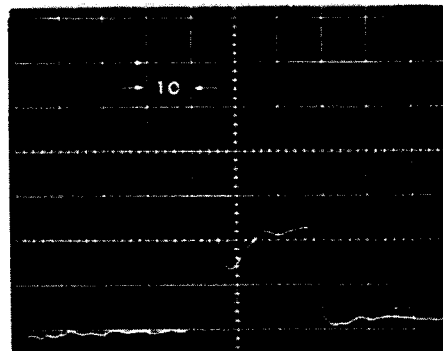
Also of interest in Fig. 32a and b is the second peak deceleration which occurred. It is believed that the second peak reflects a reduction in shear strength after the development



a) Atmosphere, $n = 0.437$

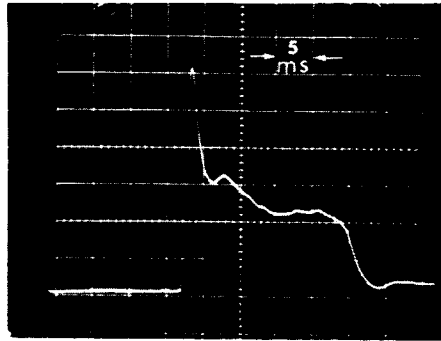


b) Rough Vacuum, $n = 0.439$

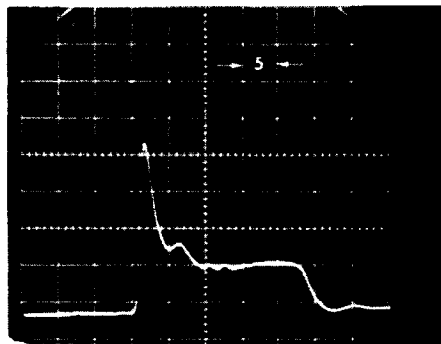


c) Ultra-High Vacuum, $n = 0.430$

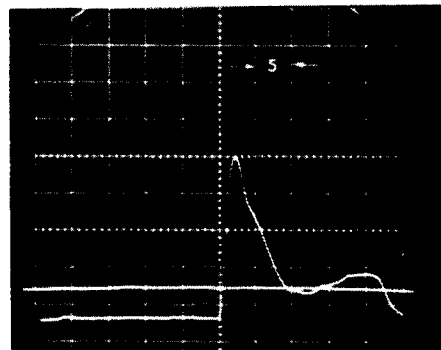
Fig. 31 TYPICAL SIGNATURES IN LOOSE QUARTZ SAND



a) Atmosphere, $n = 0.472$



b) Rough Vacuum, $n = 0.478$



c) Ultra-High Vacuum, $n = 0.469$

Fig. 32 TYPICAL SIGNATURES IN LOOSE ENSTATITE SAND

of the peak strength and the deceleration after this point is representative of the ultimate shear strength.

Rough vacuum appears to have had a small effect on the signatures but in ultra-high vacuum the deceleration decreased less rapidly after the initial spike. Also very little rebound of the penetrometer occurred after the maximum penetration.

The resistance is shown as a function of the penetration in Figs. 33 and 34. For the enstatite the second peak is clearly evident for atmospheric and rough vacuum conditions but appears to be superposed on the initial peak for high and ultra-high vacuum. It should also be noted that while the initial peak for both materials increased in ultra-high vacuum as for the powder samples, it also increased considerably in rough vacuum. In contrast to the results in the powder samples the resistance of the soil beyond the initial peak was less in vacuum than in atmosphere.

The penetration caused by 0.3 in.-lb of work is shown as a function of the vacuum level at which the experiment was performed in Fig. 35. While an increase in penetration resistance at high and ultra-high vacuum is clearly indicated the spread in the data at rough vacuum and atmosphere makes it somewhat inconclusive as to whether or not rough vacuum had a significant effect on the resistance. It was observed previously² that for the quartz, pore air pressures had a negligible effect but the difference in grain size of the two soils could account for some small pore air effects in the enstatite.

C. SUMMARY

Thus, in the powders examined the effect of vacuum was twofold. In the first place it eliminated any pore pressures which were developed in atmosphere and consequently produced an apparent increase or decrease in penetration resistance depending on the void ratio. Secondly, the changes in shear strength as

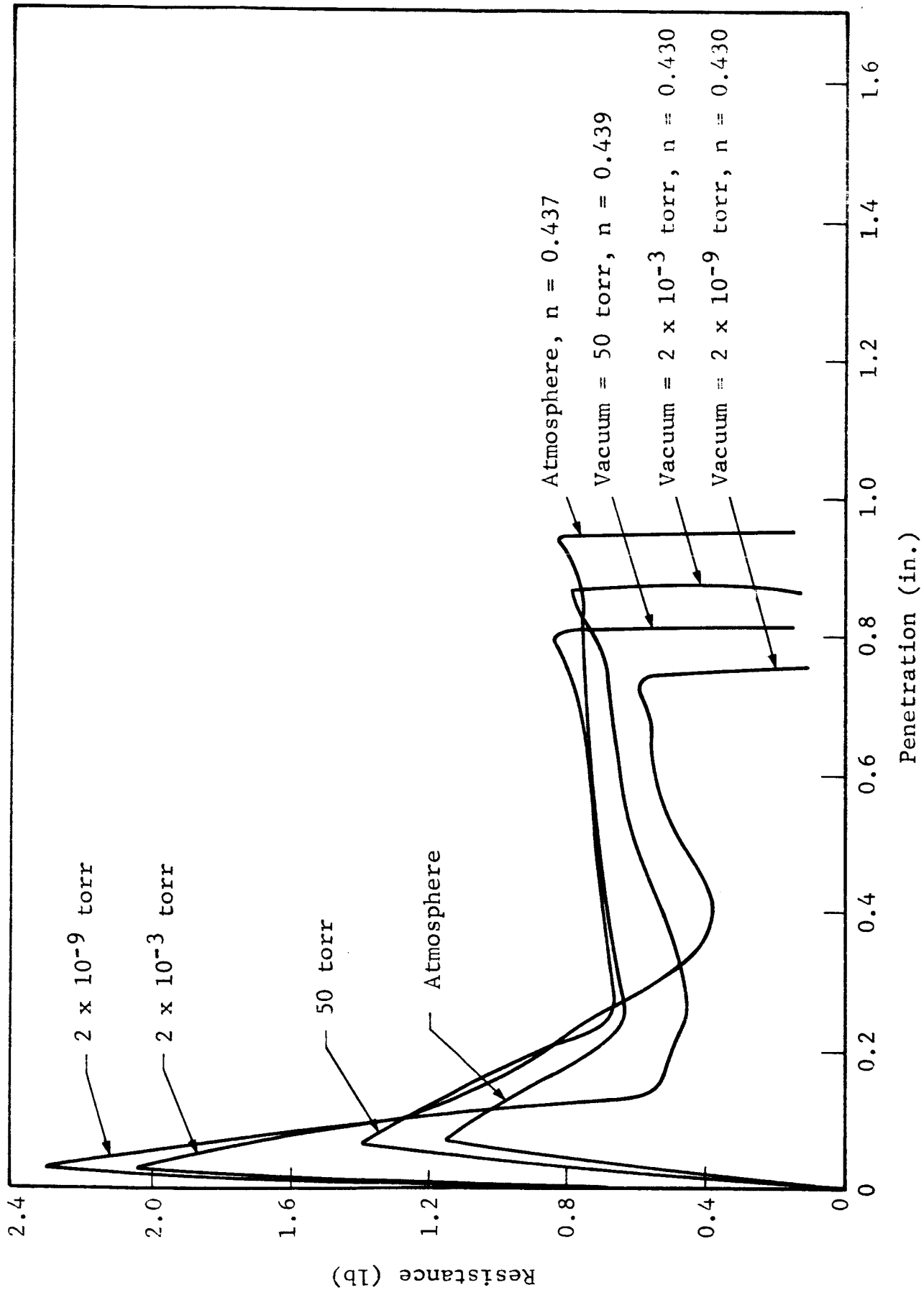


Fig. 33 RESISTANCE AS A FUNCTION OF PENETRATION IN QUARTZ SAND

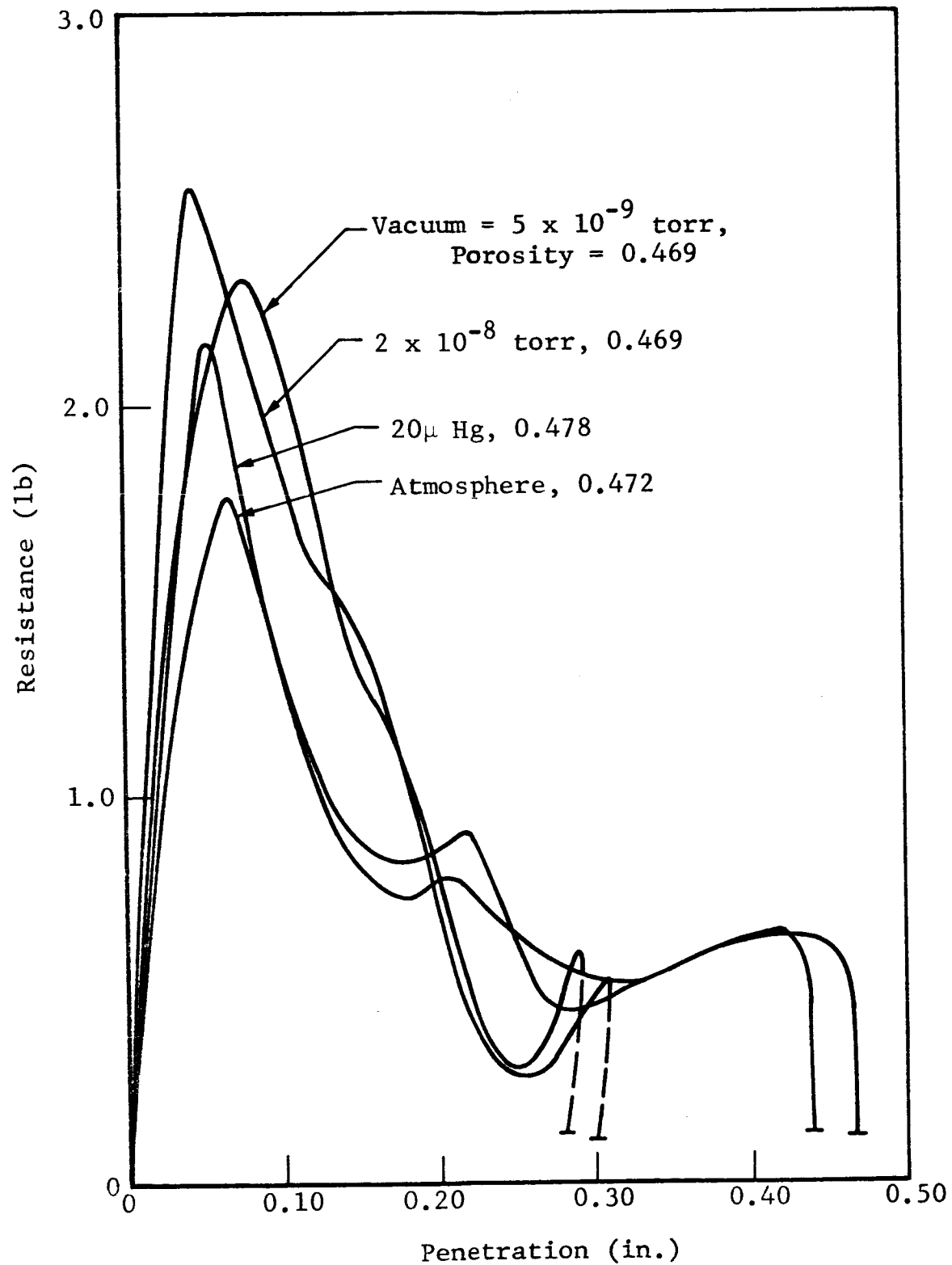


Fig. 34 RESISTANCE AS A FUNCTION OF PENETRATION IN ENSTATITE SAND

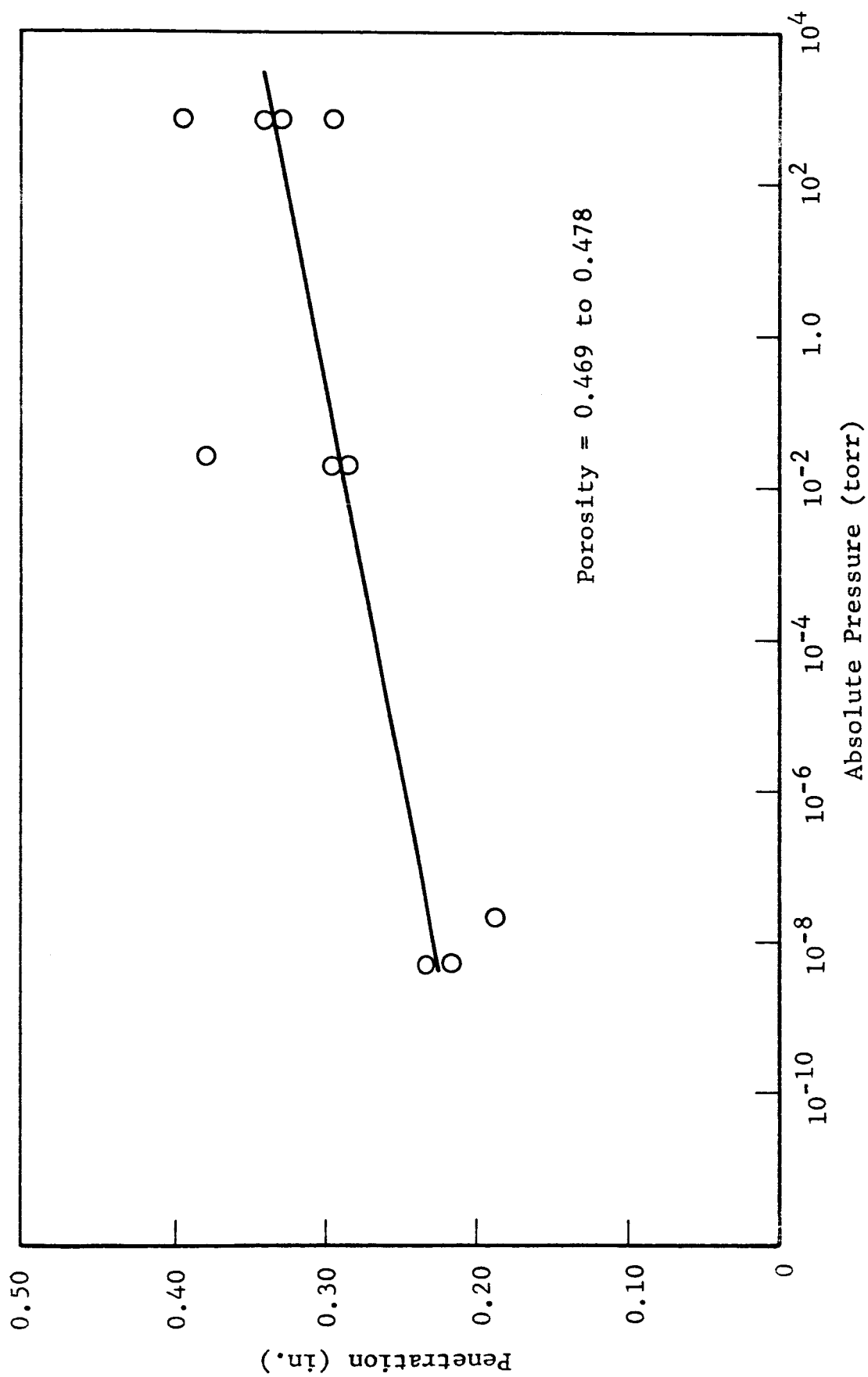


Fig. 35 EFFECT OF VACUUM ON PENETRATION AT 0.3 IN.-LB WORK IN ENSTATITE SAND

discussed in Section III resulted in a further increase in penetration resistance. The bonds at the asperities contributed to an increase in the inertial resistance of the soil and the changes in stiffness and shear strength resulted in an increase in resistance during progressive failure after the inertial resistance had been overcome.

In the sand, the effect was similar except that bonding at the asperities did not have much of an effect. Pore air pressures appeared to influence the inertial resistance but did not affect the penetration resistance at greater depths.

V. COMPOSITION OF ADSORBED GAS

It has been observed that the degree to which vacuum influences the properties of soil varies significantly with mineralogical composition. It is believed that these differences for the various materials are due primarily to differences in the nature of the adsorbate on the particle surfaces. Experiments were performed, therefore, to investigate the composition of the gas desorbed during the outgassing of soil. The purpose of these experiments was to ascertain the composition of the adsorbed gas on the different materials and to investigate any differences which might be due to sample preparation techniques and/or differences in mineralogical composition.

The experiments were conducted in an ultra-high vacuum, sputter-ion pumped vacuum system using the apparatus shown in Fig. 36. The small sample container was fabricated from 0.003 in. tantalum sheet and was supported inside the chamber by lengths of copper tubing connected to high current electrical feed throughs. Low voltage alternating current was passed through the container to heat the sample to a maximum temperature of approximately 800°C.

Two container configurations were used. The first was a rectangular box which was completely closed except for a 1/4 in. diameter hole near the top on one side. The experiments on quartz utilized this container but during heating the temperature of the container was not uniform and hot spots occurred at the corners causing the container to become brittle and finally fracture. A second type of container was fabricated, therefore, which had the configuration shown in Fig. 36. This container performed much more satisfactorily and produced a uniform temperature over its length. It was mounted in the chamber with its opening facing the inlet port of an ultra-high vacuum mass spectrometer type residual gas analyzer. The desorbed gas issuing from the container was thus directed towards the mass spectrometer where it was analyzed.

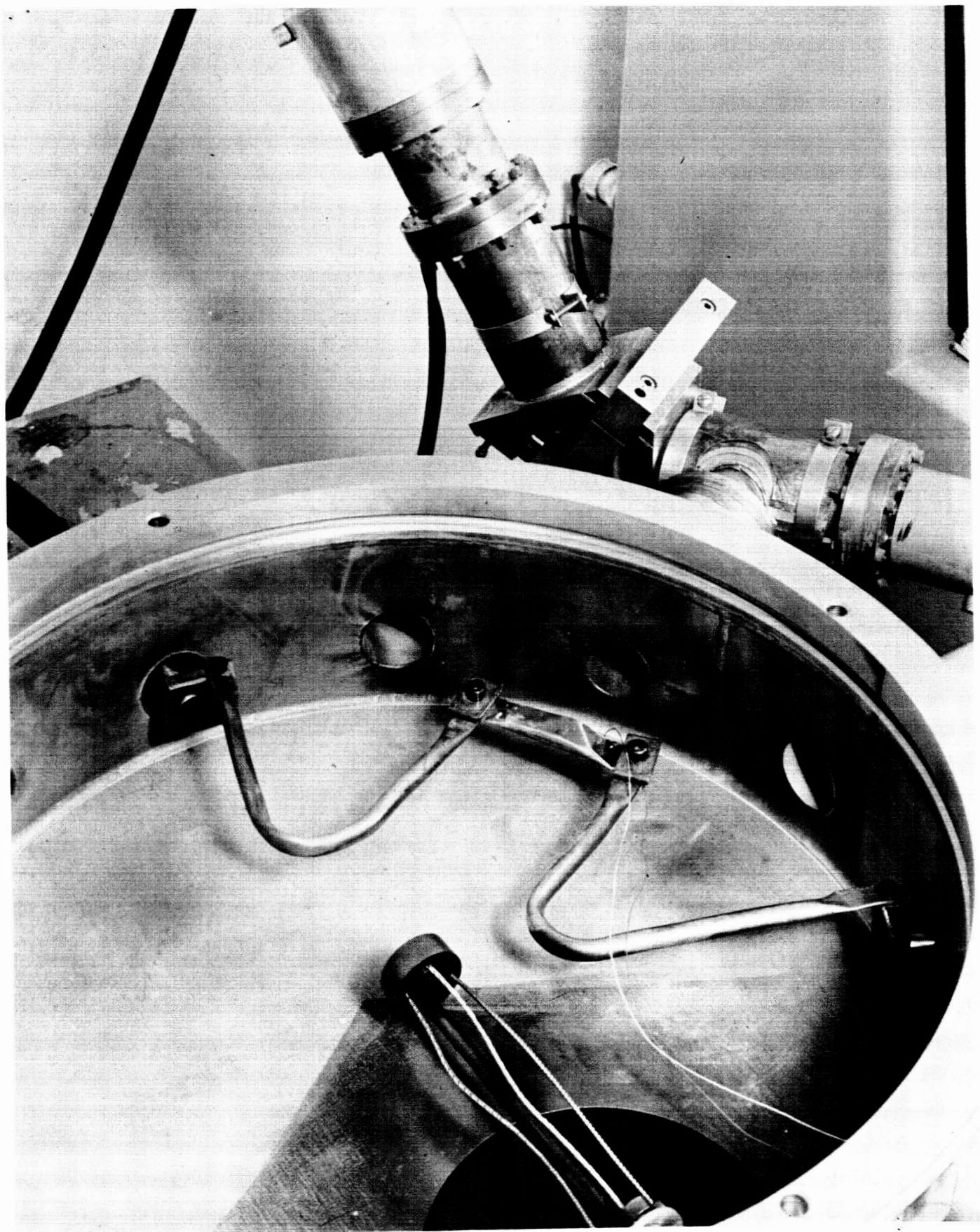


Fig. 36 DESORPTION APPARATUS

Experiments were first performed using the empty container in order to determine the spectrum of the background residual gas and its reproducibility. The system was pumped down and scans made at various temperatures. The container was allowed to cool and the system was purged with dry nitrogen. After it had remained open to the atmosphere for approximately one hour, it was pumped down again and the procedure repeated. This procedure simulated the period of time during which the container was exposed to the atmosphere during the filling operation.

Peak values of typical residual gas spectra determined at ambient temperature and at 650°C are shown in Fig. 37 and 38. All three scans were quite similar indicating that during the period in which the vacuum chamber was open, gas was readsorbed on the container of approximately the same amount and composition each time. In Fig. 37 and 38 the partial pressures were corrected for slight differences in the total pressure in the system at each scan and, hence, these figures indicate also the reproducibility of the background residual gas spectra.

A. RESULTS OF EXPERIMENTS ON QUARTZ POWDER

The container was filled with quartz powder and pumped down at ambient temperature overnight. One scan was then made with the residual gas analyzer at ambient temperature after which the temperature of the container was increased in increments of approximately 100°C and scans were made at each temperature level.

The major peaks that were observed are shown in Fig. 39 thru 45. In addition to those shown in the figures, smaller peaks were also observed at M/e values of 12, 14 and 32 and in some instances at very high temperatures a very small peak was observed at approximately 55. However, since these peaks were almost negligible in comparison to those shown they were not included in the figures. In Fig. 39 and 40 the results from

two scans are shown; the first scan (on the left) was taken approximately five minutes after raising the temperature and the second one was taken after a period of approximately 15 to 30 minutes.

The shaded portions show the differences between the peak height obtained with and without soil in the container and, hence, represent the quantity of each species desorbed from the soil. In some instances the space between two peaks is not shaded, which indicates that the peak from the background was higher than that for the container with soil. This reflects some nonreproducibility of the background spectrum but occurred only at points where very little gas was being desorbed from the soil.

From Fig. 39 and 40 it can be seen that within the reproducibility of the background spectrum the different species were present in approximately the same percentages for both scans (5 and 30 min.). Also, by comparison of Fig. 39 thru 45 it can be seen that at all temperatures the composition of the desorbed gas did not vary appreciably.

B. RESULTS OF EXPERIMENTS ON OLIVINE POWDER

In the experiments on olivine powder considerably more gas was desorbed than in those on quartz. Consequently, while the quartz could be heated to the maximum temperature in 100°C increments within a period of eight hours, it was necessary to decrease the magnitude of these increments and increase the pumping time at each for the olivine. Consequently, somewhat more than three days were required to attain the maximum temperature used.

Typical desorbed gas spectra are shown in Fig. 46 thru 49. The values of M/e at which the major peaks occurred were the same as for the quartz and it can be seen that the composition of the gas was approximately the same. It should be noted, however, that at 415°C (Fig. 49) there appears to be

an increase in the magnitude of the peaks at 44, 28 and 21 relative to the 18 peak. A similar phenomenon was observed at approximately the same temperature in another experiment on olivine but because of an inadequate background spectrum those data were inconclusive and are not presented.

It should also be noted that at all temperatures the mass range over which scans were made was from 0 to 300 and the maximum value of M/e for which any measurable peak was observed was at approximately 55. As was discussed previously, the olivine was ground in a rubber-lined mill whereas the mill lining for the other materials was stainless steel (or silex for the quartz). It was believed previously that the rubber lining may have contaminated the surfaces of the olivine and may have been responsible for the observed differences in vacuum effects. However, such contamination would be expected to result in peaks occurring in the high mass range and, hence, it appears that any contamination produced by the rubber lining was small.

Also, a sample of olivine from the same geographical region was submitted to be ground in a stainless-steel lined mill along with the obsidian and enstatite. Experiments of this type were performed on this material and spectra of the desorbed gas are shown in Fig. 50 thru 52.* Again the mass numbers at which the peaks occurred were the same as for the previous two samples and the composition of the gas was not significantly different.

One slight difference may be seen, however, in that there appears to be a somewhat larger amount of mass 18 relative to mass 2 at the higher temperature than was observed for the other olivine sample or the quartz.

*In order to differentiate this sample from the previous olivine sample it is referred to as olivine A.

C. RESULTS OF EXPERIMENTS ON OBSIDIAN AND ENSTATITE

Experiments were performed on the obsidian and enstatite sand having a grain size from 105 to 149 μ . The desorbed gas spectra for these materials are shown in Fig. 53 thru 61. It is worthy of note that at ambient temperatures the background spectrum was approximately the same as that for the desorbed gas. While this indicates that at these temperatures very little desorption occurred it also shows the validity of the background which had been determined some time previously.

For all of these materials no measurable peaks other than those previously mentioned were observed and as can be seen from the spectra the major peaks are very similar in relative magnitude to those for the quartz and olivine. Also, as was observed for olivine A, there appears to be a greater percentage of mass 18 relative to mass 2, particularly at the highest temperature.

D. GAS SPECIES DESORBED

The identification of the species of gas desorbed on the basis of the M/e values observed is quite complex and is somewhat subject to the interpretation of the experimenter. The comminution of the material in air undoubtedly resulted in the adsorption of nitrogen on the particles with oxygen forming a chemisorbed layer on the fresh surfaces. After some time, however, a portion of the nitrogen was probably displaced by preferential adsorption of water vapor. Thus, the high peak at mass 18 can be attributed primarily to water vapor and the peak at 28 and 14 to nitrogen. As evidenced by the very small peak at 32 probably very little oxygen was desorbed because of its chemisorption rather than physical adsorption. Also, a part of the peak at 32 as well as those at 2, 16 and 17 may have been caused by the breakdown of water.

The high peak at mass 2 is common in ion pumped vacuum systems and its increase at high temperatures could be due to the generation of hydrogen by the pump as the pressure in the

system increased. Similarly, hydrocarbons from the pump may have contributed to the peaks at 12, 14, 15 and 16.

Of interest in this regard is the fact that the peak at 18 increased more than the one at 2 at elevated temperatures for the materials ground in the stainless steel mill. If the 18 peak was due primarily to water vapor this would provide an indication of the amount of H_2 present due to the H_2O and would indicate that in the olivine and quartz a larger portion of the peak at 2 was due to impurities (such as hydrocarbons) and/or a greater amount of H_2 from the pump. The difference, however, is not great.

In the olivine it was seen that the peaks at 2, 28 and 44 increased in a greater proportion to the one at 18 at the highest temperature. Also in one experiment on small olivine crystals for which an accurate residual gas analysis was not obtained it was observed that the crystals had lost their olive green color after heating. The mineral had undergone a chemical change and was reduced to a very dark material which was magnetic mixed with a very light material which was nonmagnetic. This would indicate the reduction of the silicates resulting in the separation of the iron and magnesium.

Consequently, if SiO_2 was formed during this process, it could react with carbon to form SiO and CO which would account for the increases at 44 and 28 respectively. Also if the carbon resulted from the breakdown of hydrocarbons the hydrogen so released could cause the increase at mass 2.

In summary, it is apparent that the composition of the desorbed gas was predominantly water vapor for all materials investigated. Furthermore, the absence of peaks in the high mass range indicates that differences in vacuum effects on materials of different mineralogical compositions were not due to contamination of the particle surfaces during sample preparation.

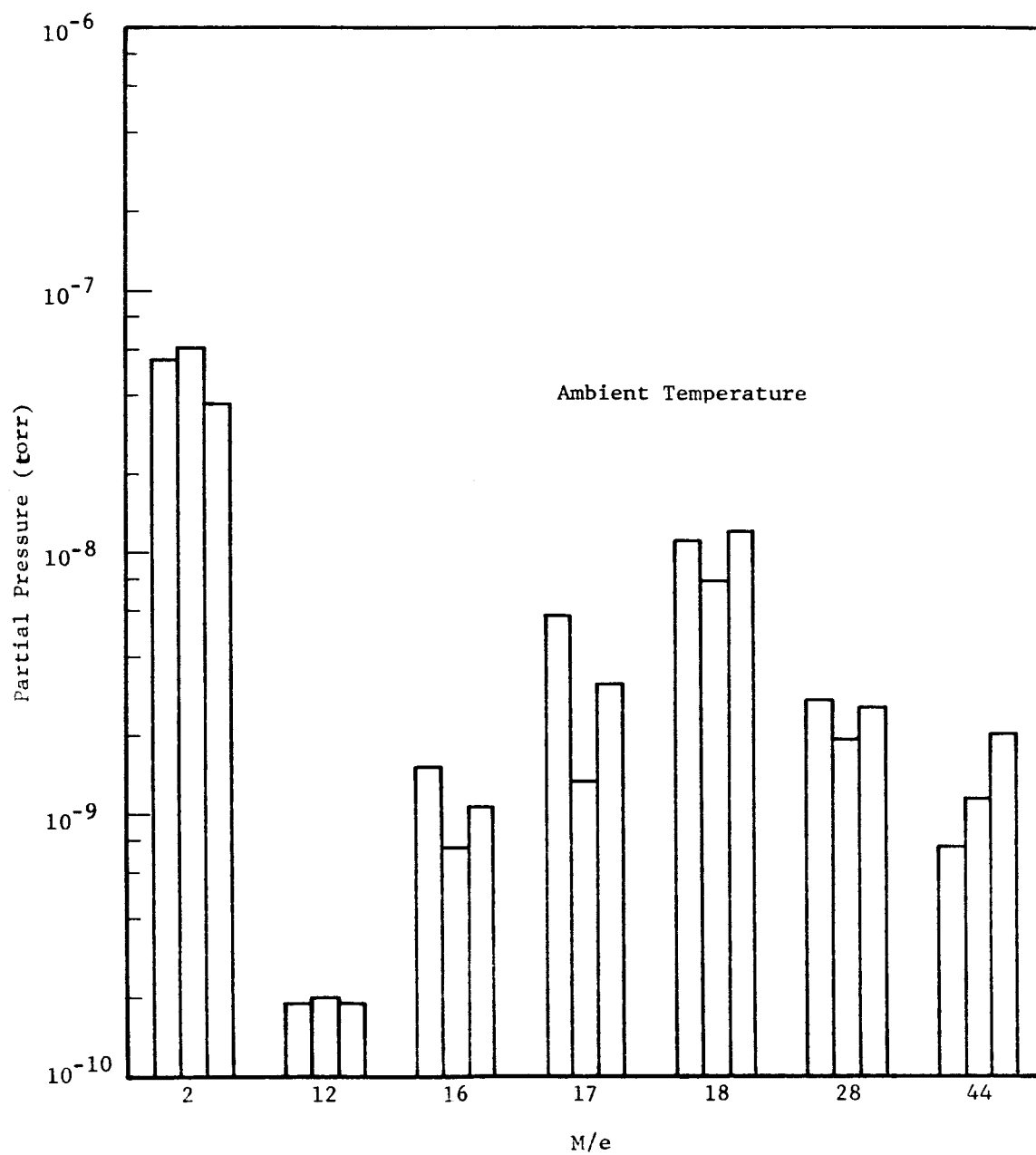


Fig. 37 BACKGROUND RESIDUAL GAS SPECTRUM

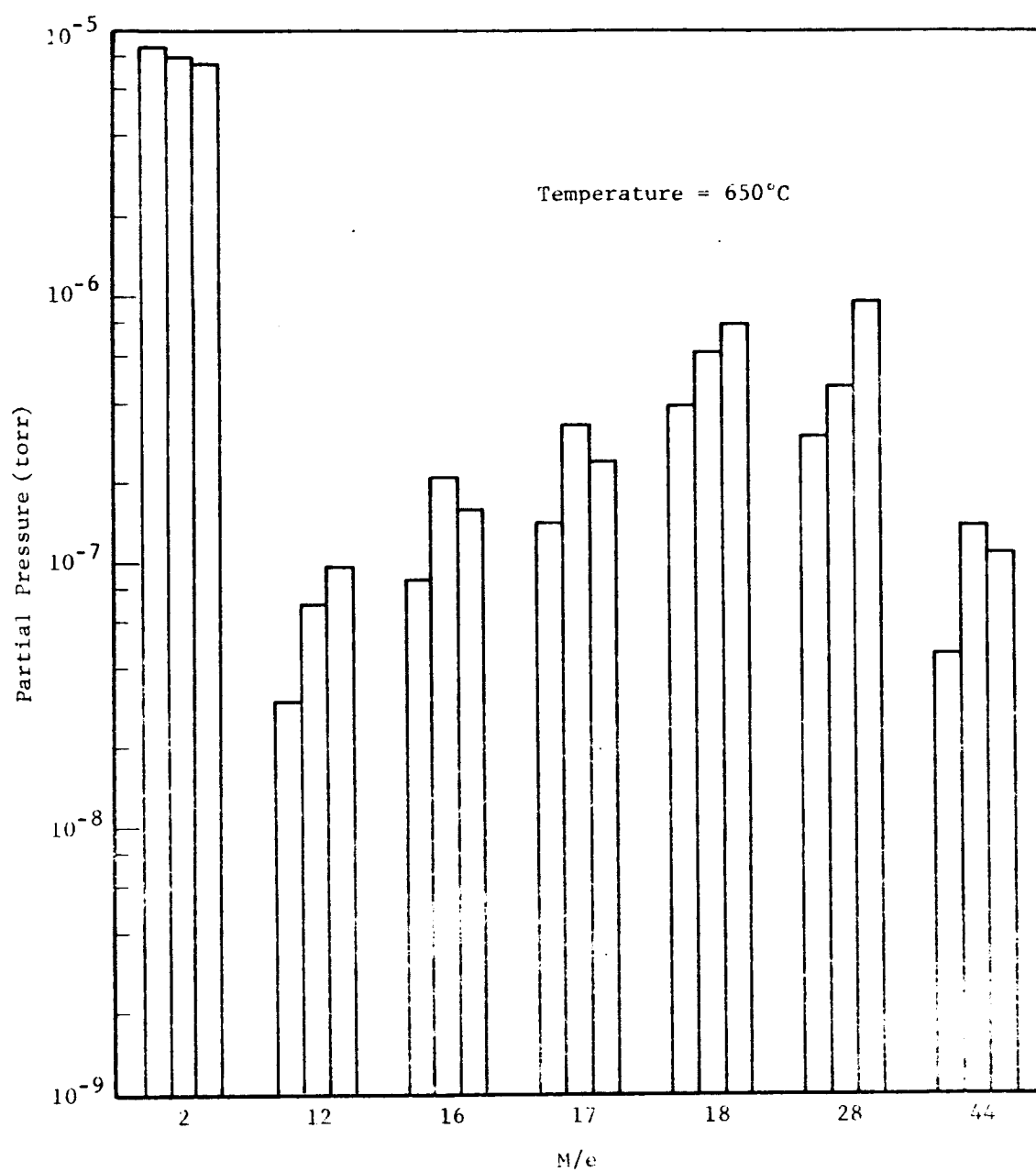


Fig. 38 BACKGROUND RESIDUAL GAS SPECTRUM

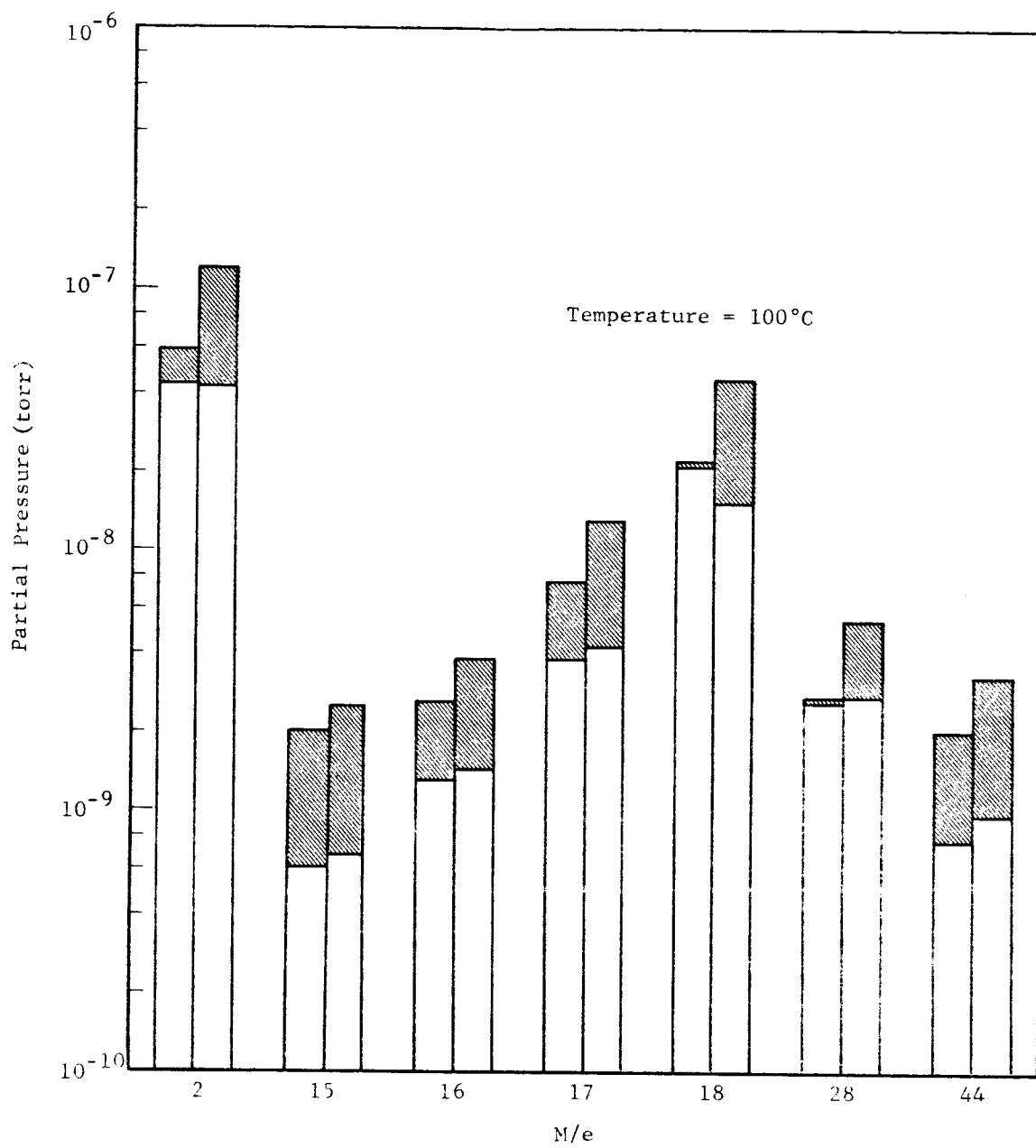


Fig. 39 DESORBED GAS SPECTRUM FOR QUARTZ POWDER

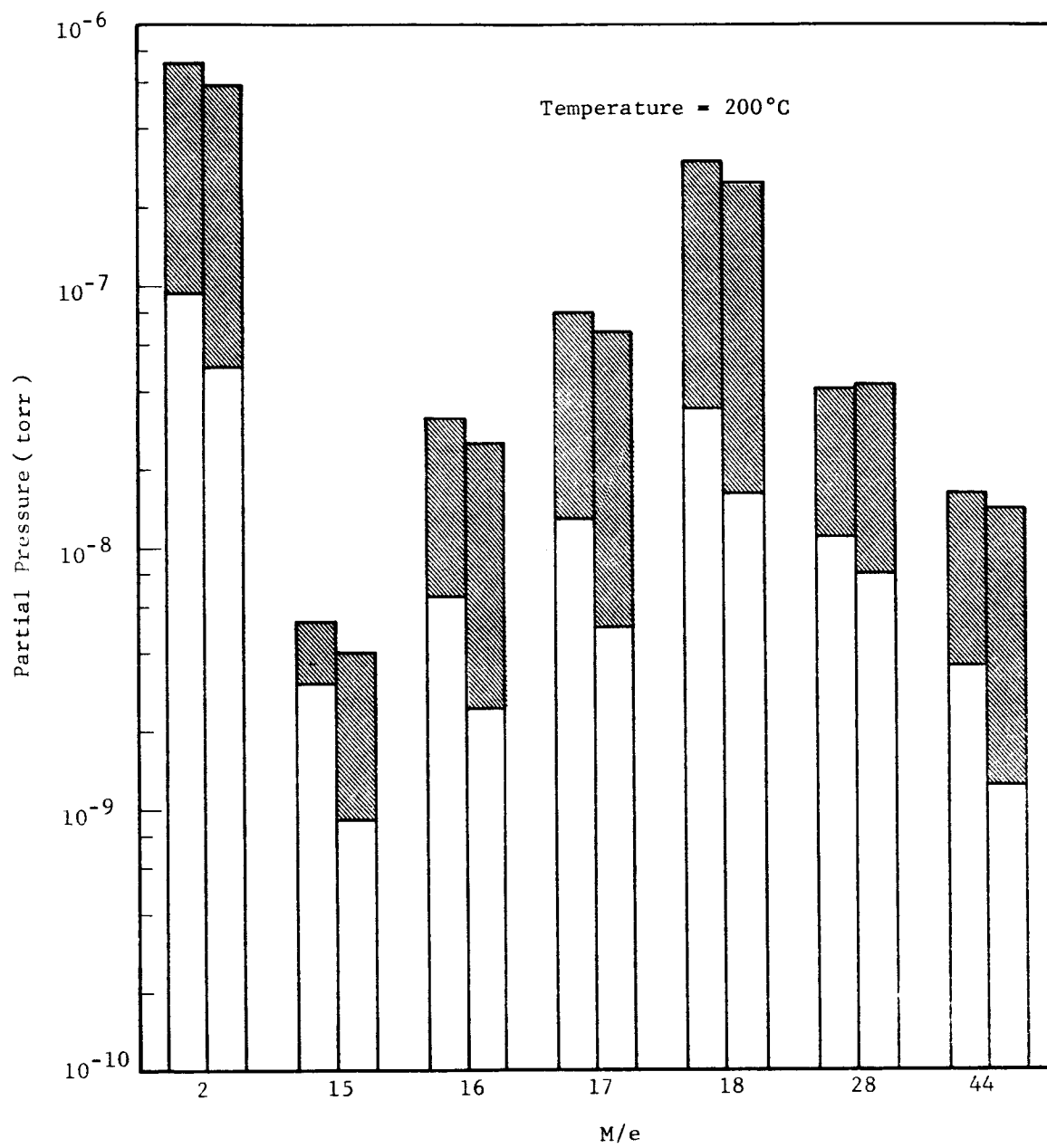


Fig. 40 DESORBED GAS SPECTRUM FOR QUARTZ POWDER

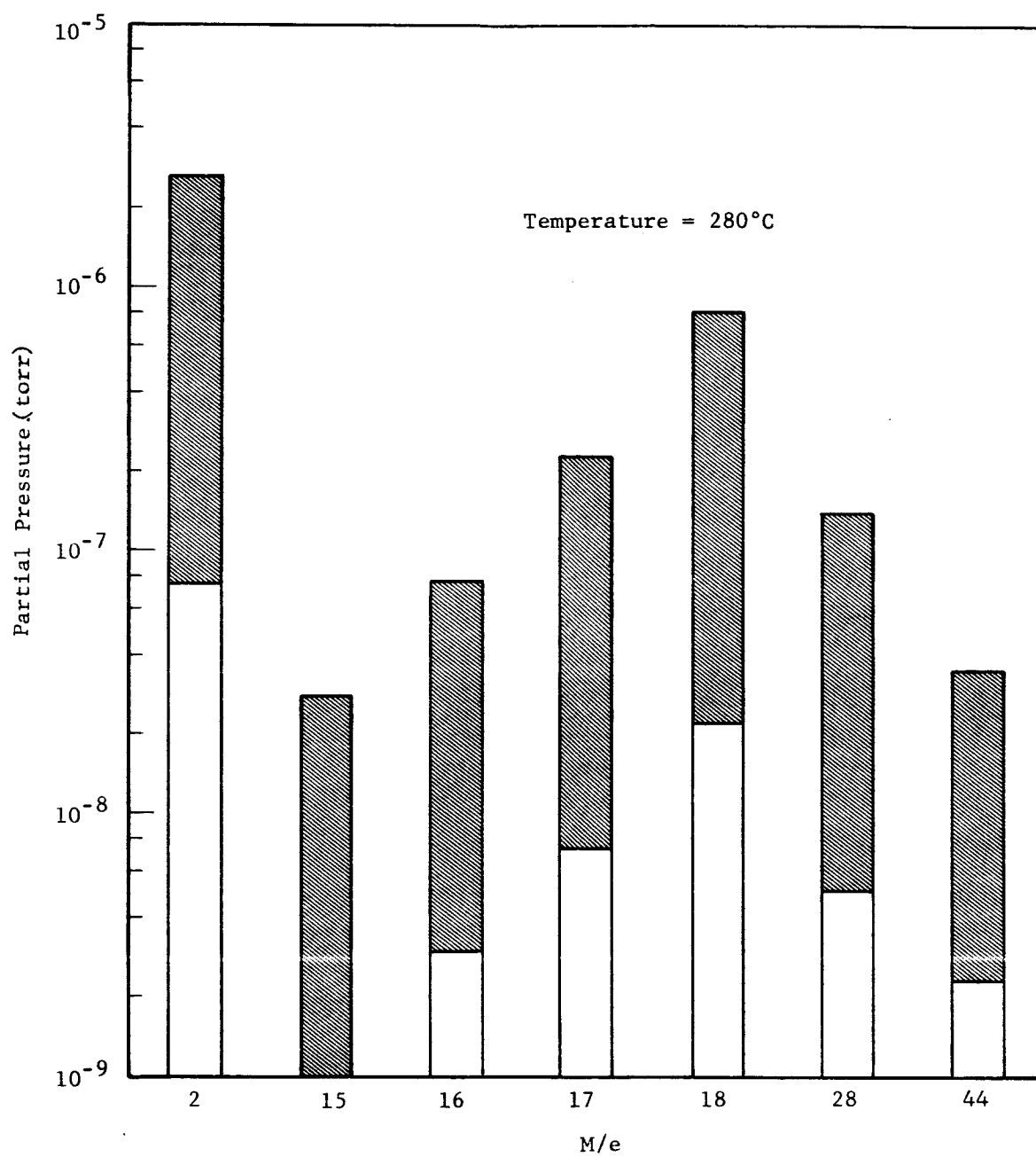


Fig. 41 DESORBED GAS SPECTRUM FOR QUARTZ POWDER

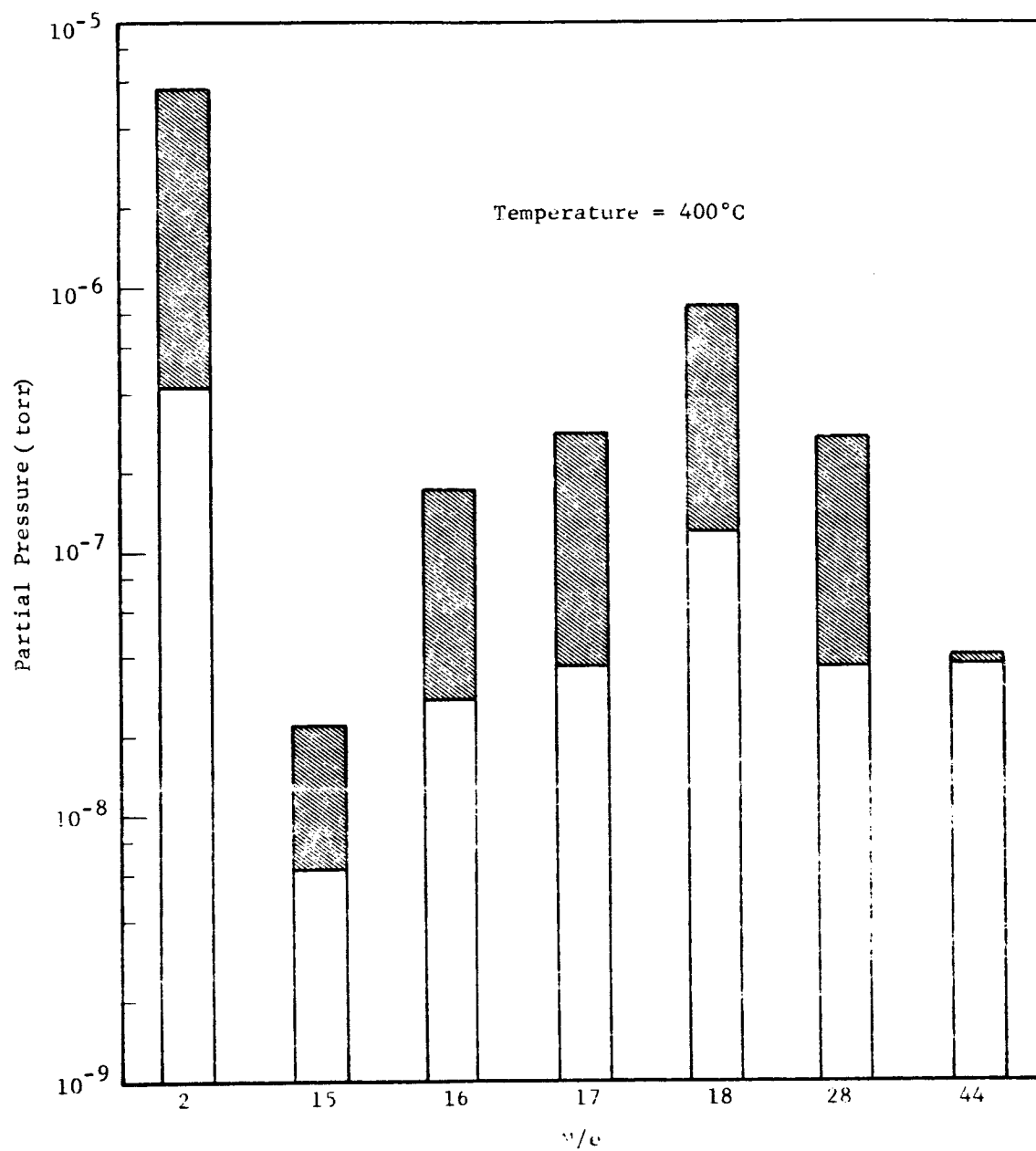


Fig. 42 DESORBED GAS SPECTRUM FOR QUARTZ POWDER

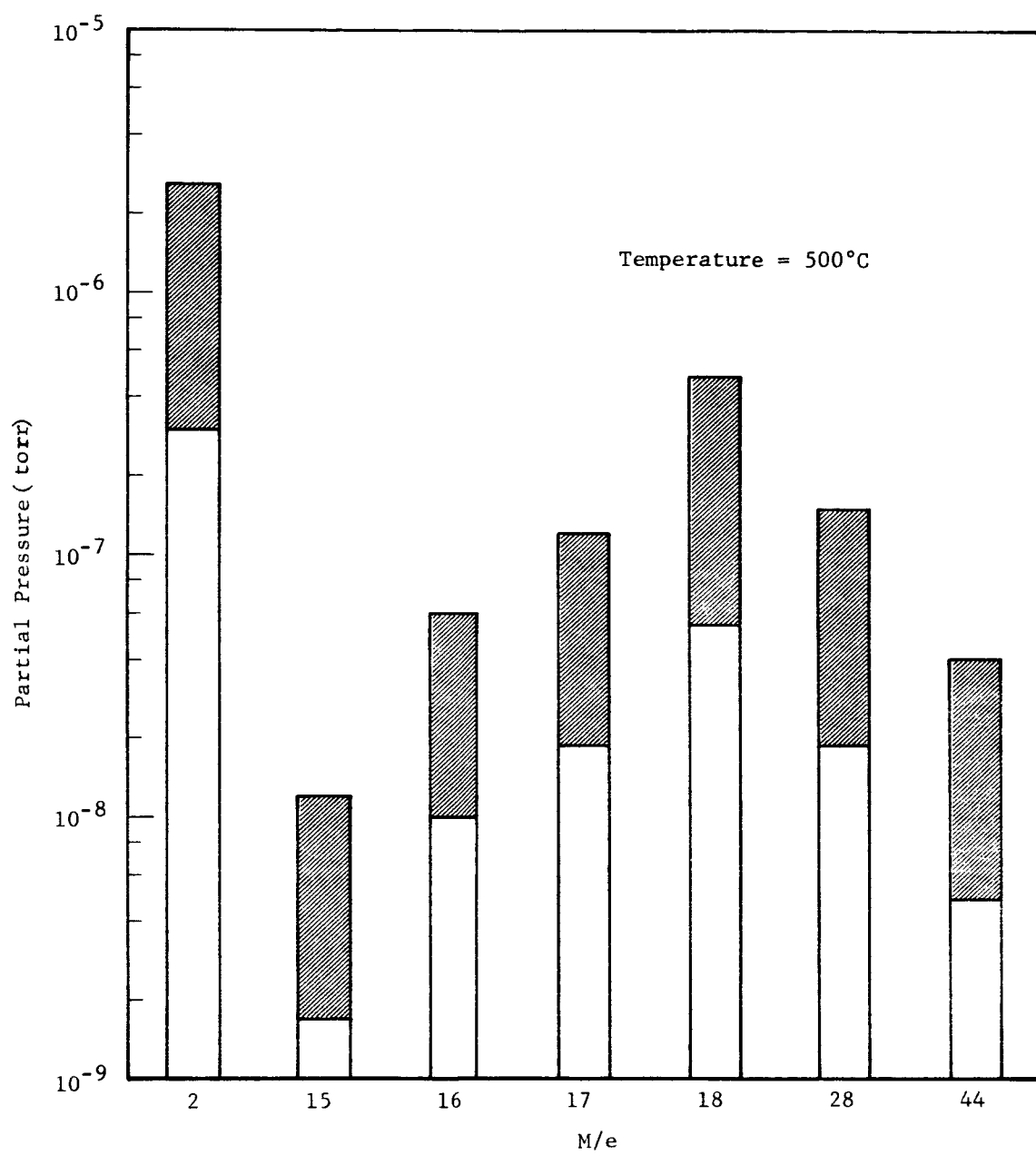


Fig. 43 DESORBED GAS SPECTRUM FOR QUARTZ POWDER

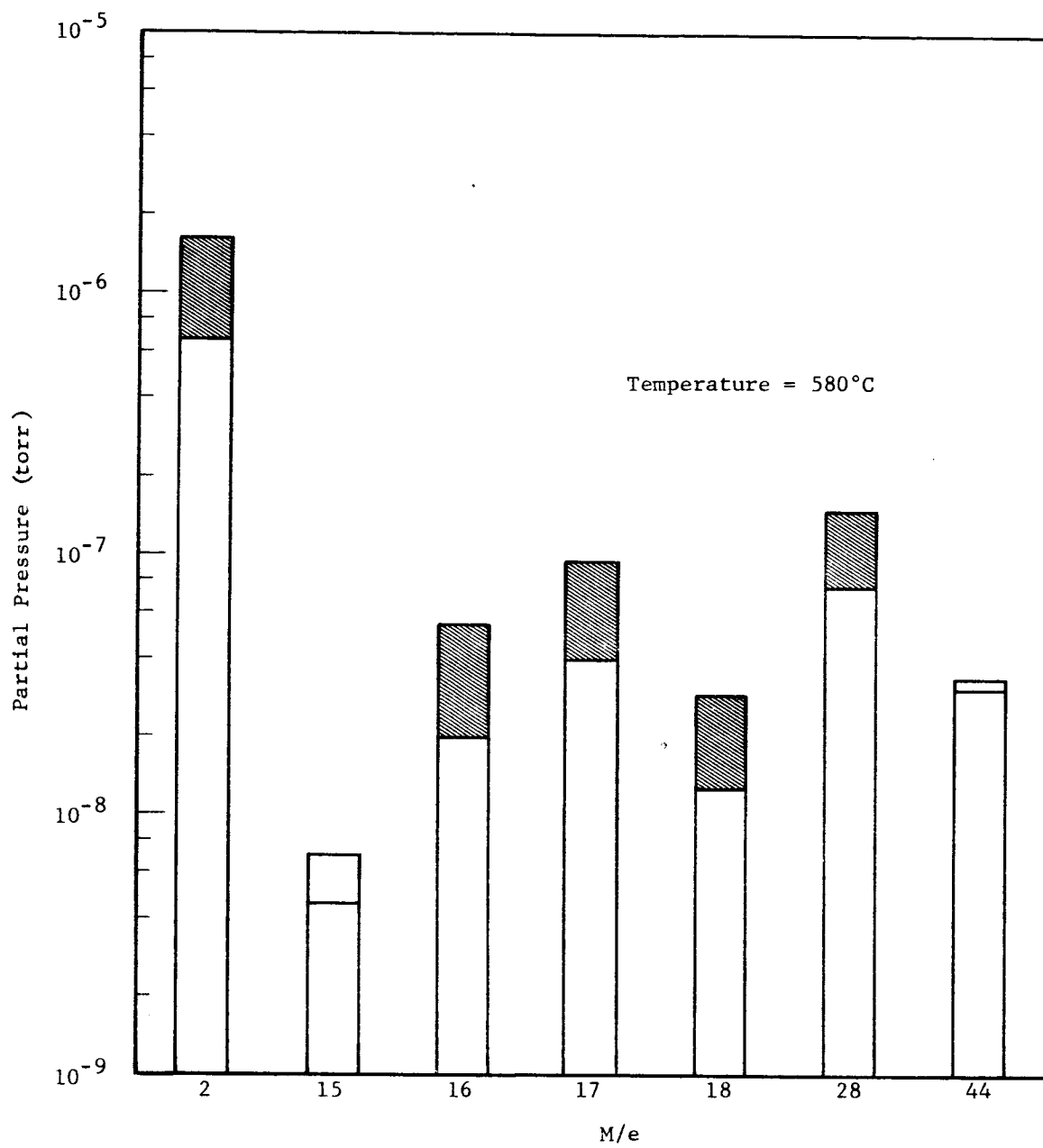


Fig. 44 DESORBED GAS SPECTRUM FOR QUARTZ POWDER

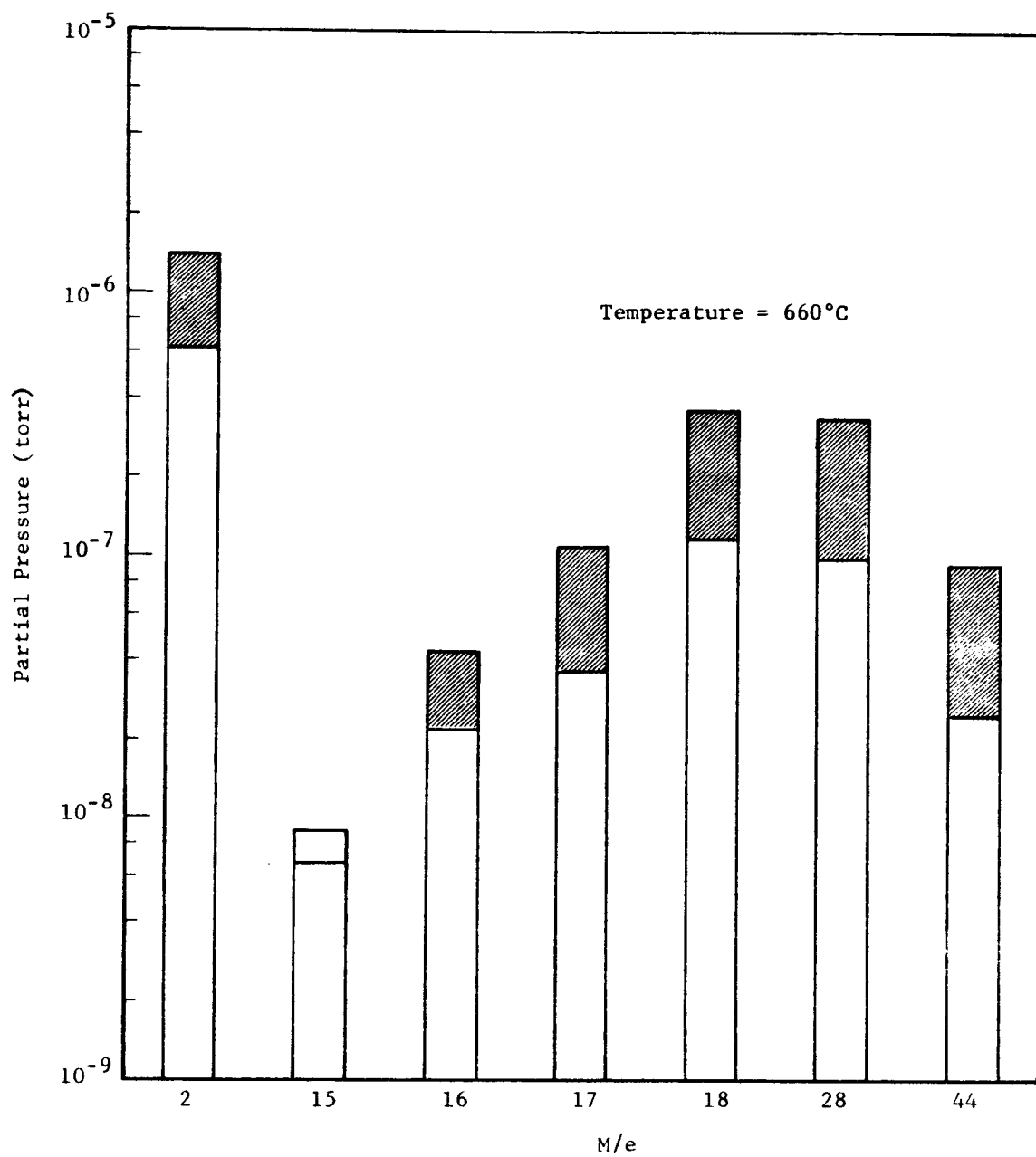


Fig. 45 DESORBED GAS SPECTRUM FOR QUARTZ POWDER

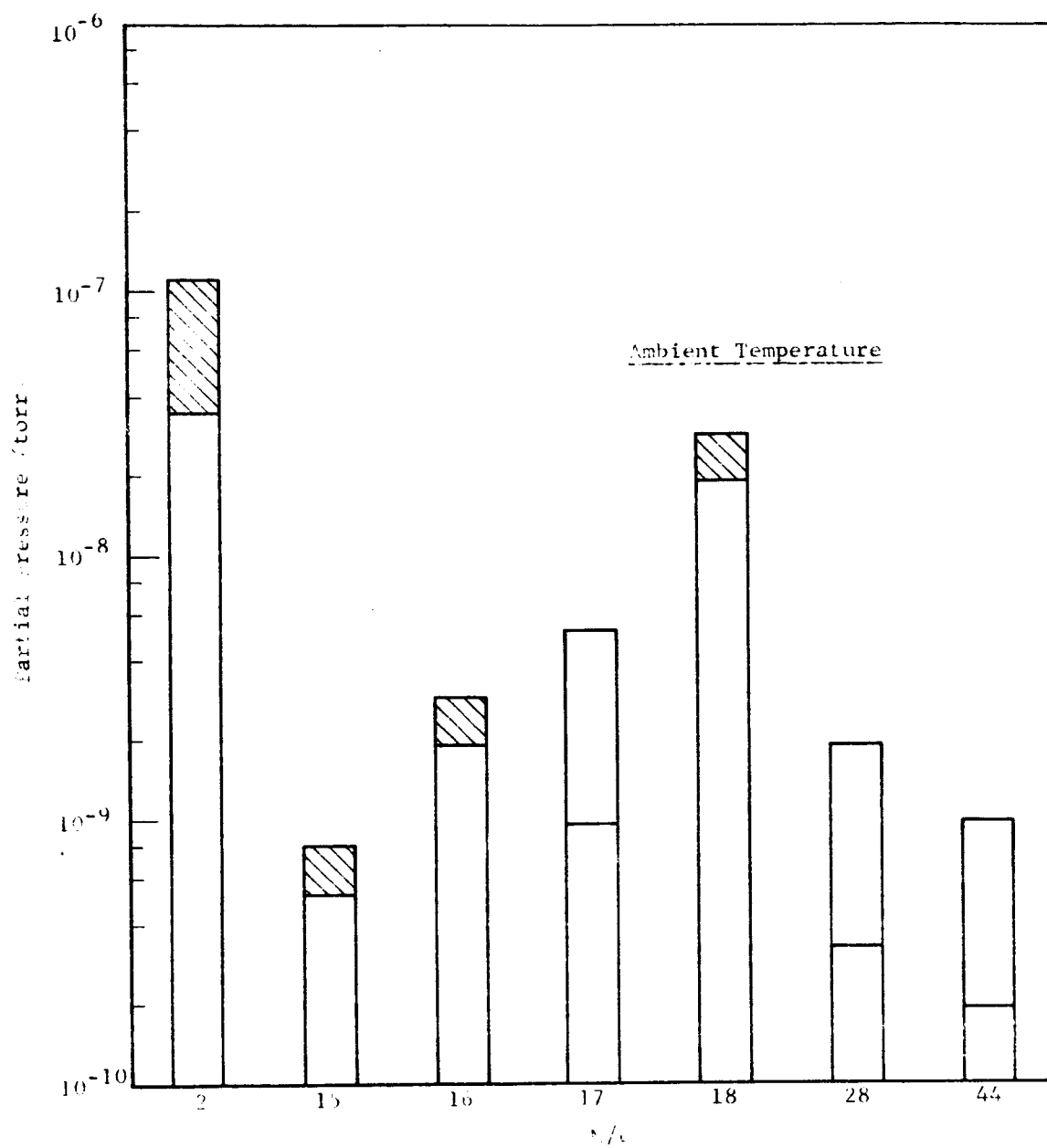


Fig. 46 DESORBED GAS SPECTRUM FOR OLIVINE POWDER

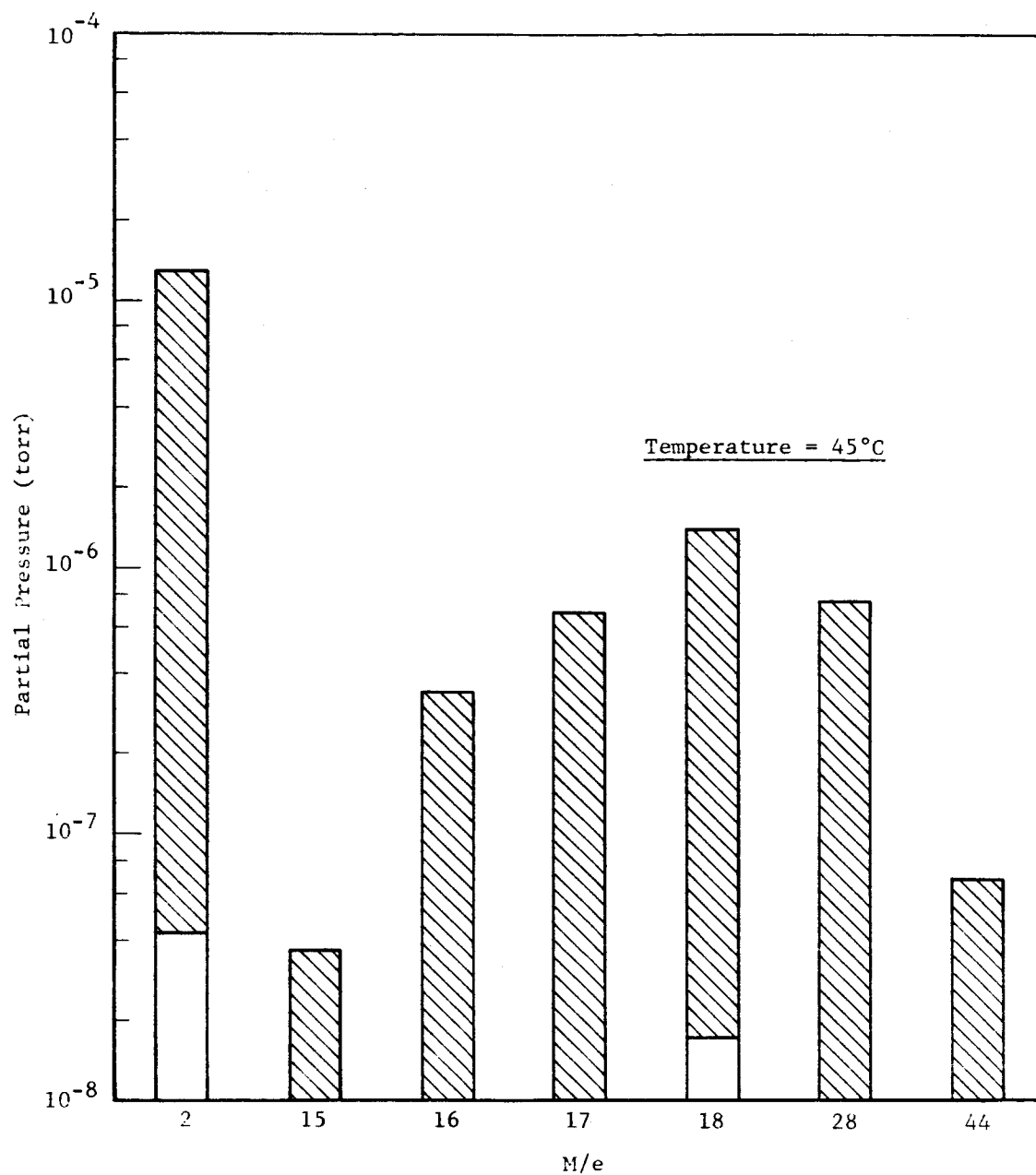


Fig. 47 DESORBED GAS SPECTRUM FOR OLIVINE POWDER

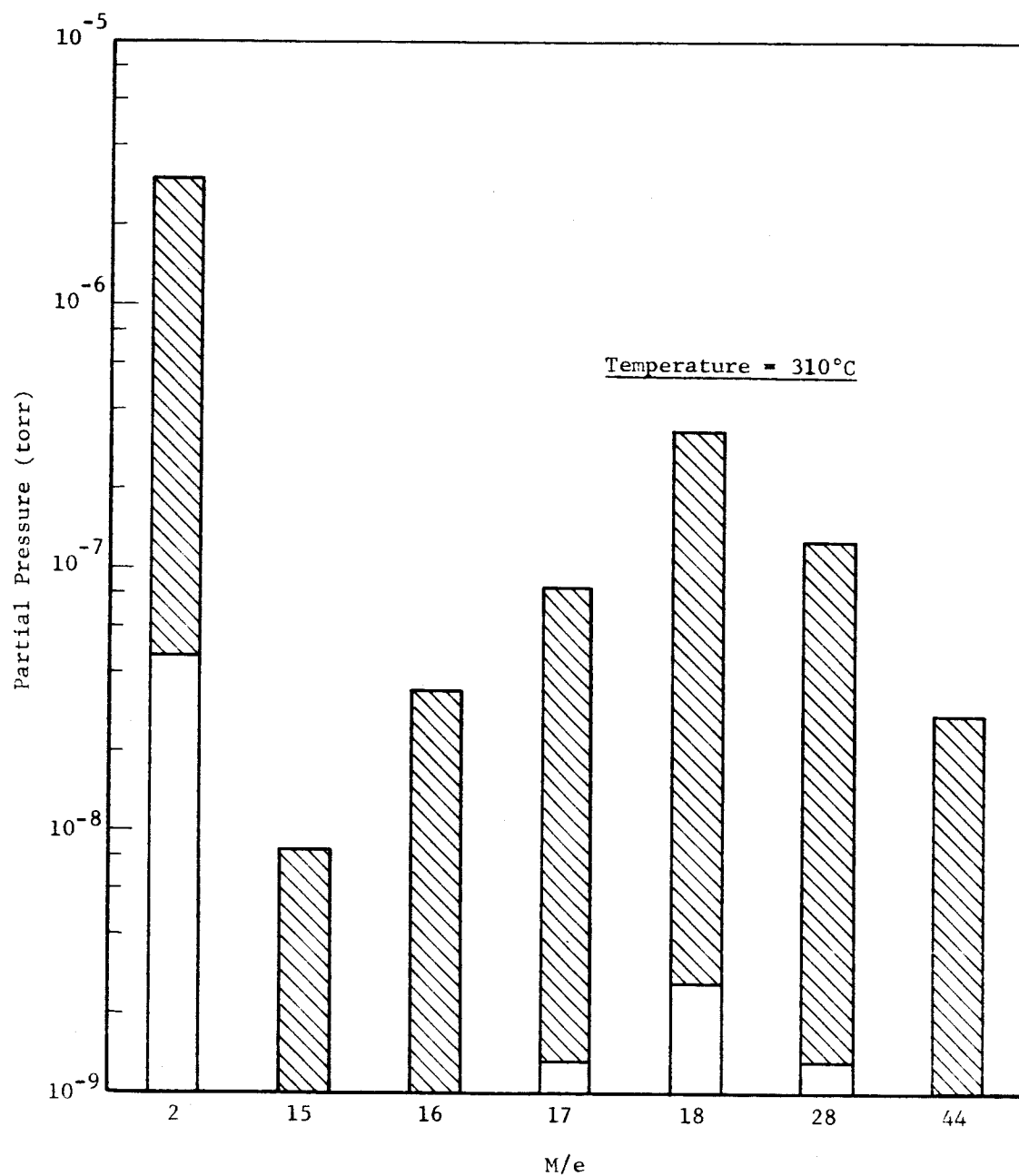


Fig. 48 DESORBED GAS SPECTRUM FOR OLIVINE POWDER

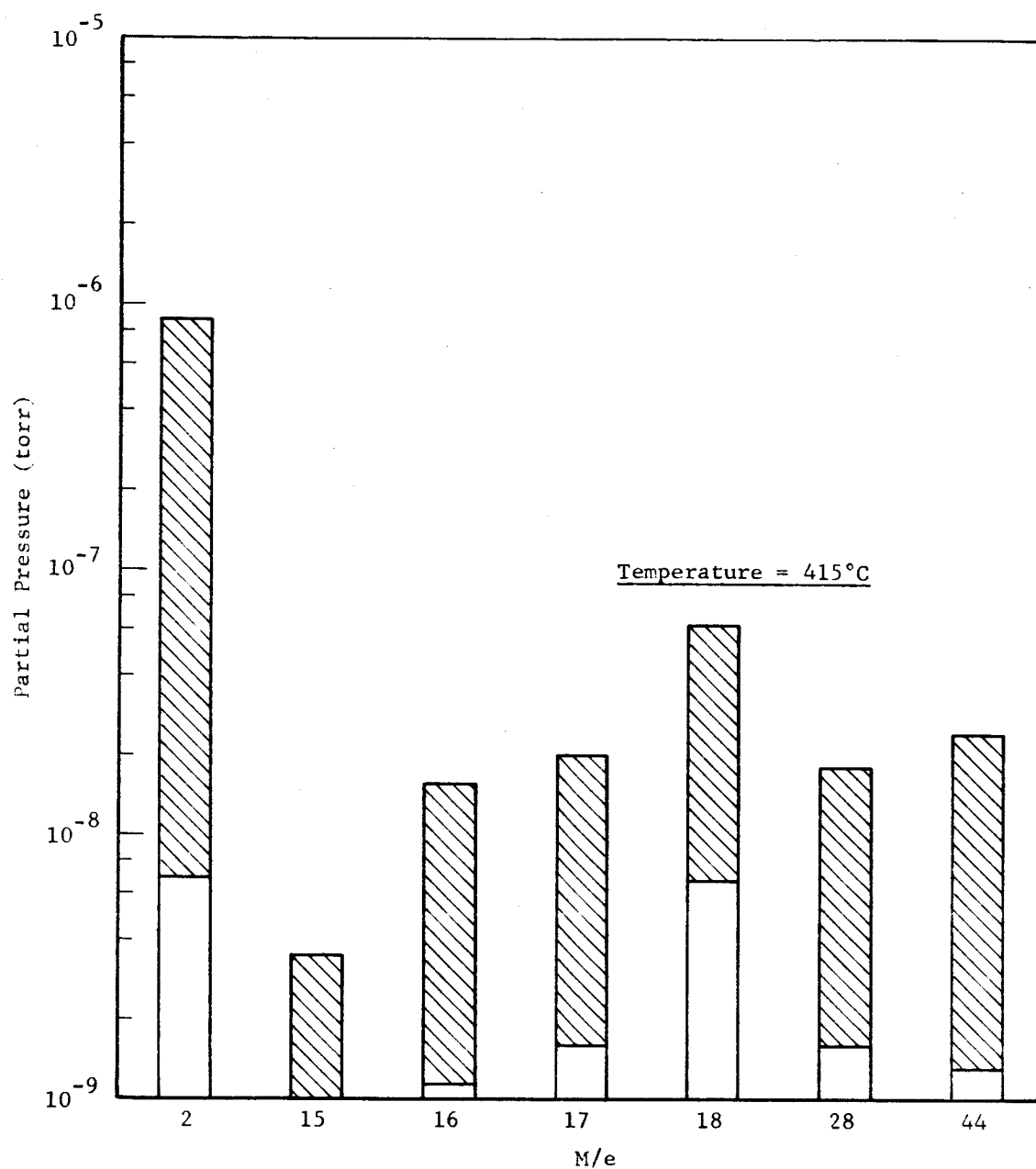


Fig. 49 DESORBED GAS SPECTRUM FOR OLIVINE POWDER

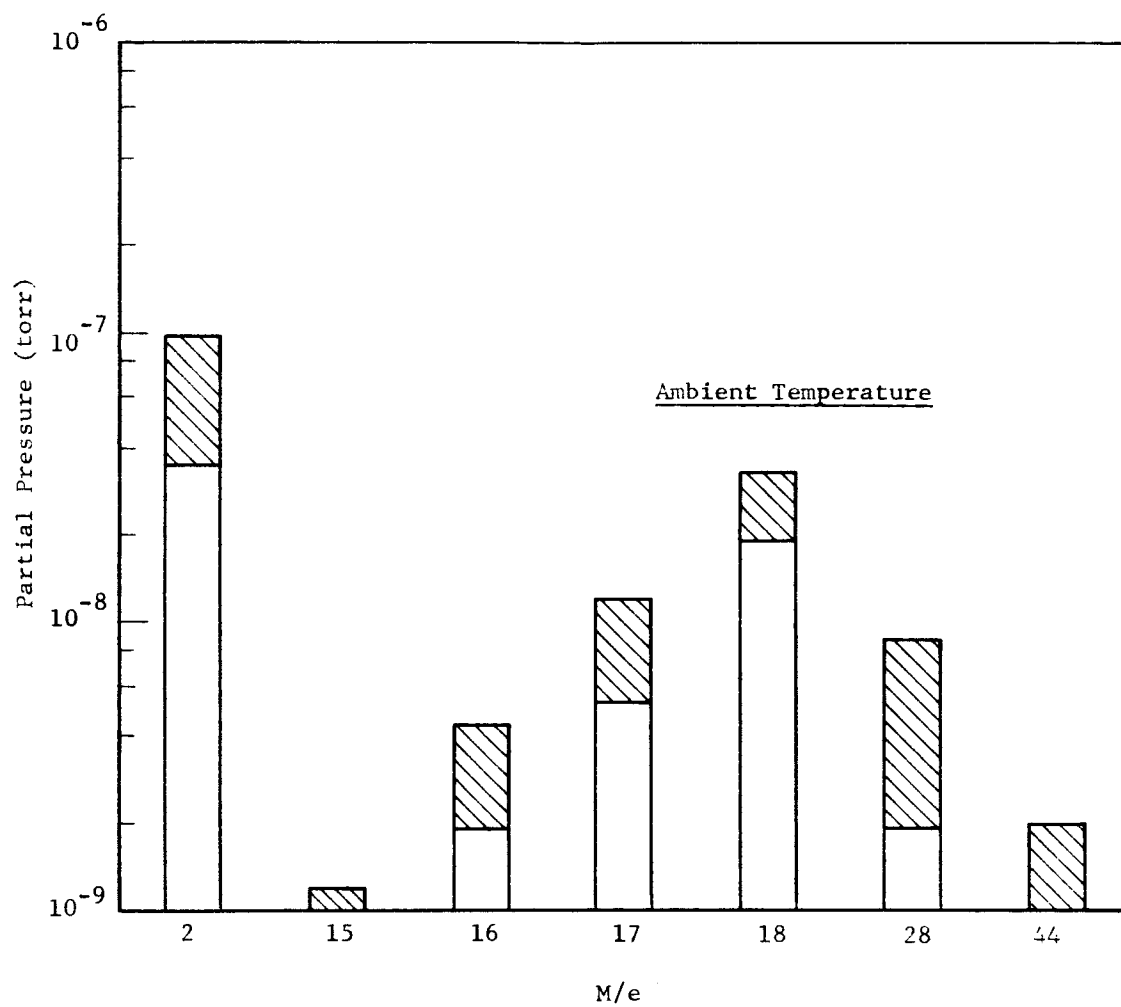


Fig. 50 DESORBED GAS SPECTRUM FOR OLIVINE A

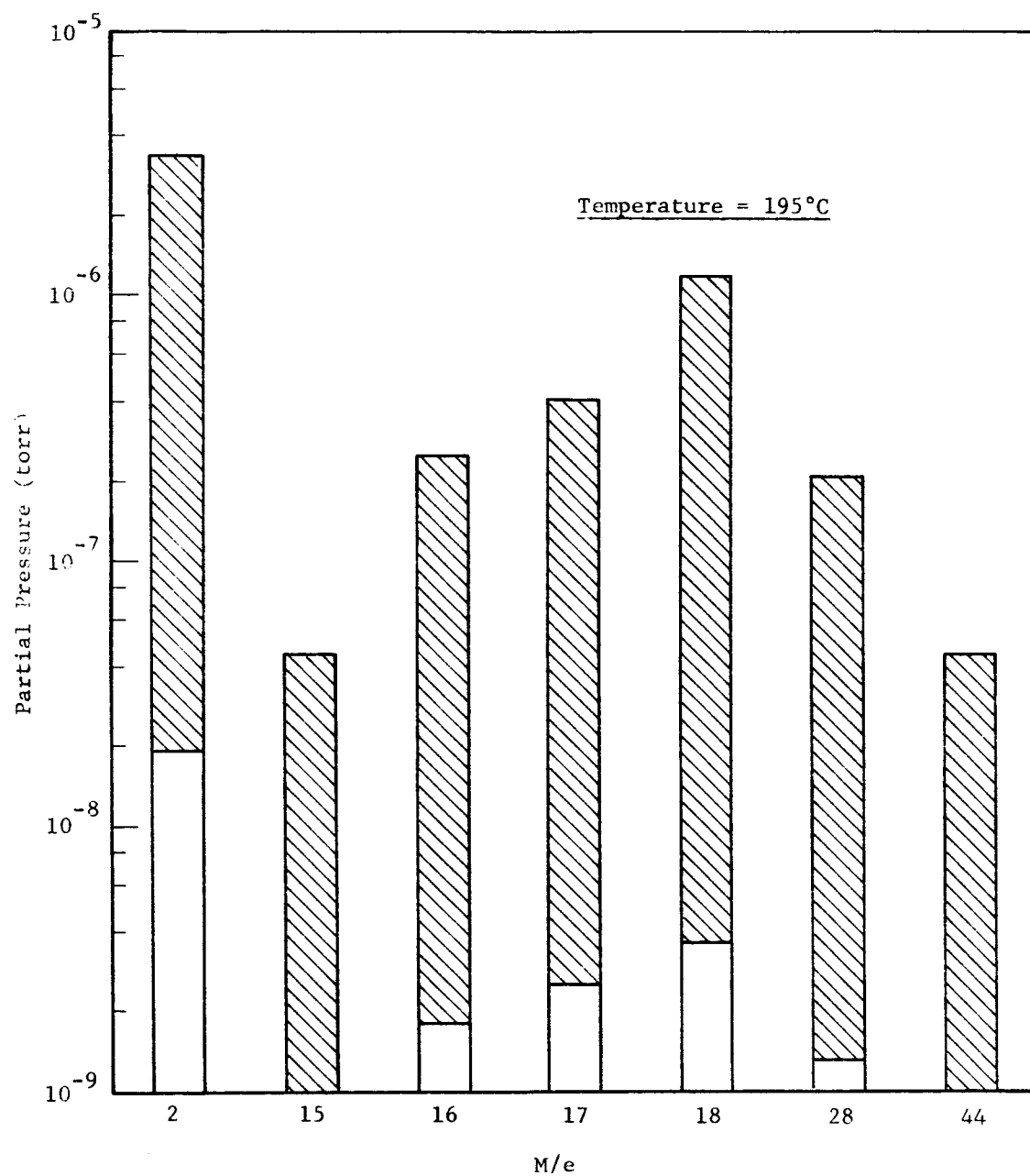


Fig. 51 DESORBED GAS SPECTRUM FOR OLIVINE A

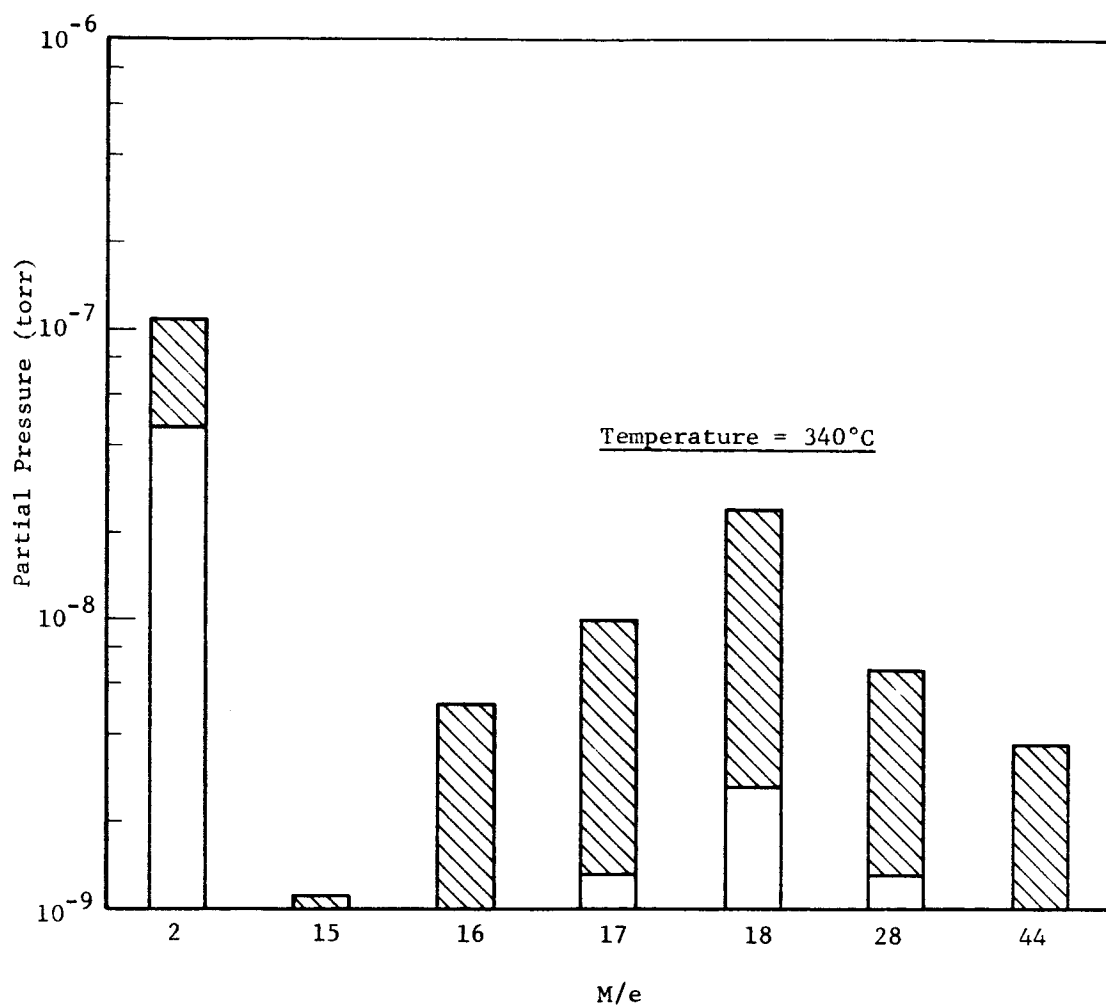


Fig. 52 DESORBED GAS SPECTRUM FOR OLIVINE A

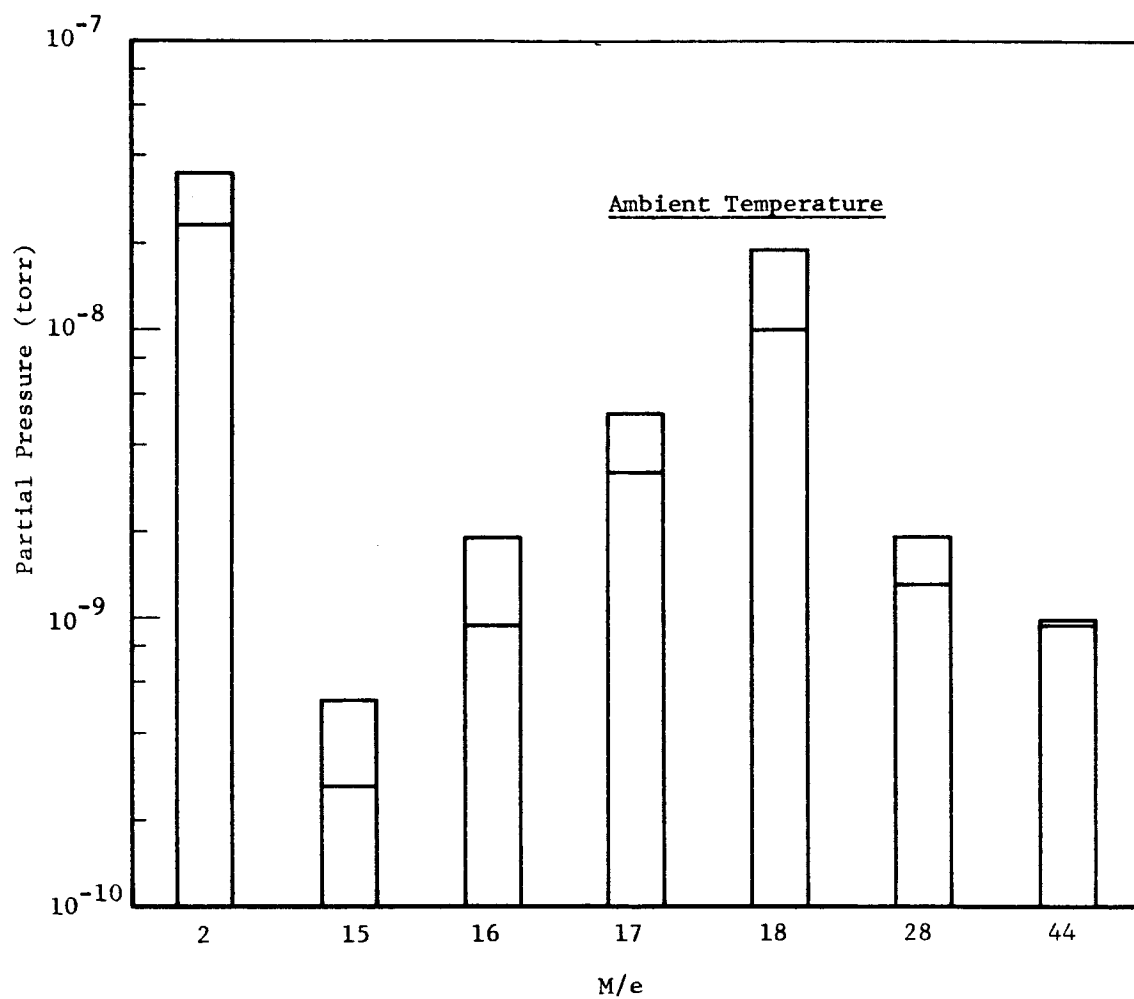


Fig. 53 DESORBED GAS SPECTRUM FOR OBSIDIAN POWDER

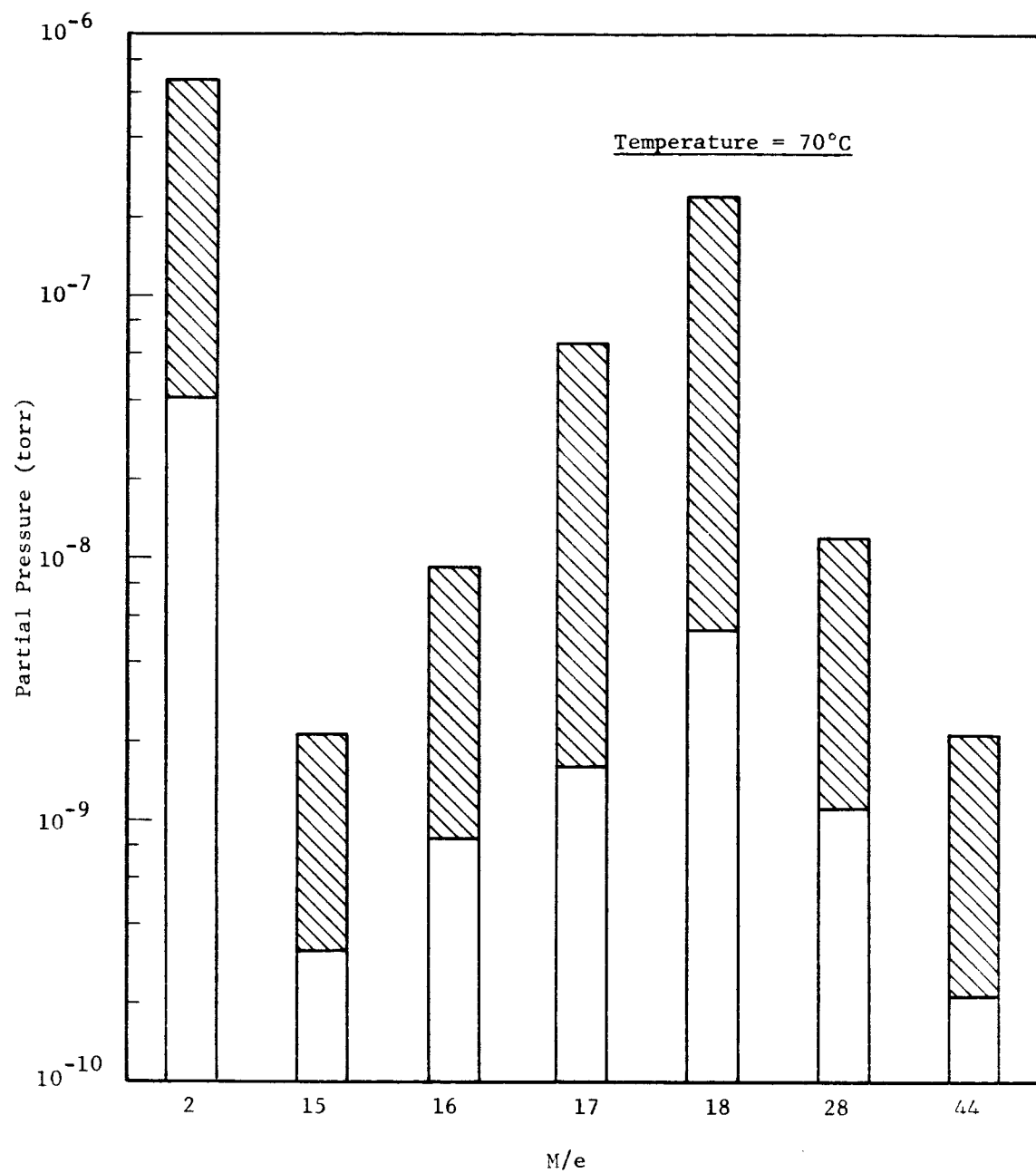


Fig. 54 DESORBED GAS SPECTRUM FOR OBSIDIAN POWDER

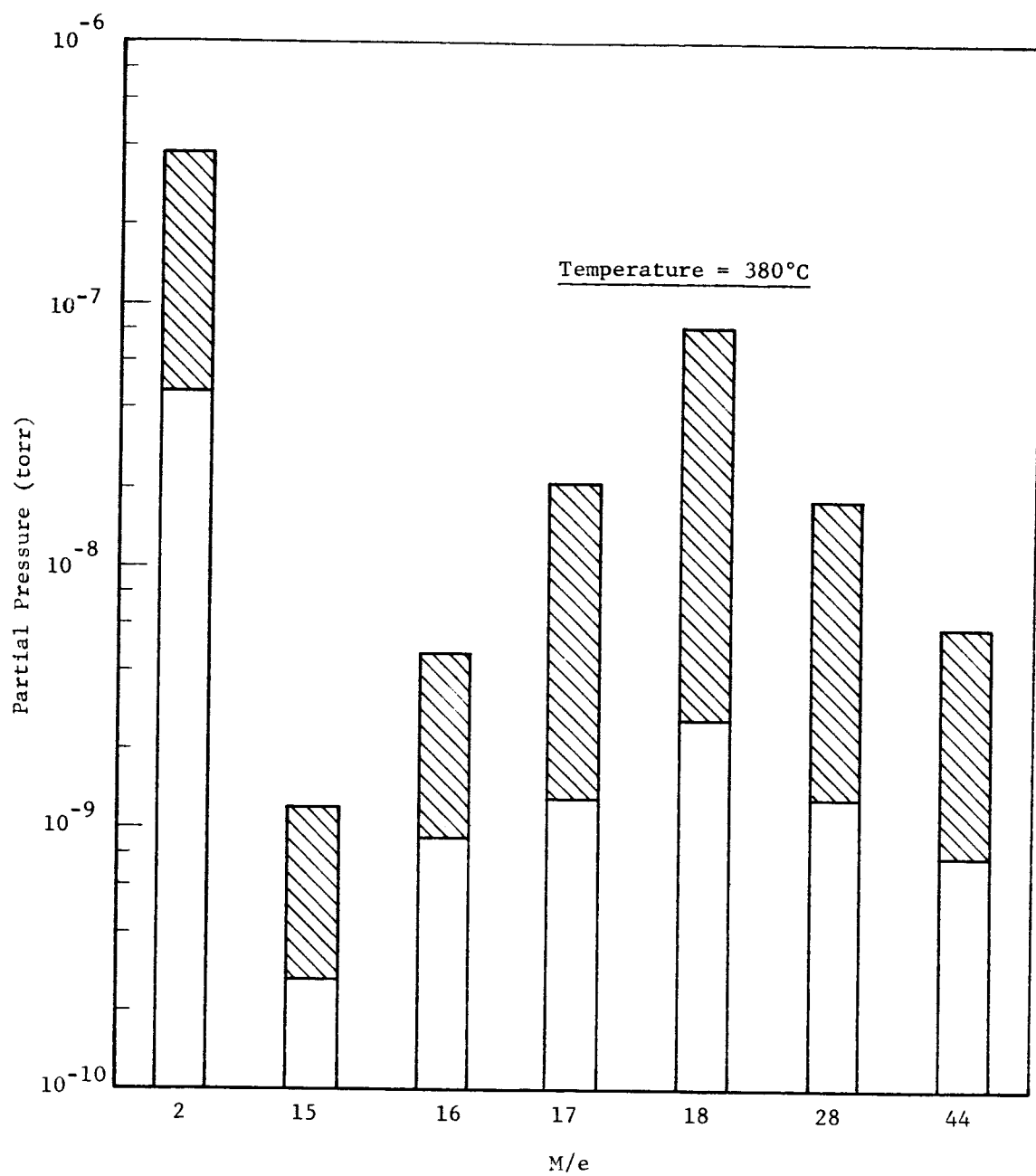


Fig. 55 DESORBED GAS SPECTRUM FOR OBSIDIAN POWDER

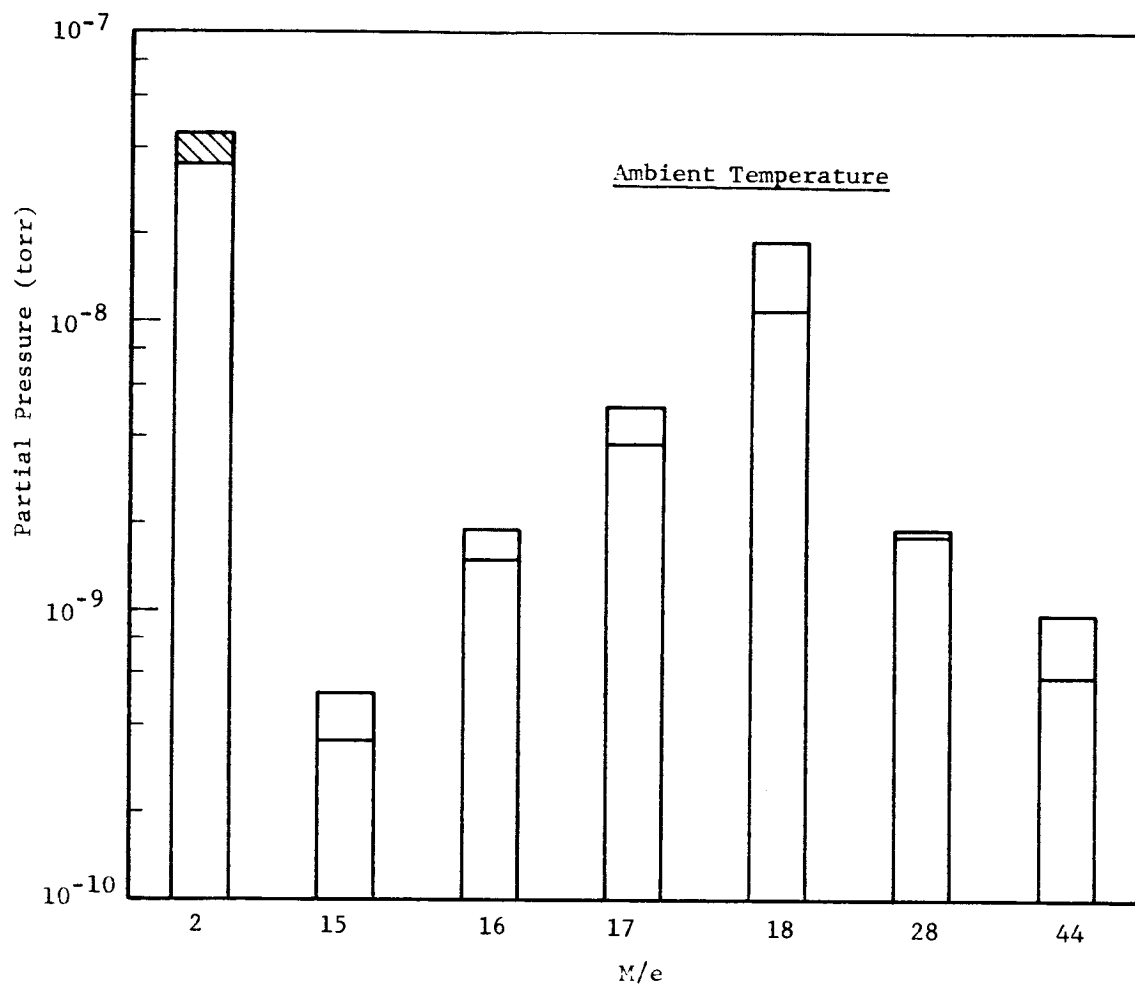


Fig. 56 DESORBED GAS SPECTRUM FOR ENSTATITE POWDER

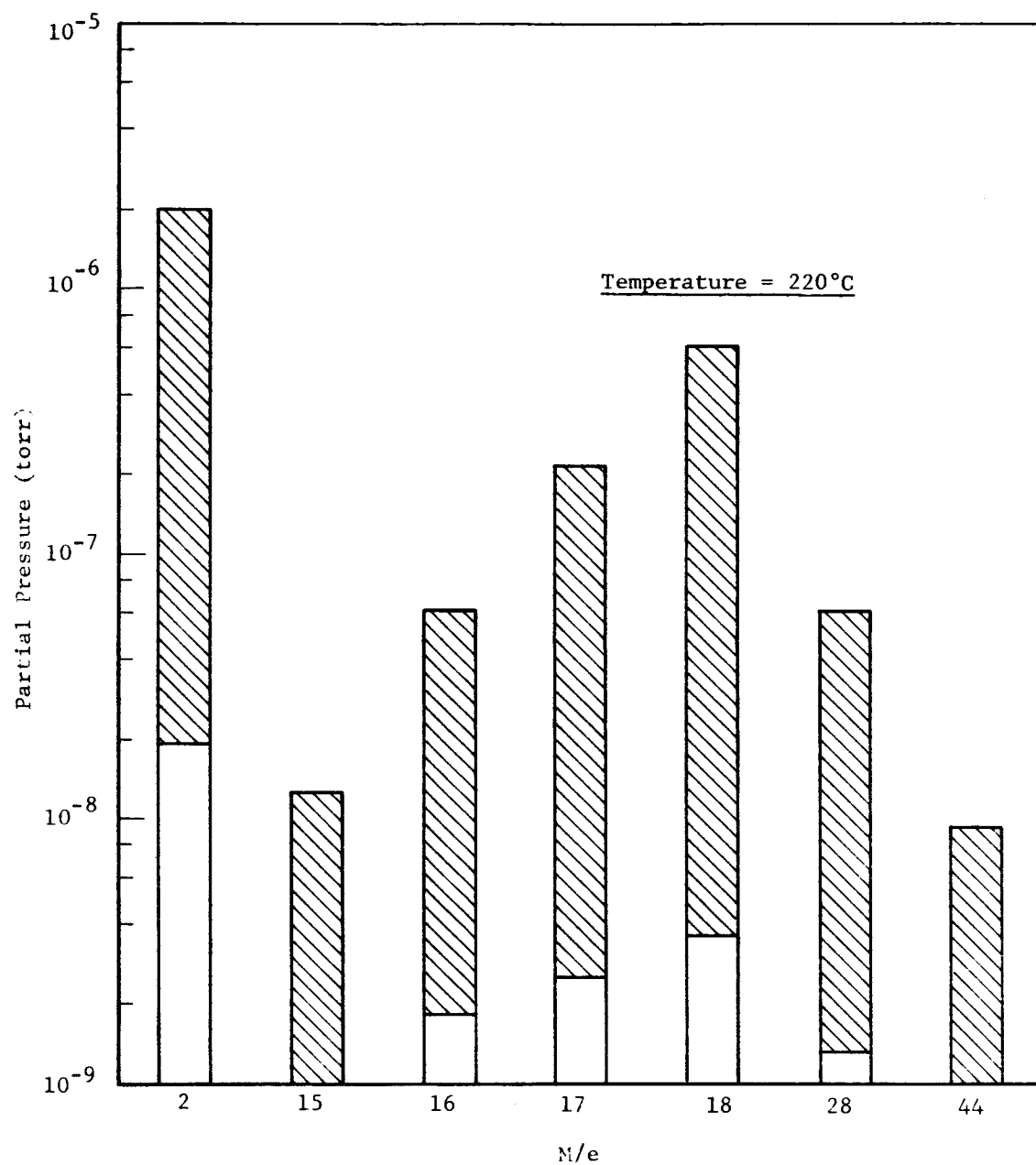


Fig. 57 DESORBED GAS SPECTRUM FOR ENSTATITE POWDER

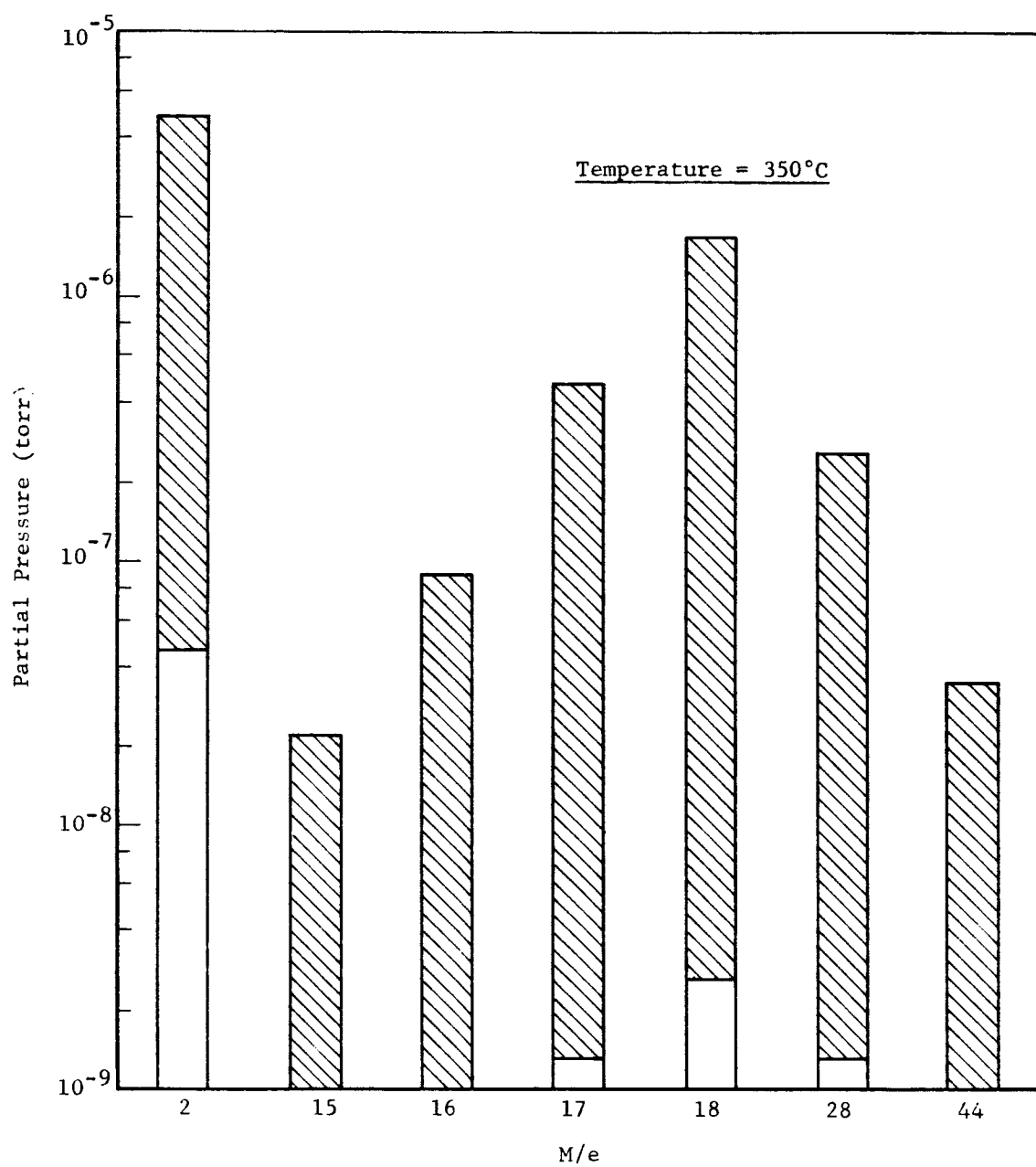


Fig. 58 DESORBED GAS SPECTRUM FOR ENSTATITE POWDER

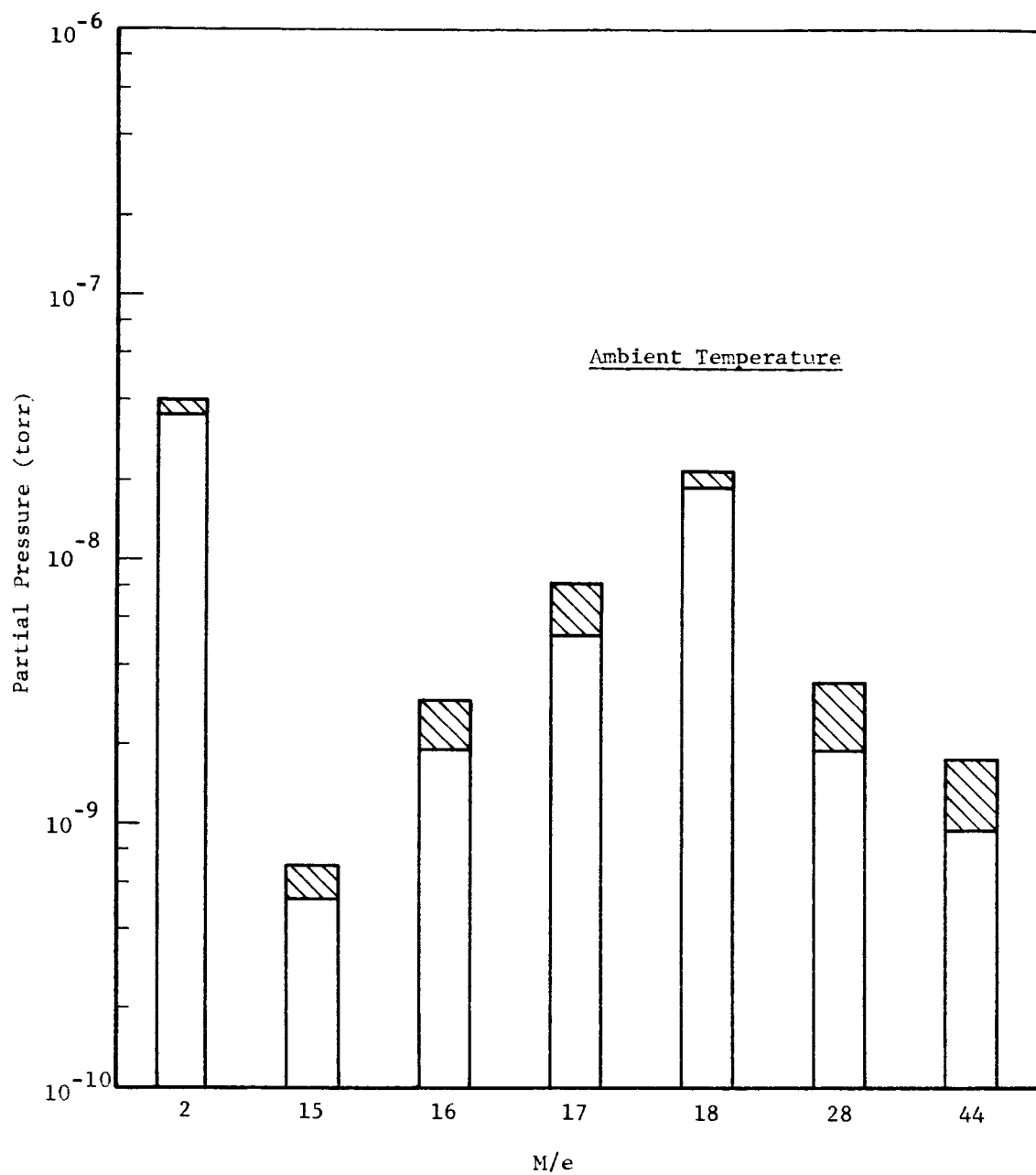


Fig. 59 DESORBED GAS SPECTRUM FOR ENSTATITE SAND

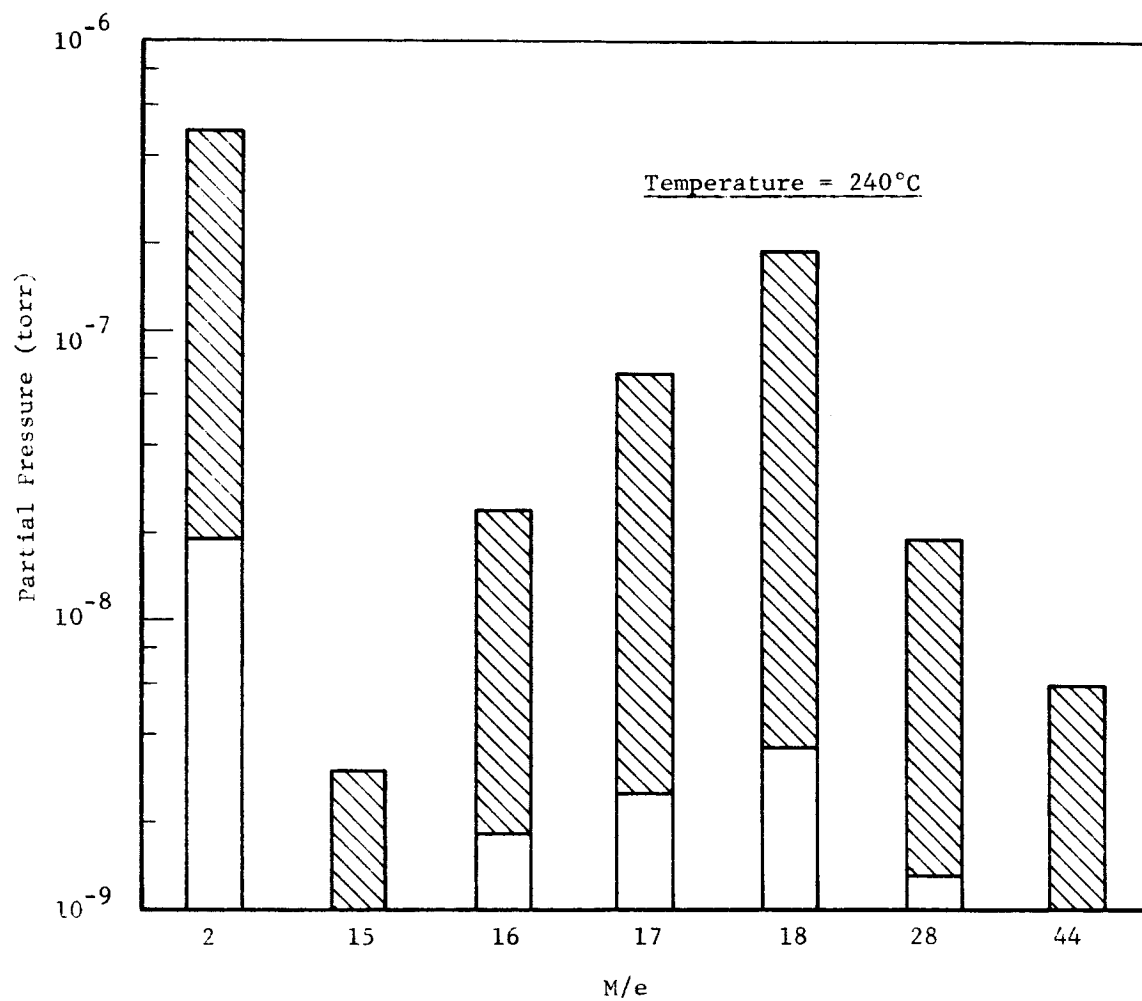


Fig. 60 DESORBED GAS SPECTRUM FOR ENSTATITE SAND

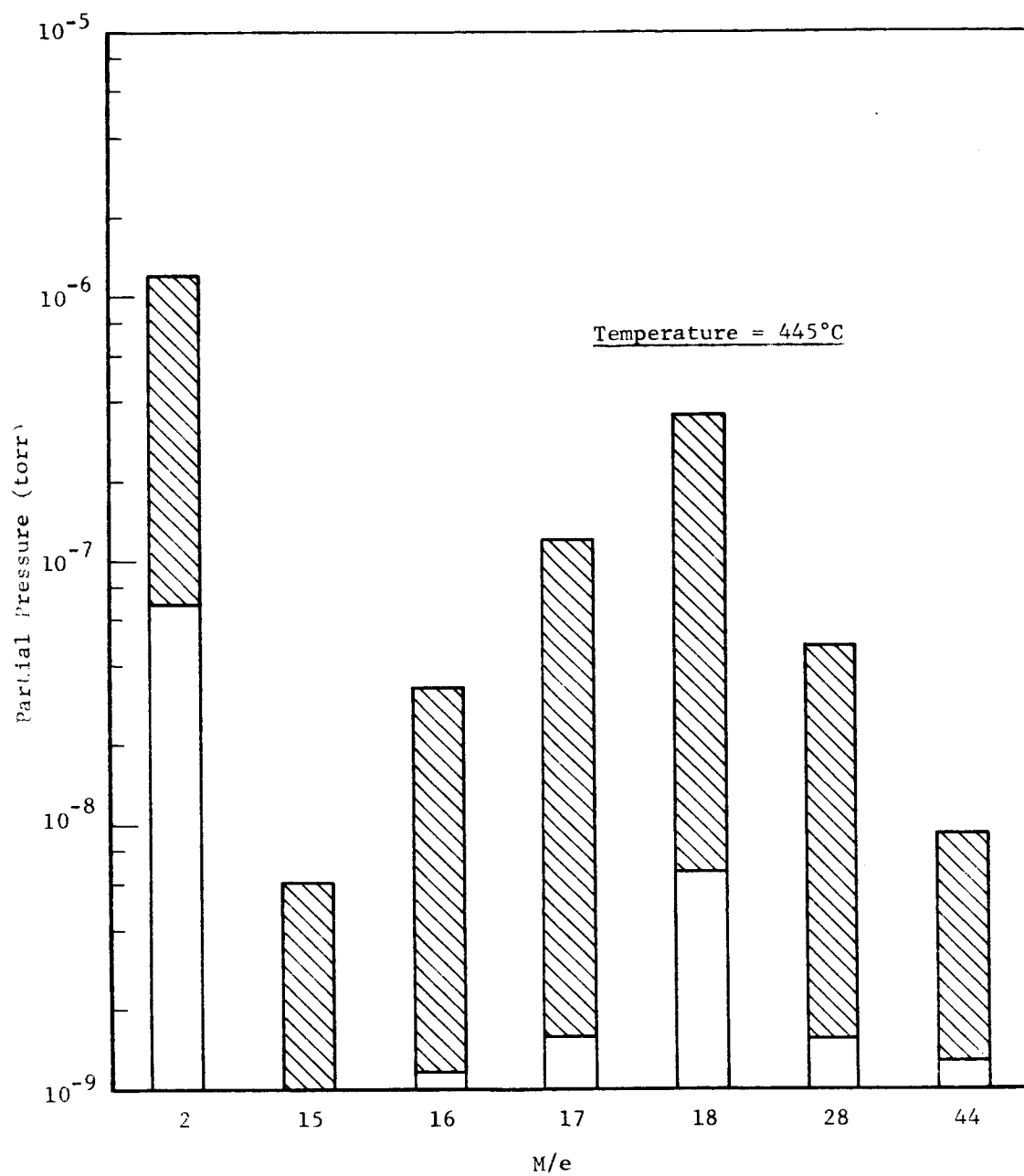


Fig. 61 DESORBED GAS SPECTRUM FOR ENSTATITE SAND

VI. GENERATION OF CLEAN PARTICLE SURFACES

In the previous section it was seen that the composition of the desorbed gas did not vary significantly enough with mineralogical composition to account for the magnitudes of the observed differences in vacuum effects. Consequently, the quantity of adsorbed gas on the different materials was investigated also as a possible explanation of the dependence of vacuum effects on mineralogical composition.

During the experiments to study the composition of the desorbed gas, the pressure was monitored as a function of time and from the differences in the pressure-time curves for both the empty system and the system containing soil the amount of gas desorbed from the soil mass could be determined. The pumpdown curve for the vacuum system both with and without quartz powder is shown in Fig. 62. At ambient temperatures both curves followed essentially the same path indicating very little desorption from the soil. When the temperature was increased the pressure in the empty system rose and then decreased sharply. With soil in the system the pressure decreased much less after the initial increase and leveled off at a higher pressure.

At temperatures of 400°C or higher the pressure began to drop more rapidly and decreased at approximately the same rate as in the empty system. This would indicate that the maximum rate of desorption had been reached and the major part of the adsorbed gas had been removed. Also, as can be seen the two curves tend to converge, indicating that the amount of gas removed at the highest temperatures was quite small and was undoubtedly the more tightly bound gas closest to the particle surface.

In another experiment the sample was allowed to cool in ultra-high vacuum after the initial heating and was then heated again in approximately the same increments as the first time. The pumpdown curves for the first and second heating periods of this experiment are shown in Fig. 63. The difference

IIT RESEARCH INSTITUTE

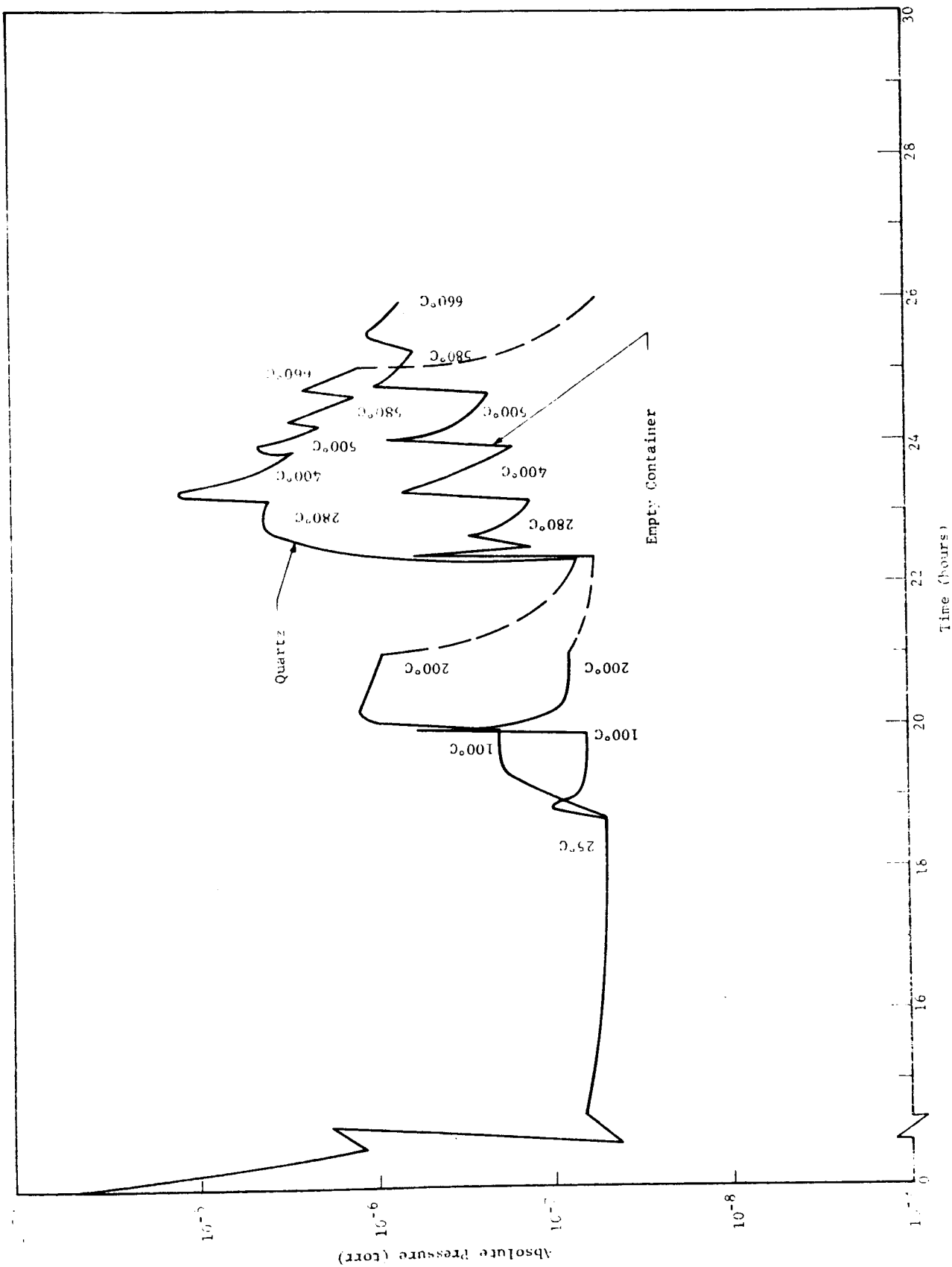


Fig. 62 PUMPDOWN CURVE FOR QUARTZ POWDER

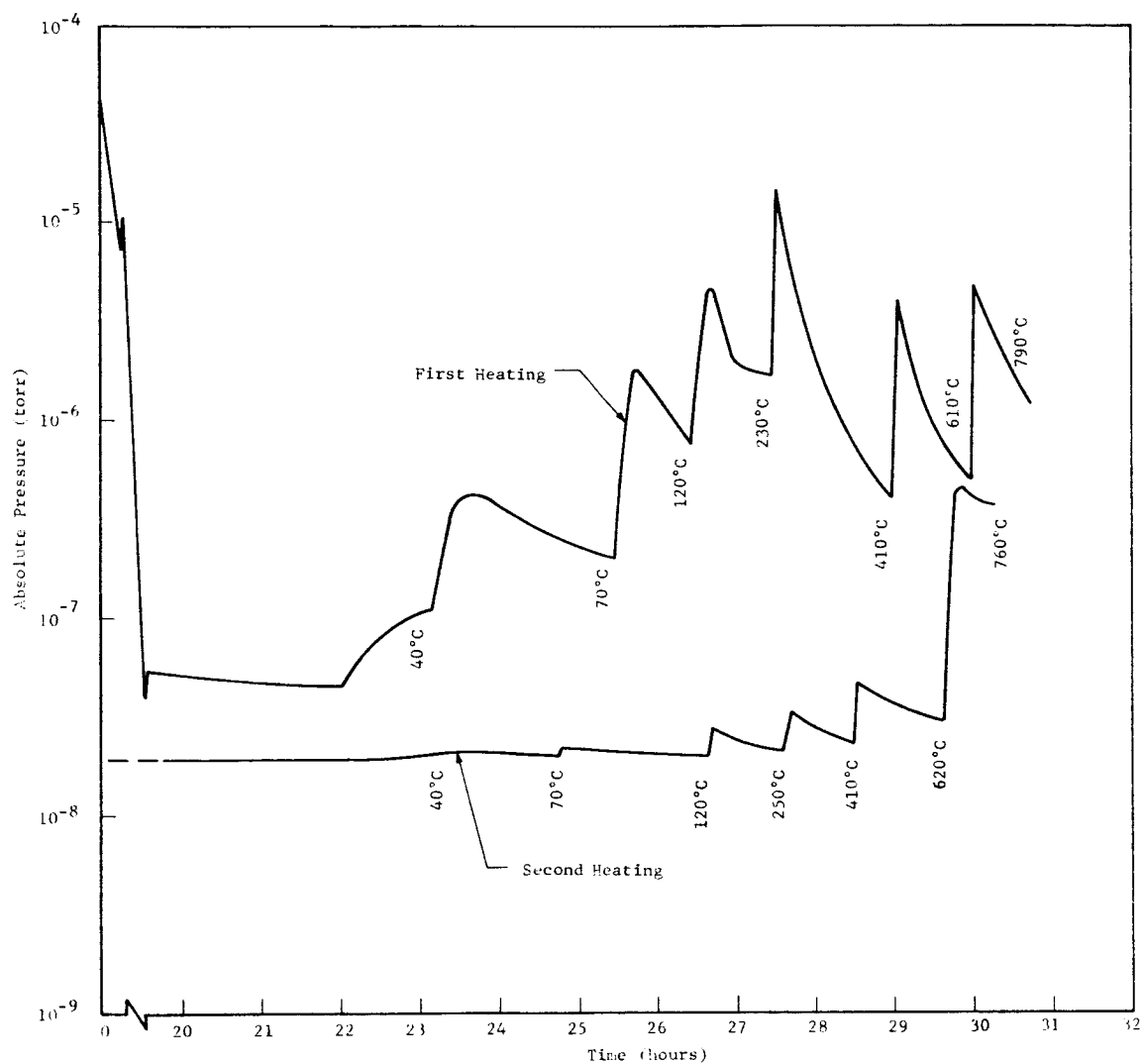


Fig. 63 PUMPDOWN CURVE FOR QUARTZ POWDER

between the two curves represents the amount of gas that was desorbed but not readsorbed during the cooling period. While the curve for the second heating is actually an extension of that for the first heating it has been transposed for purposes of comparison. It can be seen that very little gas was readsorbed and since it is known that even at vacuum levels of 10^{-8} torr a sufficient amount of gas is present to form a monolayer in minutes, it would appear that the sticking coefficient was quite low and the gas remaining on the particle was in equilibrium with the surrounding environment. Thus, if a soil sample is baked out in vacuum and allowed to cool the cleanliness of the soil would be relatively unaffected by readsorption during the cooling period.

In most experiments in this program oven dried soil was used whenever possible. However, in some cases, the preparation time was such that it was necessary to use air dried soil and, hence, desorption experiments were performed to investigate the influence this would have on the degassing history. The pump-down curves for similar experiments using air dry and oven dry soil are shown in Fig. 64. The difference between the two curves is quite small and within the reproducibility of the pumpdown curves of the system. Thus, it is evident that the bakeout in atmosphere which removed only the hygroscopic moisture had little effect on the total quantity of gas which was removed. Also, it indicates that the initial part of the pump-down period removed a very large portion of the hygroscopic moisture.

In order to make more specific comparisons between different experimental conditions and different materials it is desirable to compute actual quantities of desorbed gas from the pumpdown curves. In order to derive an expression for this quantity a system with a chamber volume, V , and a characteristic pressure, P_0 , as a function of time during pump-down will be considered. The pumping speed will be denoted by

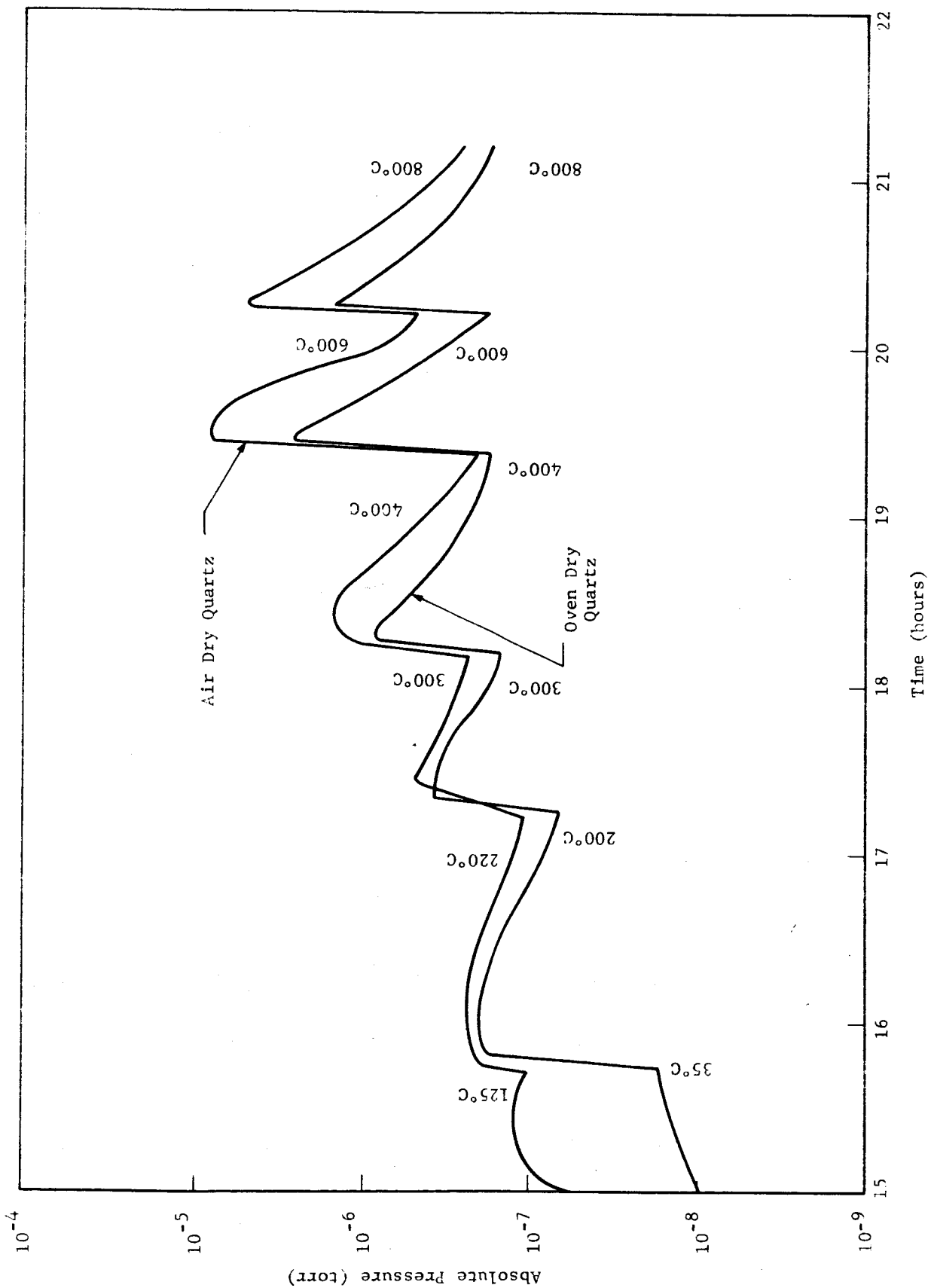


Fig. 64 PUMPDOWN CURVES FOR OVEN DRY AND AIR DRY QUARTZ

S which in the general case is a function of the pressure at the pump.

First, one may consider an empty system after pumping has continued for a sufficient amount of time such that its pressure, P_o , is at the ultimate attainable vacuum level. If it is assumed that the pressure is uniform throughout the system the total amount of gas entering the system by virtual leaks, desorption from chamber walls, back diffusion of gas molecules from the pump, etc. would be equal to that which the pump removes (i.e. steady state). Denoting the rate of flow of incoming gas by Q_i , then

$$Q_i = P_o S_o \quad (3)$$

where S_o is the pumping speed at the pressure P_o . This term Q is commonly termed throughput in the field of vacuum technology.

For the system containing soil, the amount of gas entering the system will be greater than Q_i by an amount Q_s which may vary with time depending on the temperature conditions and amount of gas still adsorbed. Thus, in some time period from t_1 to $t_1 + \Delta t$ the pressure changes from P_1 to $P_1 + \Delta P$ and the mass of gas which is stored in the chamber changes by the amount

$$\Delta m = \Delta P \frac{V}{RT} \quad (4)$$

where

Δm is the change in mass
 R is the universal gas constant
 T is the absolute temperature.

Considering continuity of the system

$$(Q_i + Q_s) \frac{\Delta t}{RT} = \frac{PS\Delta t}{RT} + \Delta P \frac{V}{RT} \quad (5)$$

where $P = P_1 + \alpha \Delta P$, $0 < \alpha < 1$.

Solving for Q_s and taking the limit as Δt approaches zero,

$$\dot{Q}_s = PS - P_o S_o + \frac{\partial P}{\partial t} V. \quad (6)$$

It should be noted that if the constituents of the gas desorbed from the soil are not the same as those of the residual gas in the empty system, different values of R must be used for the different terms in Eq. (5). However, the results of the previously discussed experiments have shown that for the soils being considered, the compositions of both the desorbed and residual gases are nearly the same. Similarly, if the temperature of the desorbed gas is different than that of the residual gas different values of T must be used. However, it will be assumed that within a very short period of time after leaving the soil container the desorbed molecules experience a sufficient number of collisions with the chamber walls and other gas molecules to reduce their thermal energy to that of the residual gas.

In arriving at Eq. (6), it was assumed that P_o did not vary with time which may or may not be true depending on the experimental conditions. However, if P_o changes by an amount ΔP_o during the increment of time Δt , the change in mass as given in Eq. (4) represents two contributions; one from the soil and one from a change in Q_i . Considering the continuity of the empty system the average change in Q_i during Δt is found to be

$$\Delta Q_i = \frac{\Delta P_o}{\Delta t} V. \quad (7)$$

If this term is added to Q_i in Eq. (5), solving for Q_s and taking the limit as Δt approaches zero yields,

$$Q_s = PS - P_o S_o + \frac{\partial}{\partial t} (P - P_o) V. \quad (8)$$

Equation (8) may then be integrated to determine the total amount of gas, q , which is desorbed during the period from times t_1 to t_2 . Hence,

$$q = \int_{t_1}^{t_2} [PS - P_0 S_0 + \frac{\partial}{\partial t} (P - P_0)V] dt. \quad (9)$$

It should be noted that since S is a function of P the pumpdown curves cannot be integrated directly to determine q . However, for most systems S is nearly constant over fairly wide ranges of pressure and may be adequately represented by a step function to facilitate numerical integration of the pumpdown curves. Experiments were performed on a number of different materials for which the pumpdown curves are shown in Fig. 65 thru 69. These curves and Fig. 62 were integrated over the total time of the experiments to determine the total quantity of gas desorbed (Eq. 9). The entire pumpdown curve of the empty system is shown in Fig. 65 and while the total time for the different experiments varied somewhat it can be seen that the curve for the empty system is fairly constant for all temperatures. Also the term $\frac{\partial}{\partial t} (P - P_0)V$ in Eq. (9) was observed to be a second order term and, hence, the small "spikes" in the pumpdown curve can be neglected.

The value of q so obtained for the various materials are shown in Table 2 in order of ascending values of q . While it is evident that some gas still remained on the particles at the end of the experiments it is believed that the amount desorbed at the temperatures that were used represents the major amount of adsorbed gas and the amount remaining at the end was negligible. This is supported by the fact that the pumpdown curves for the empty system and the system with soil tend to converge and are very close at the highest temperatures.

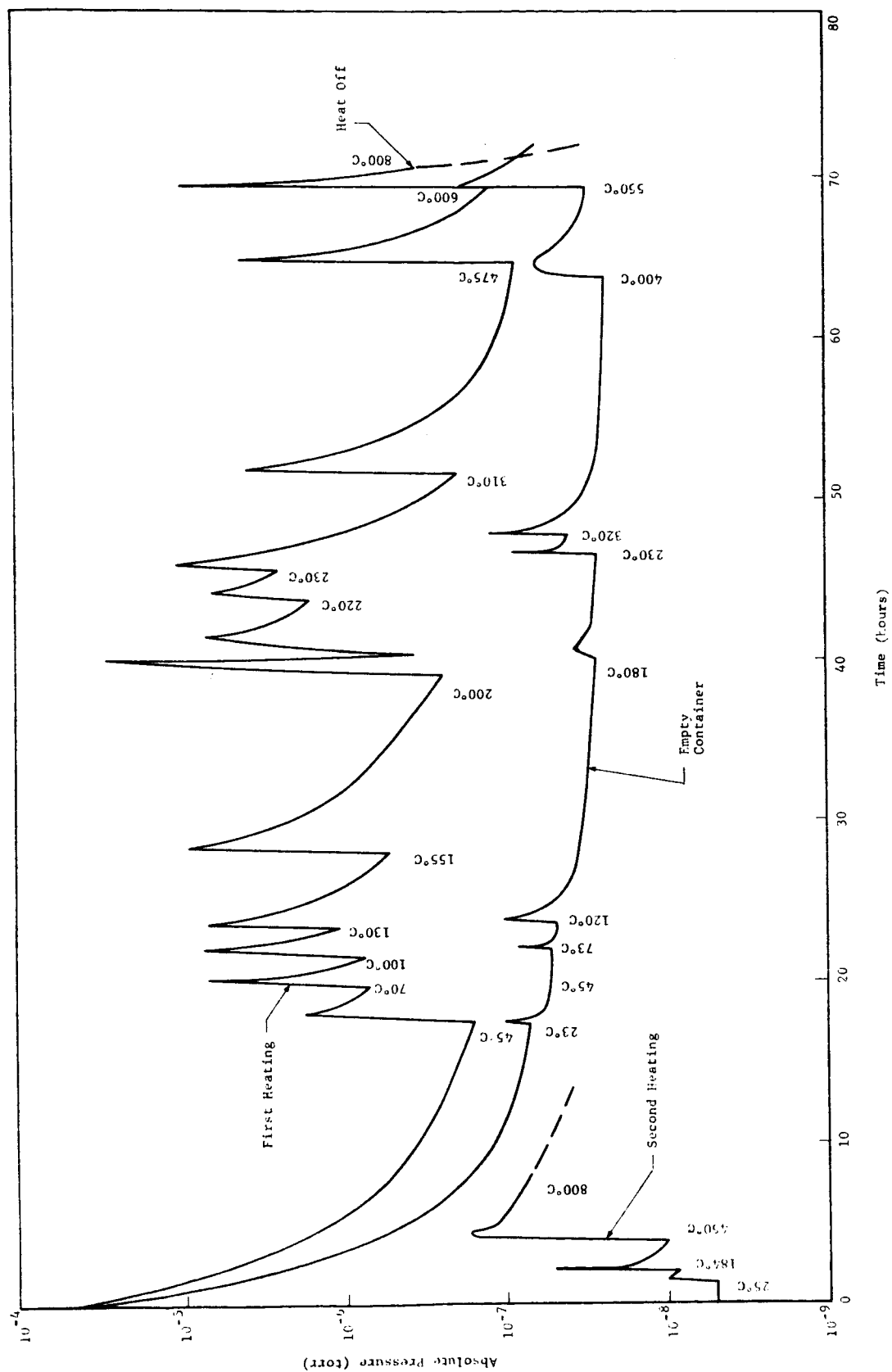


Fig. 65 PUMPDOWN CURVE FOR OLIVINE POWDER

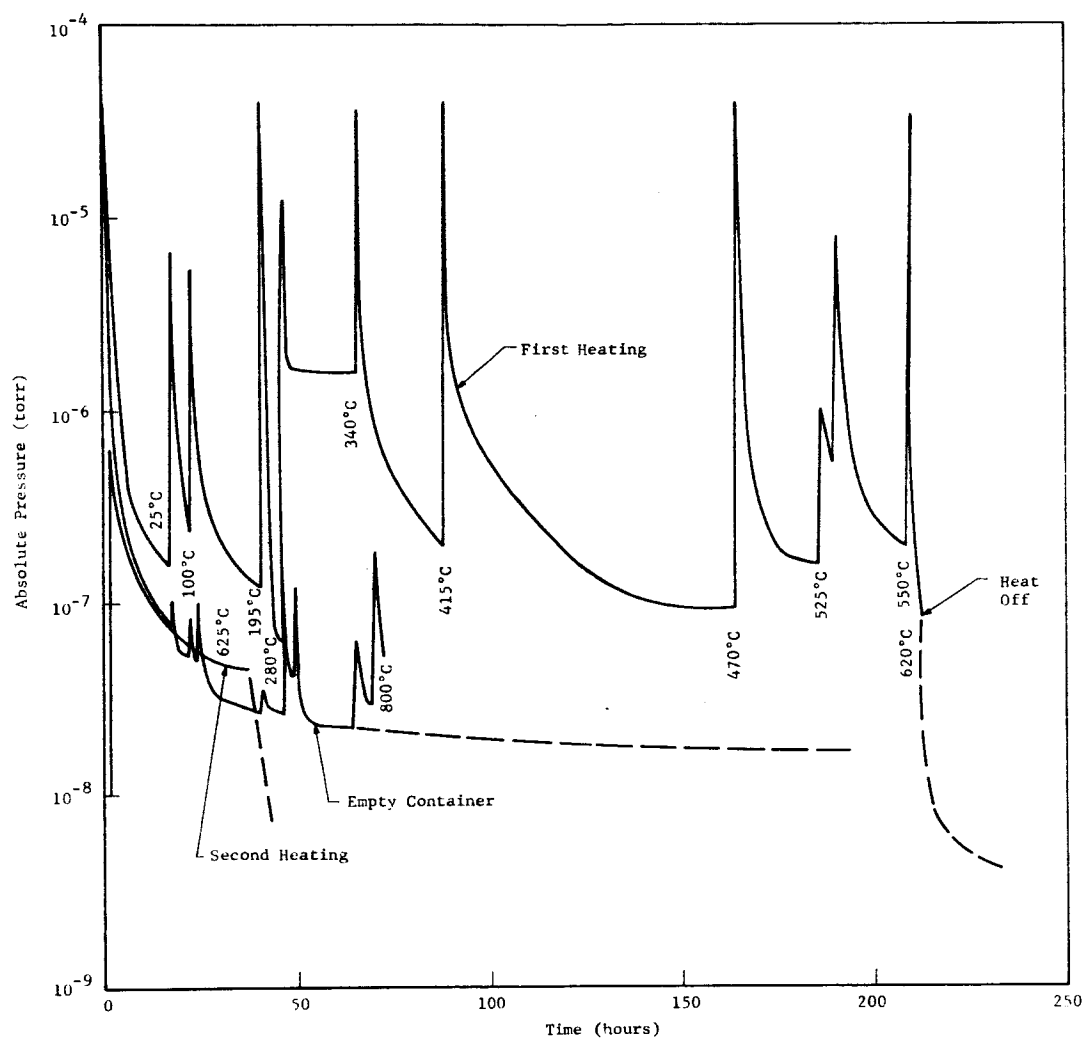


Fig. 66 PUMPDOWN CURVE FOR OLIVINE A

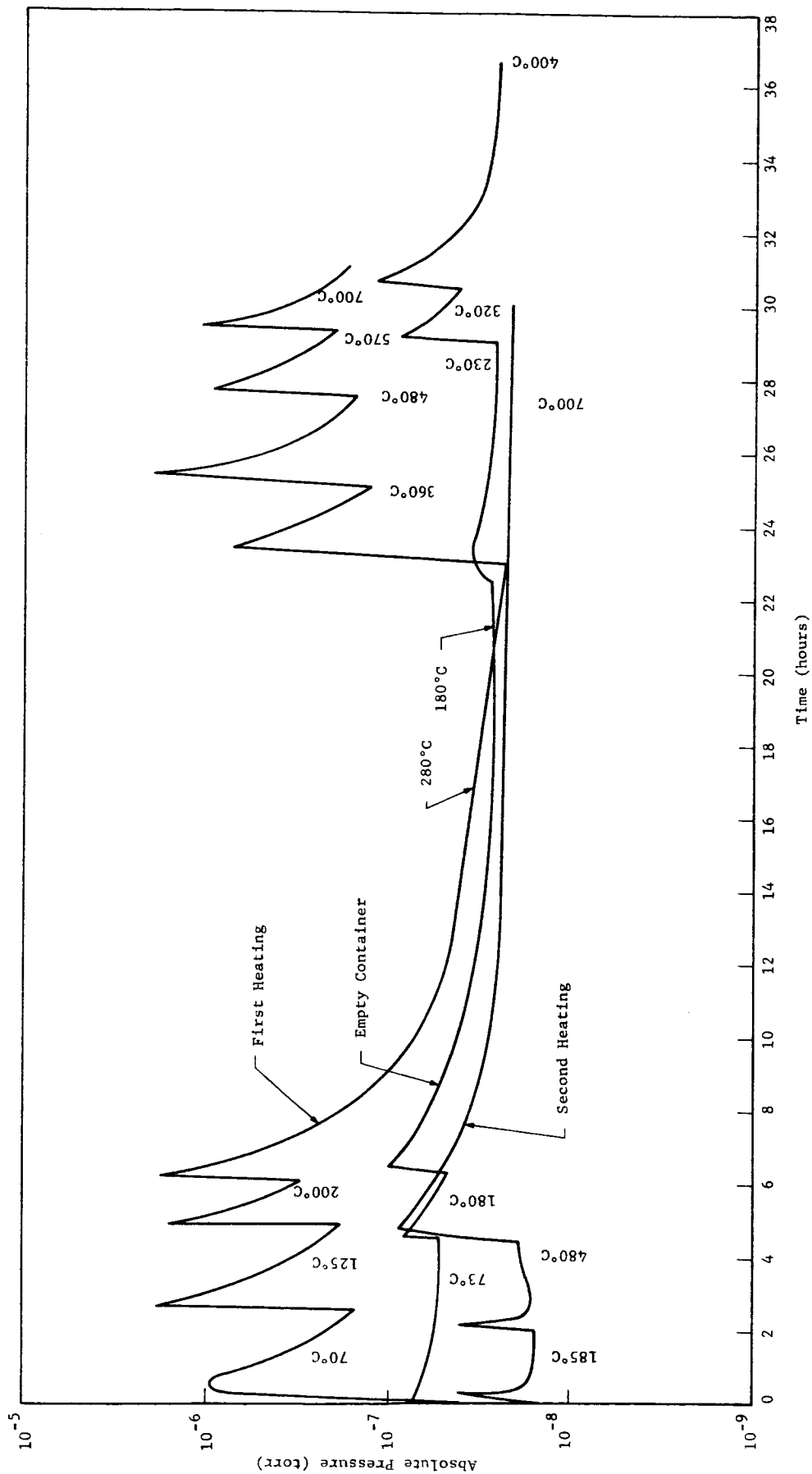


Fig. 67 PUMPDOWN CURVES FOR OBSIDIAN POWDER

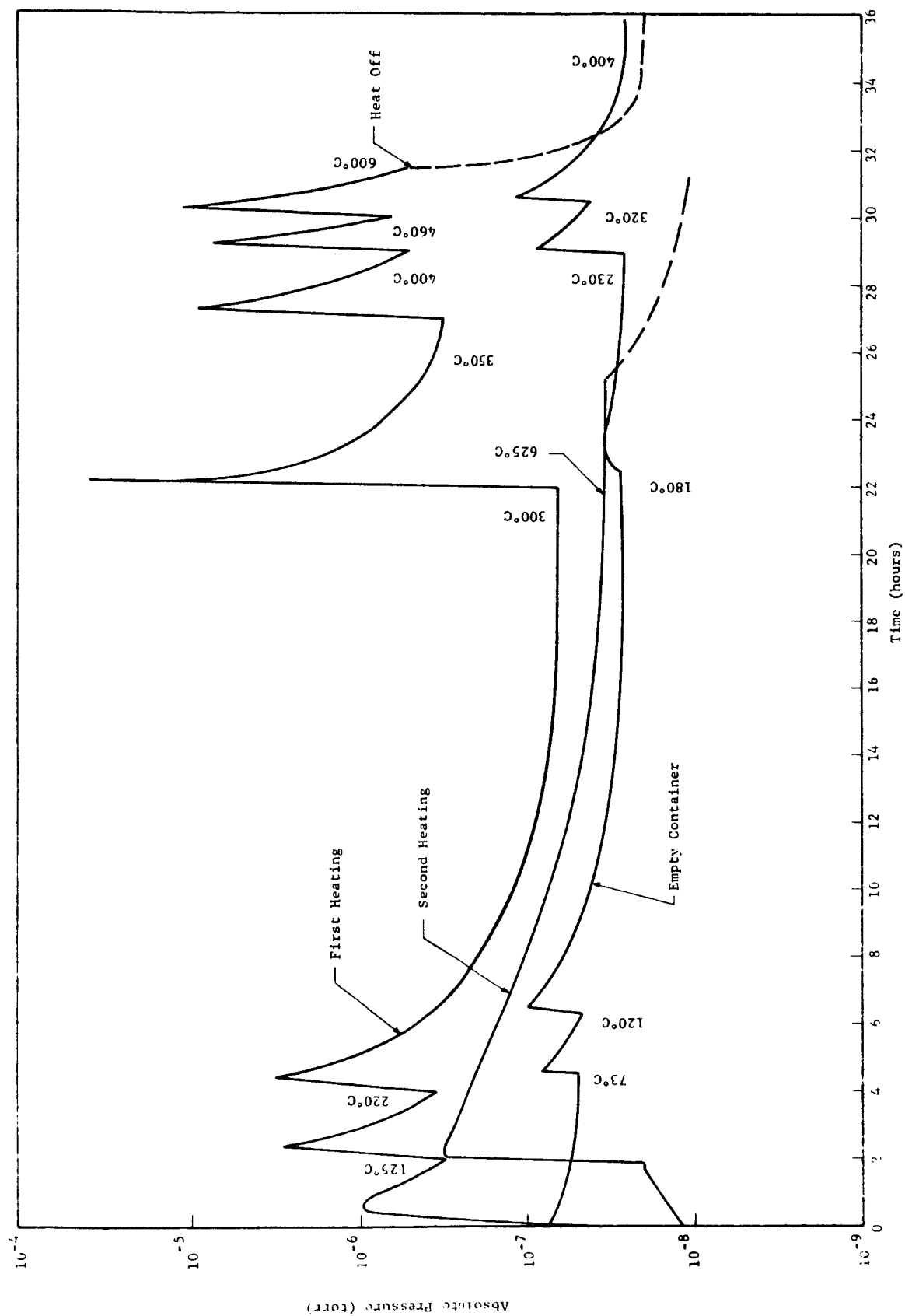


Fig. 68 PUMPDOWN CURVES FOR ENSTATITE POWDER

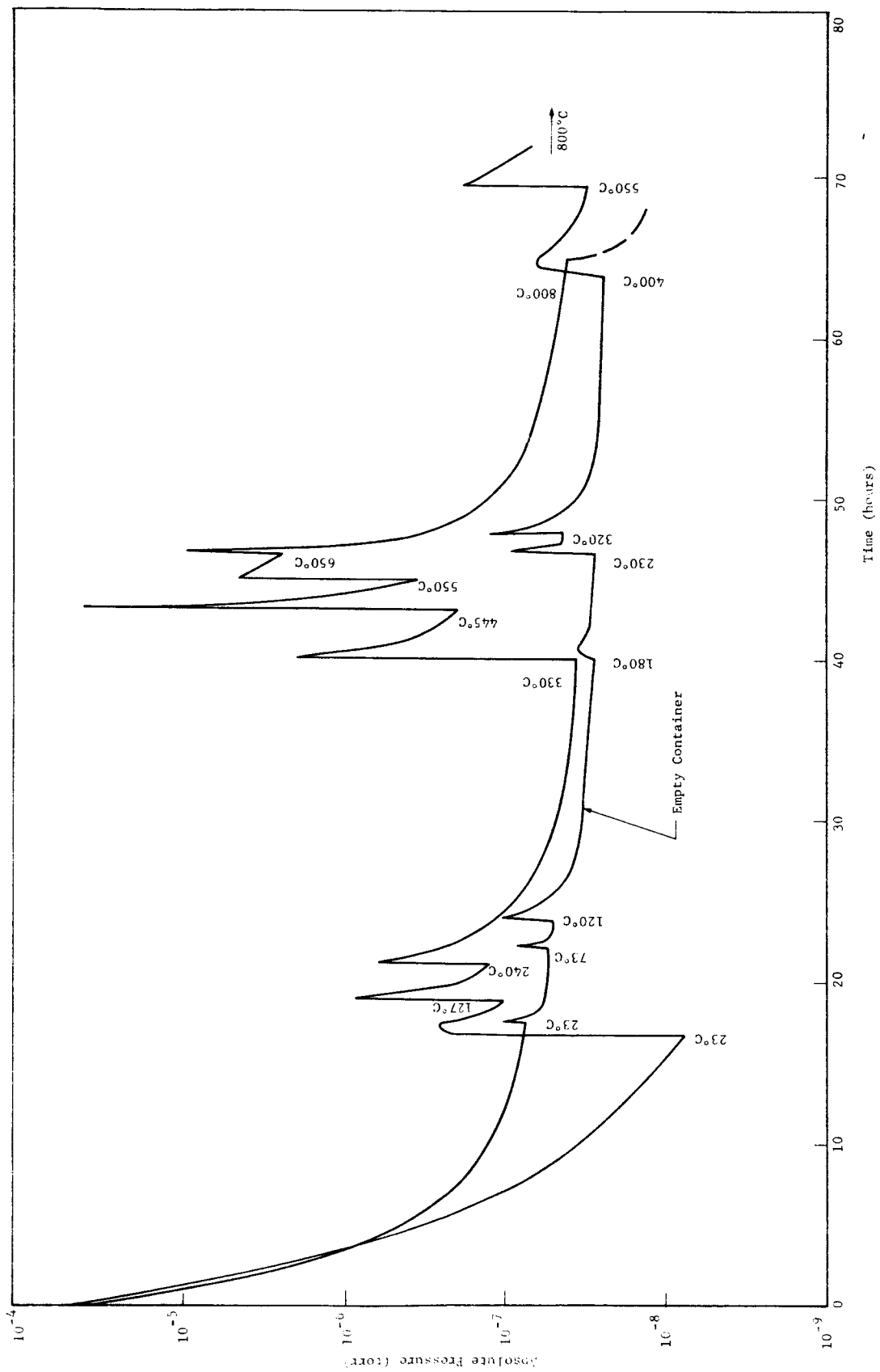


Fig. 69 PUMPDOWN CURVES FOR ENSTATITE SAND (105 to 149 μ)

Table 2
TOTAL AMOUNT OF DESORBED GAS

<u>Material</u>	<u>q, torr liters/gram</u>
Quartz Powder	1.8
Obsidian Powder	4.3
Enstatite Sand	26.8
Enstatite Powder	40.8
Olivine Powder	78.2
Olivine A	278.0

The values in Table 2 show a very significant difference in sorbed gas for the different materials, with a difference of more than two orders of magnitude between the maximum and minimum. As might be expected, the olivine exhibited the greatest and the quartz the least with the obsidian closer to the quartz and the enstatite closer to the olivine.

The sample identified as olivine A was the same soil as described in the previous section. It is interesting to note that although this sample was ground under the same conditions as the obsidian and enstatite and its grain size distribution was very nearly the same as the quartz and the coarser grained olivine the total amount of gas desorbed from it was almost four times that of the other olivine sample. It may be concluded rather definitely, therefore, that the grinding of the material in a rubber lined mill had a minor if any affect on the adsorbed gas on the soil.

Another point which is quite significant is the fact that although the grain size of the enstatite sand was approximately 30 times greater than that of the enstatite powder and the specific surface of a granular material varies inversely with the grain diameter, the amount of gas desorbed from the powder sample differed from that of the sand by less

IIT RESEARCH INSTITUTE

than a factor of 2. This could be due to either or both of two factors: 1) the greater permeability of the sand permitted a more efficient outgassing, and 2) the material may have contained a large amount of absorbed gas initially which was released and readsorbed on the surface.

Since it was observed in Phase II of this project² that the pressure at a point 18 inches below the surface of a soil mass (quartz powder) responded to a leak in the chamber almost simultaneously with the chamber pressure, it is believed that differences in permeability would not account for the differences in q of the two materials. Hence, it is believed that the enstatite and consequently the olivine contained a much greater amount of absorbed gas than either the obsidian or quartz. Furthermore, it is believed that this gas was removed from within the soil particles in the vacuum and then readsorbed on the surfaces.

In general it may be stated that the amount of gas which can be desorbed from the different materials is highly dependent on the mineralogical composition. Thus, it is evident that the difference in vacuum effects on the physical properties of the different materials may be attributed to differences in the amount of gas remaining on the various materials even when subjected to the same outgassing procedure.

VII. EFFECT OF SURFACE CLEANLINESS ON SHEAR STRENGTH

It is evident from the previous results that the effect of vacuum on soil properties is primarily one of removing the adsorbed gas which in turn increases the interaction between particles both by the development of interparticle forces and by increasing the coefficient of friction between grains. However, normal outgassing procedures remove only an unknown portion of the adsorbed gas and, therefore, experiments were performed to investigate the changes in soil shear strength in relation to the amount of gas remaining on the soil particles rather than in relation to the vacuum level of the surrounding environment alone.

In these experiments it was necessary to use a relatively simple measurement of shear strength which could be duplicated exactly both with respect to soil sample and test procedure. It was also desirable that as much of the sample as possible be exposed to the vacuum to aid in outgassing and hence, a minimum quantity of soil was specified. To eliminate variations due to sample preparation it was required that a number of experiments be performed on each sample. In consideration of these requirements the measurement selected for these experiments was static penetration resistance.

A series of experiments were first performed in atmosphere to determine the optimum size of penetrometer and the minimum size of container for which boundary conditions would be negligible. Penetrometer experiments were performed in a container 10 in. in diameter and 7.3 in. deep at various distances from the penetrometer centerline to the edge of the container ranging from 5 to 0.5 in. The sizes of penetrometers selected were 0.75, 0.50 and 0.25 in. in diameter. The penetration resistance for the three penetrometers at various edge distances is shown in Fig. 70 through 72. Experiments were then performed using the three penetrometers and containers

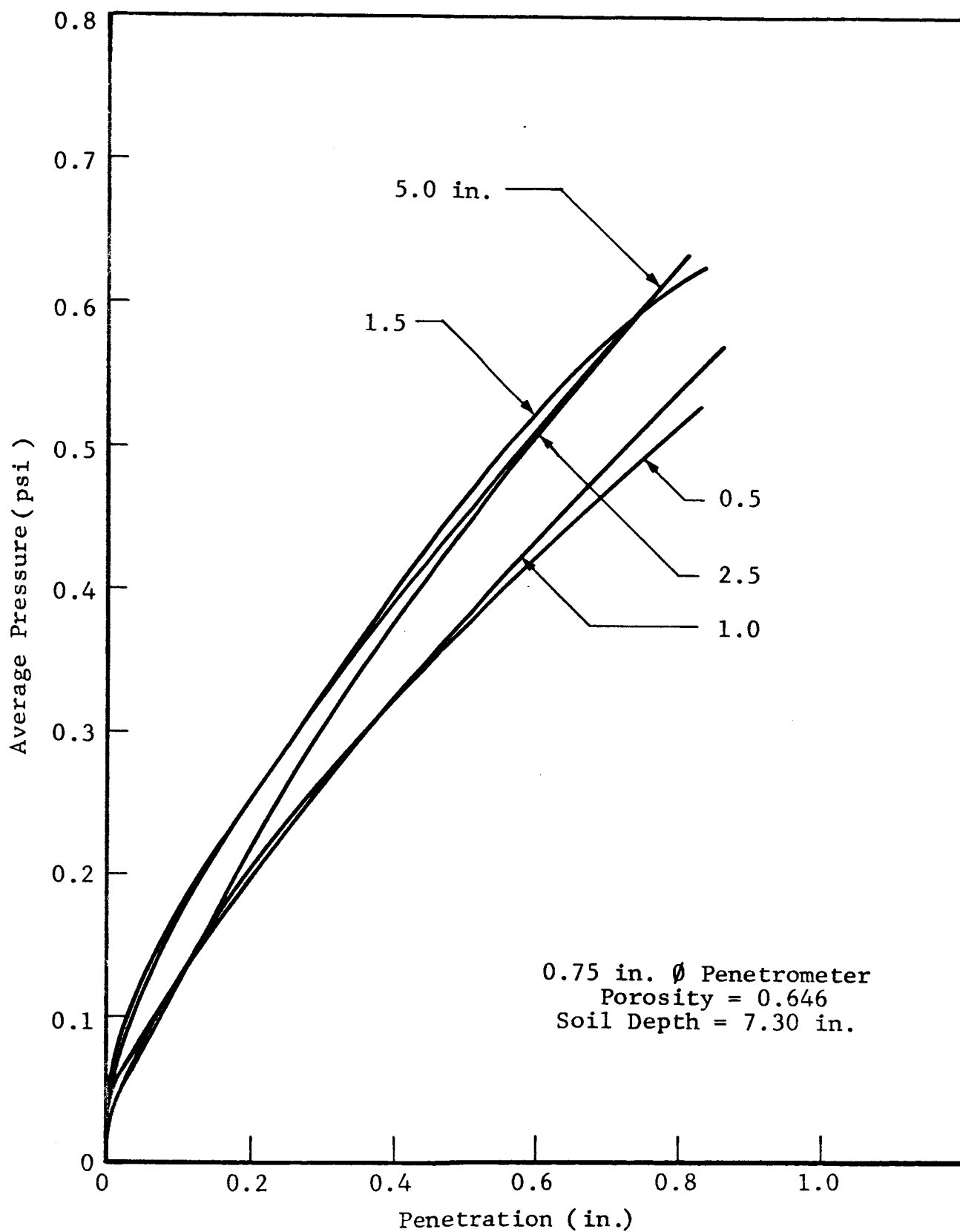


Fig. 70 PENETRATION RESISTANCE FOR VARIOUS EDGE DISTANCES

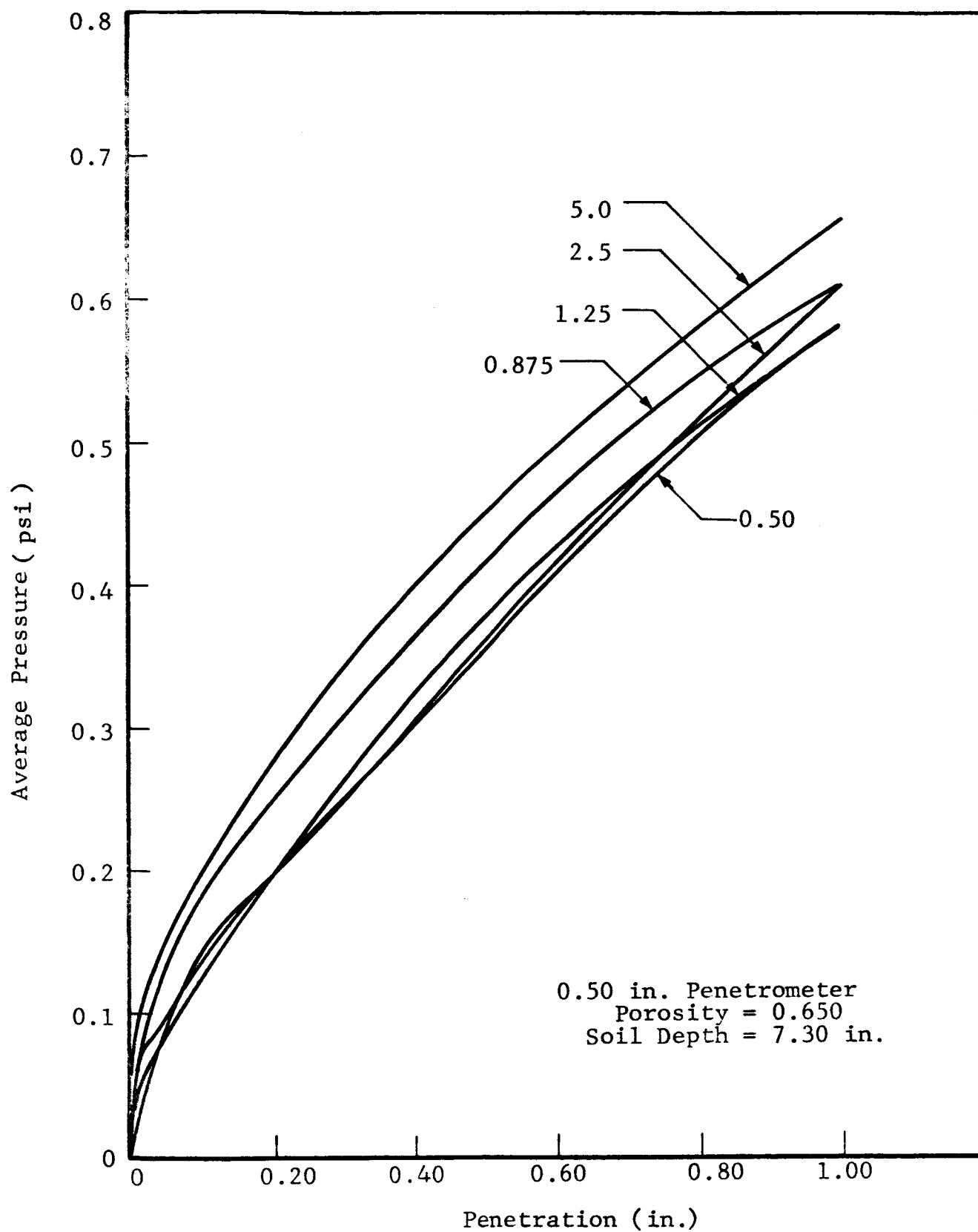


Fig. 71 PENETRATION RESISTANCE FOR VARIOUS EDGE DISTANCES

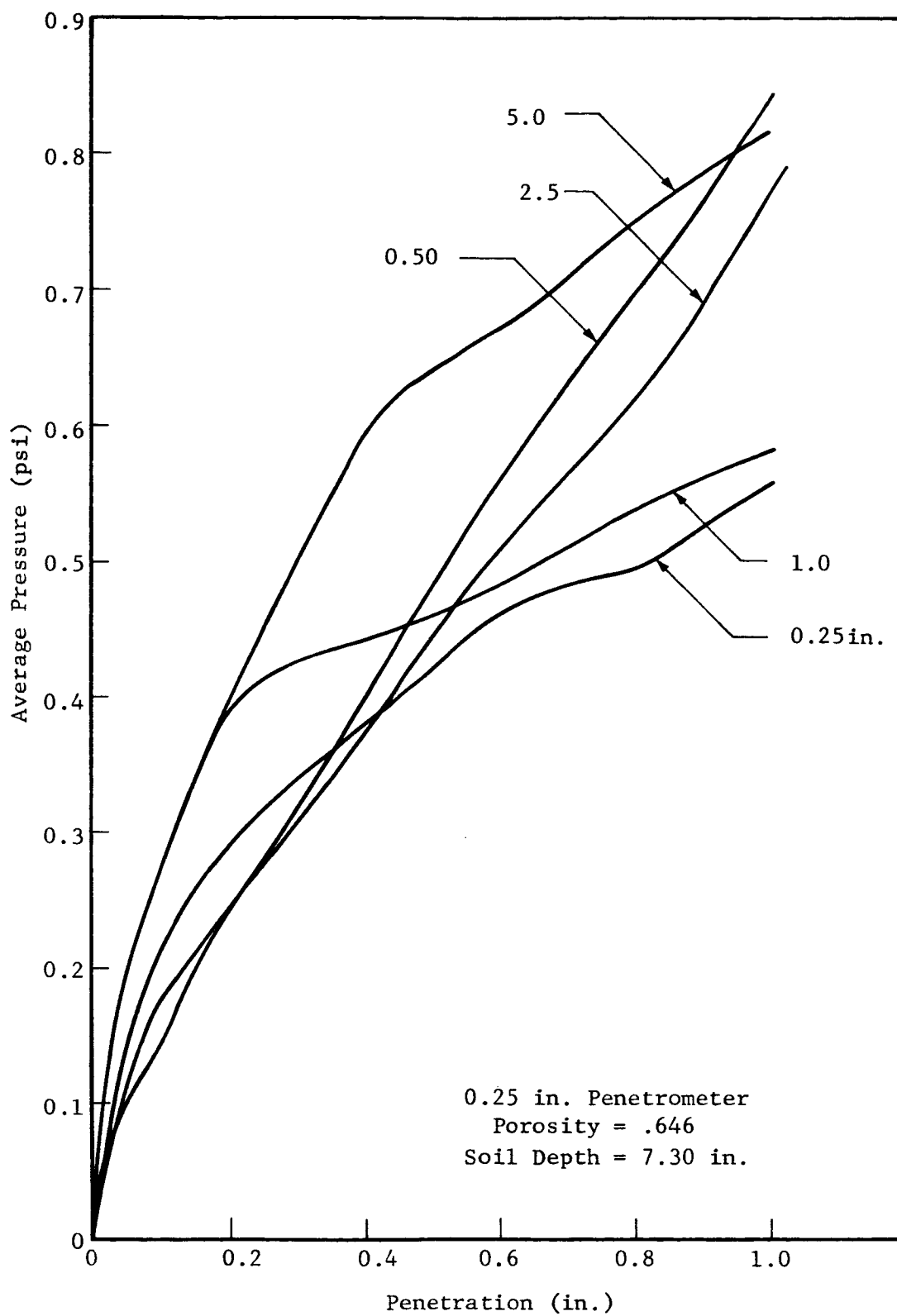


Fig. 72 PENETRATION RESISTANCE FOR VARIOUS EDGE DISTANCES

having depths of 3.0, 2.0 and 1.5 in. and the results of these experiments are shown in Fig. 73 through 75.

It is evident that very small distances from the edge had a small effect on the shape of the curve. As may be seen from Fig. 72 and 75, however, the 0.25 in. penetrometer provided data which was not very reproducible. This was most probably due to nonhomogeneity in the soil density and the small cross sectional area necessitating the measurement of very small loads. From Fig. 73 and 74 it can be seen that the 0.50 in. penetrometer will permit a greater penetration before the container effects become noticeable than will the 0.75 in. penetrometer. However, since penetration resistance is a function of the shear along the circumference as well as the compressibility of the material directly below the penetrometer it was believed that the use of two sizes of penetrometer would provide a means of comparing the relative effects on shear-strength and compressibility.

On the basis of these preliminary experiments a soil container having a diameter of 3.0 in. and a depth of 2.0 in. was designed and both 0.50 in. and 0.75 in. penetrometers were used. The apparatus is shown in Fig. 76. It consisted of a soil container of the aforementioned dimensions which was mounted on ball bearings on top of a frame. The penetrometer was mounted on the top of the chamber through a bellows. After an experiment had been performed the penetrometer was retracted and the container was rotated by means of a flexible shaft connected to a rotary feedthrough. In this way a number of experiments could be performed on the same soil sample as evidenced in Fig. 76. Nichrome wire in ceramic beads were wound around the container to permit electric heating of the sample. To reduce outgassing the entire apparatus was fabricated from polished stainless steel except for the container, penetrometer and load cell which were fabricated from

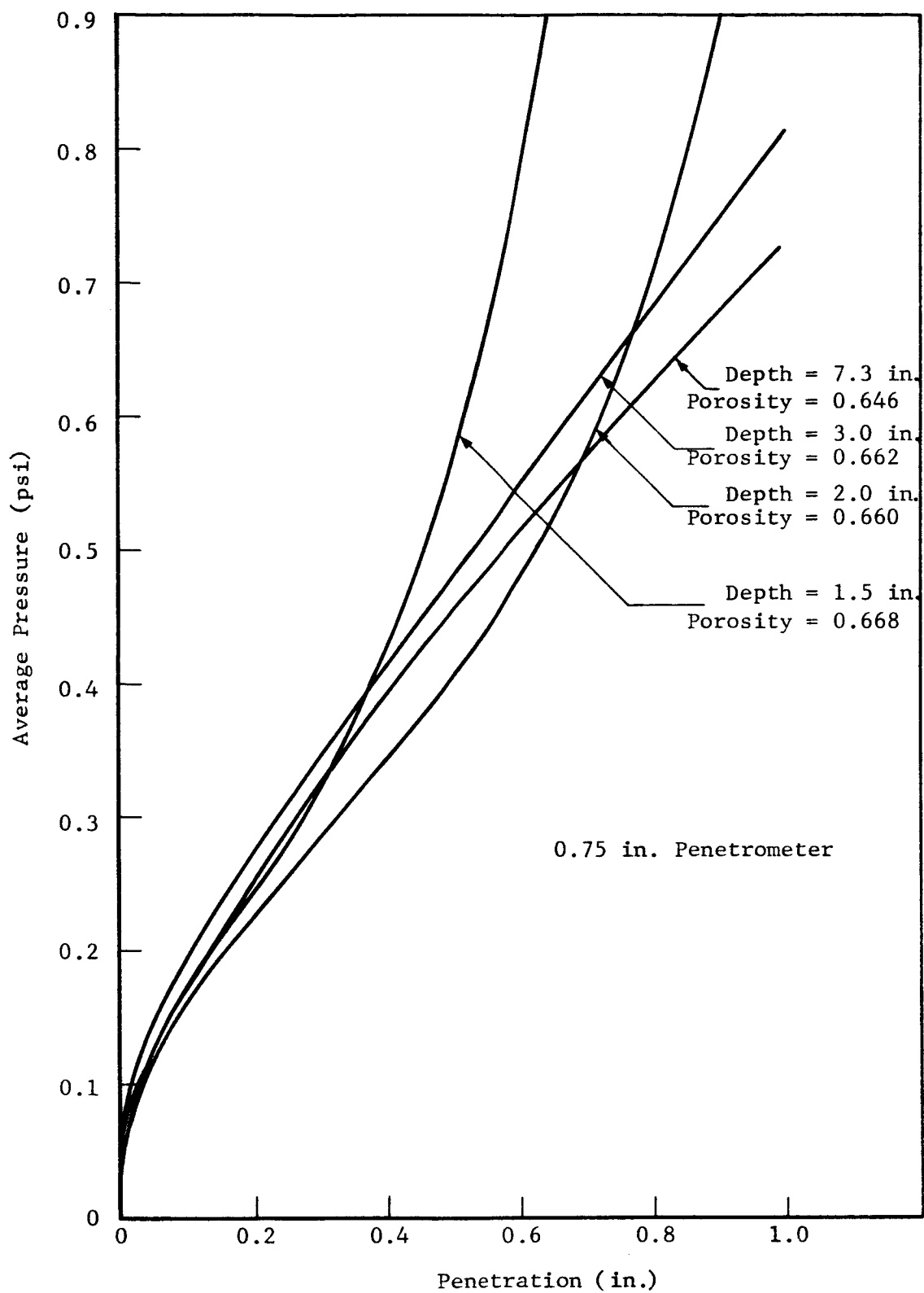


Fig. 73 PENETRATION RESISTANCE FOR VARIOUS SOIL DEPTHS

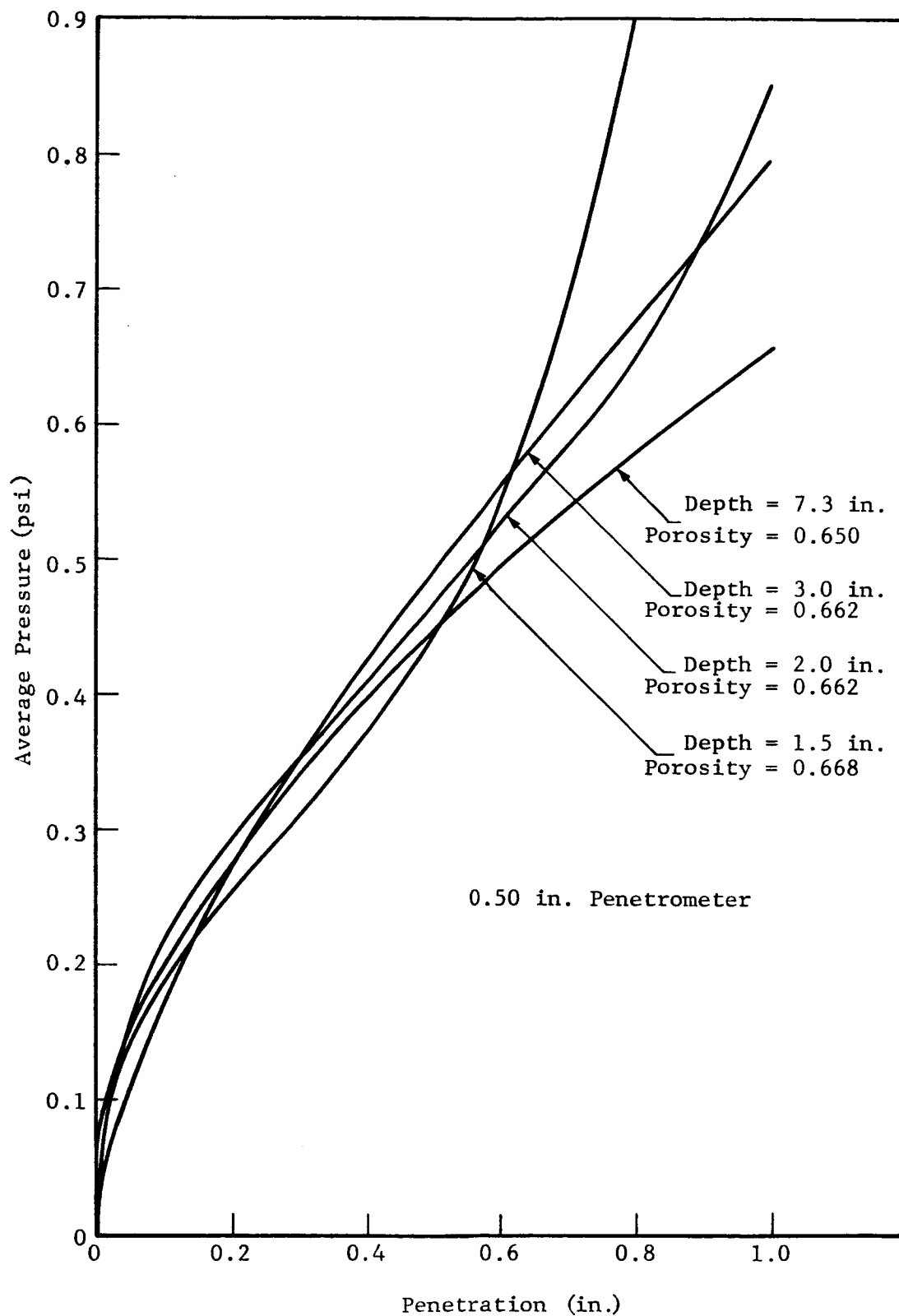


Fig. 74 PENETRATION RESISTANCE FOR VARIOUS SOIL DEPTHS

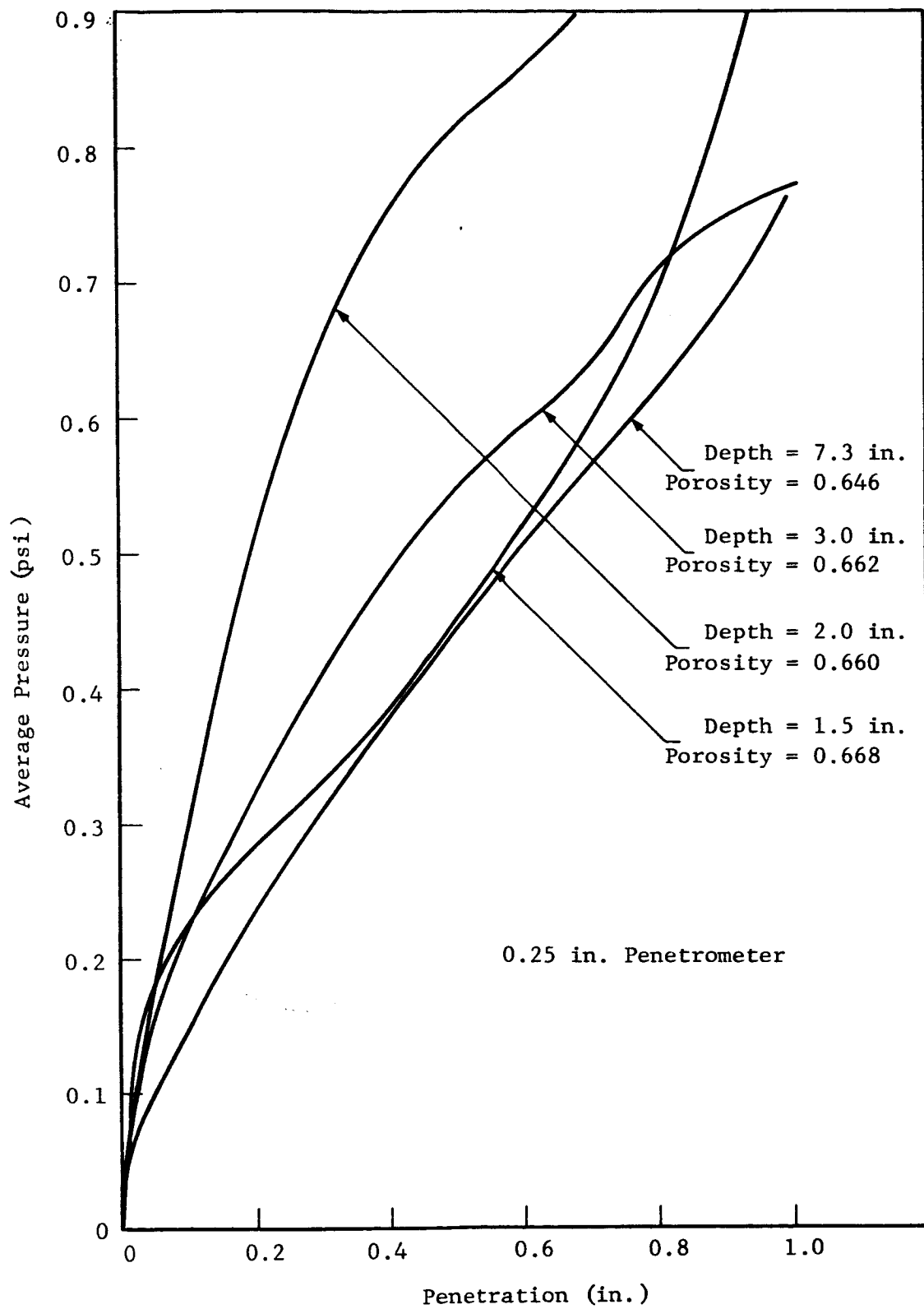


Fig. 75 PENETRATION RESISTANCE FOR VARIOUS SOIL DEPTHS

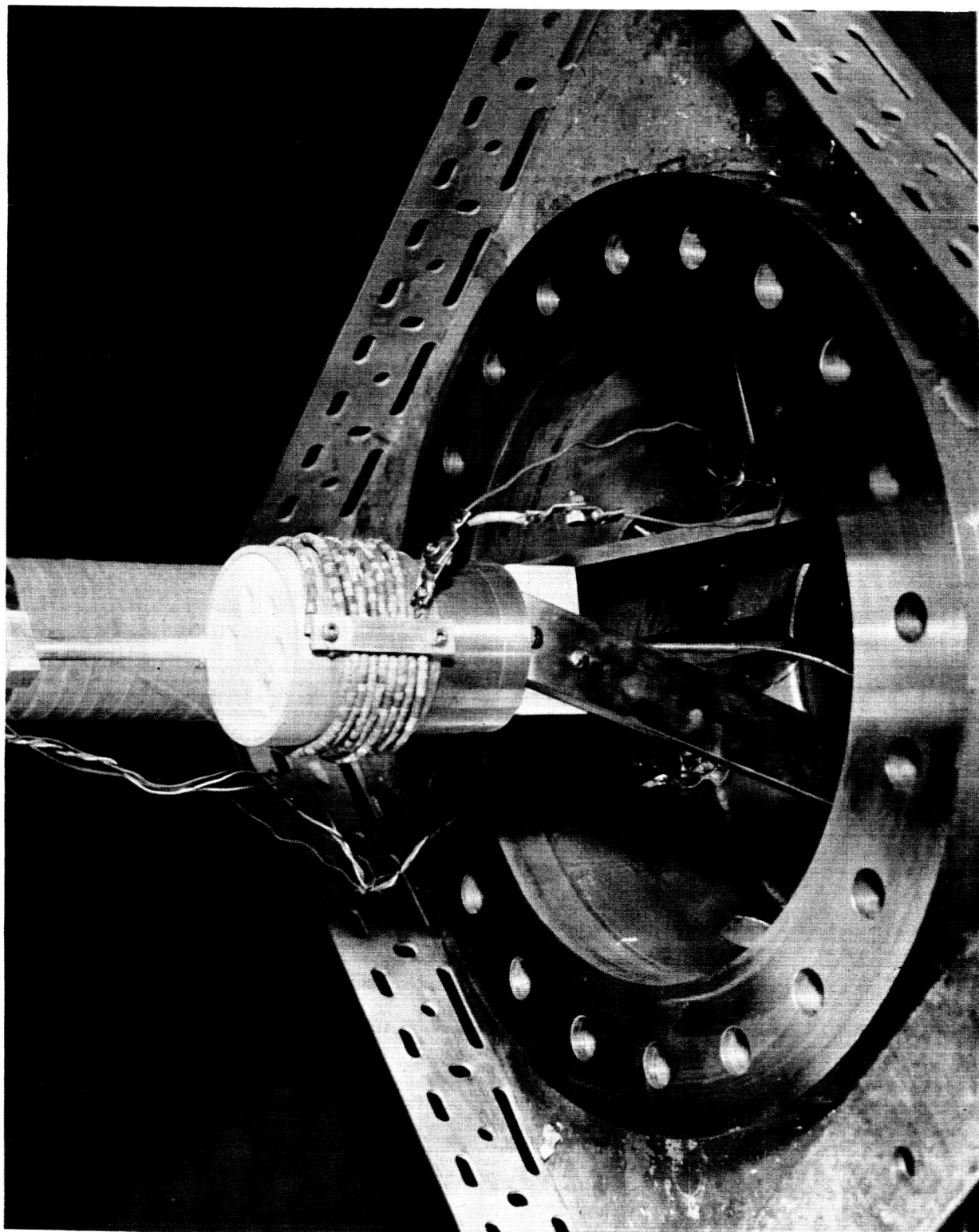


Fig. 76 STATIC PENETRATION APPARATUS

polished aluminum. The load cell was similar to those used in the direct shear experiments and its temperature was maintained at ambient temperature by cooling the bellows on which it was mounted.

To eliminate any possible contamination by backstreaming of pump oil the experiments were all performed in a 125 l/sec ion-pumped system.

After the sample had been prepared and the apparatus assembled in the vacuum system one experiment was performed in atmosphere. The system was then pumped down and after three days another experiment was performed. The temperature of the soil was then increased to 143°C in increments and another experiment was performed after an additional three days of pumping. The temperature was increased again and another experiment was performed after a total of 10 days.

After this series of experiments the apparatus was placed in the vacuum system without soil and the temperature-time history was repeated. From the two pumpdown curves the total quantity of desorbed gas could be determined for each point at which an experiment was performed.

To facilitate the integration in Eq. (9) and to provide a greater amount of accuracy in the computations the throughput was plotted as a function of time rather than just the pressure (Fig. 77). Since time did not permit the calibration of the pumping speed of the pump as a function of pressure, the manufacturer's rated pumping speed was used in the computations. While it is recognized that the actual speed of the pump may not be the same as the rated pumping speed, it is expected that its variation with pressure would conform fairly well with the data supplied and hence, any inaccuracies introduced would not be great and would be the same for all experiments.

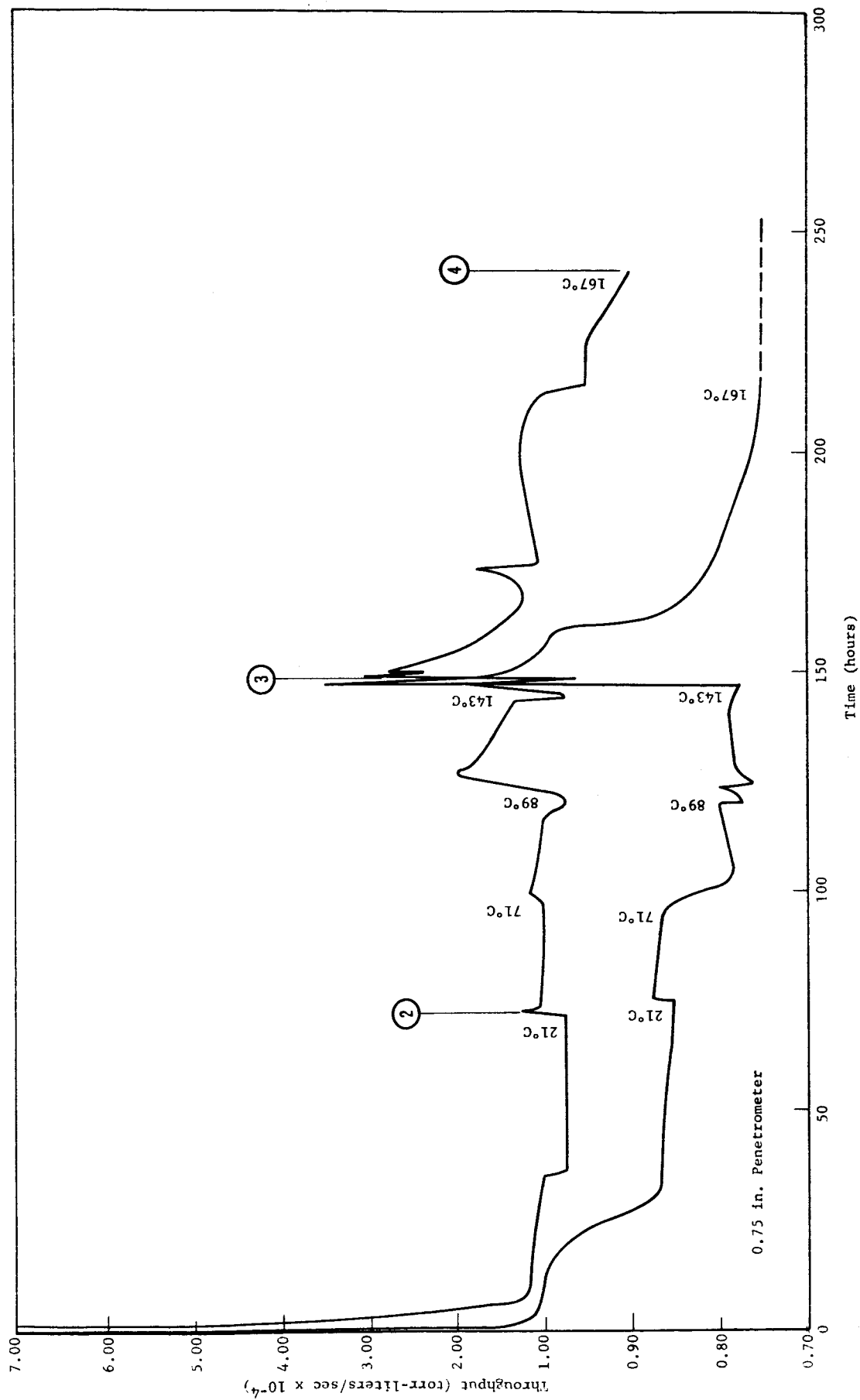


Fig. 77 THROUGHPUT AS A FUNCTION OF TIME FOR PENETRATION EXPERIMENTS

A complete series of experiments was performed using the 0.75 in. penetrometer but during the experiments with the 0.50 in. penetrometer the heating wire broke. Unfortunately, time did not permit further work and, hence, only two experiments could be performed with this apparatus. Also, because of this, it was not possible to accurately determine the pump-down characteristics for the empty system under the same conditions and, hence, it was necessary to estimate this pumpdown curve (Fig. 78) on the basis of the one for the previous series of experiments.

After the experiments in vacuum had been performed a series of experiments were performed in atmosphere in the same container and at the same positions to determine any container effect which may have been present.

The penetration resistance of the soil at the different times is shown in Fig. 79 and 80 for the two penetrometers. The solid lines indicate experiments in the vacuum chamber and the broken lines are for the experiments in atmosphere. The numbers in the circles by each curve refer to the corresponding numbers on the throughput-time curves (Fig. 77 and 78) and, thus indicate the times at which the experiments were performed. The numbers in squares refer to the experiments in atmosphere at the same position in the container and in the same order of performance as the corresponding number in the circles.

From Fig. 79 it is evident that some container effects were present for the 0.75 in. penetrometer but none were observed for the 0.50 in. penetrometer (Fig. 80). The effects, however, were quite small relative to the effects due to outgassing of the soil. It is clearly indicated that for increasing degrees of outgassing the penetration resistance increased quite rapidly.

In order to compare relative changes in the penetration resistance a term denoted the "strength ratio" was defined as the average bearing pressure at a particular value of penetration

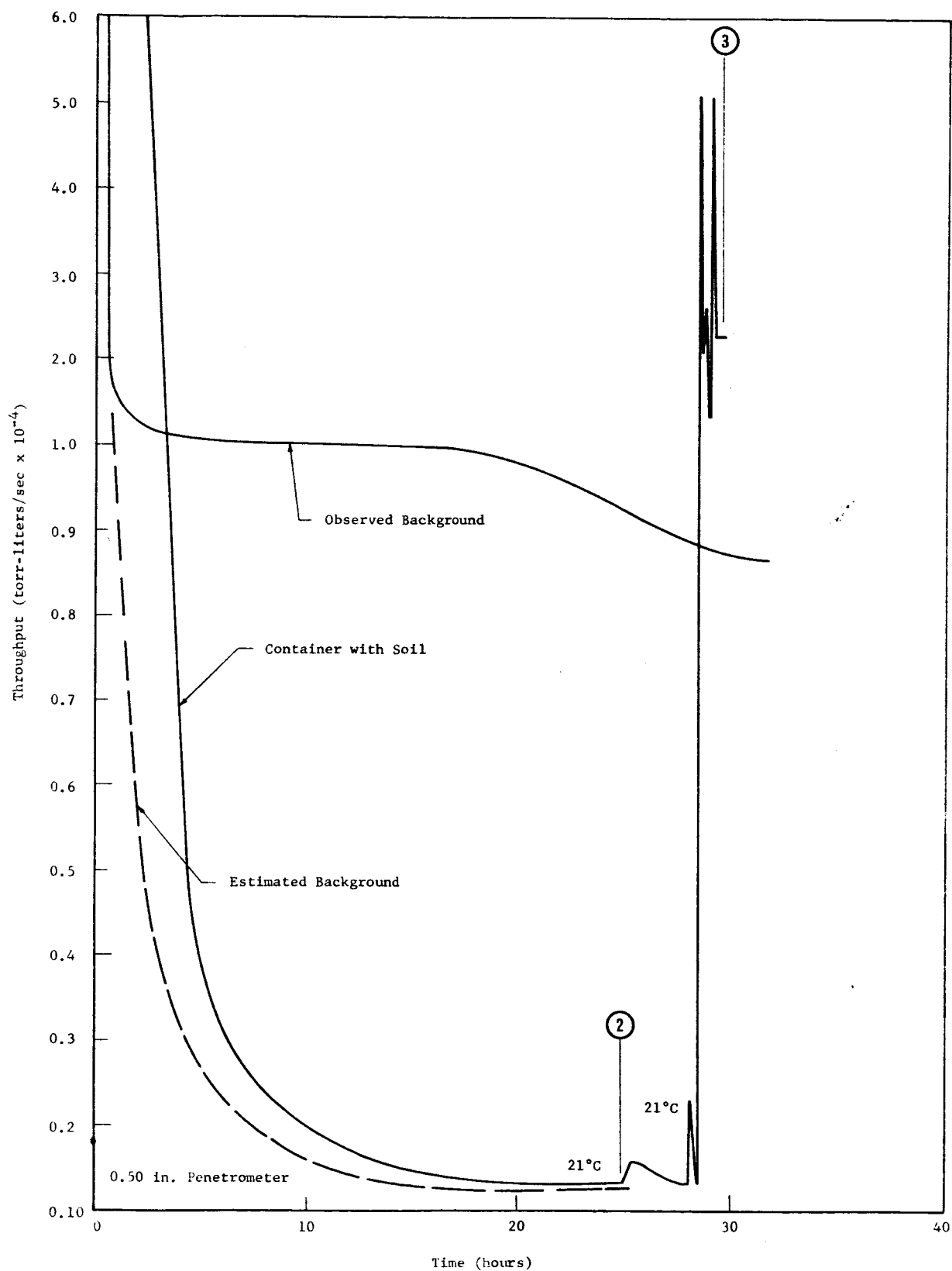


Fig. 78 THROUGHPUT AS A FUNCTION OF TIME FOR PENETRATION EXPERIMENTS

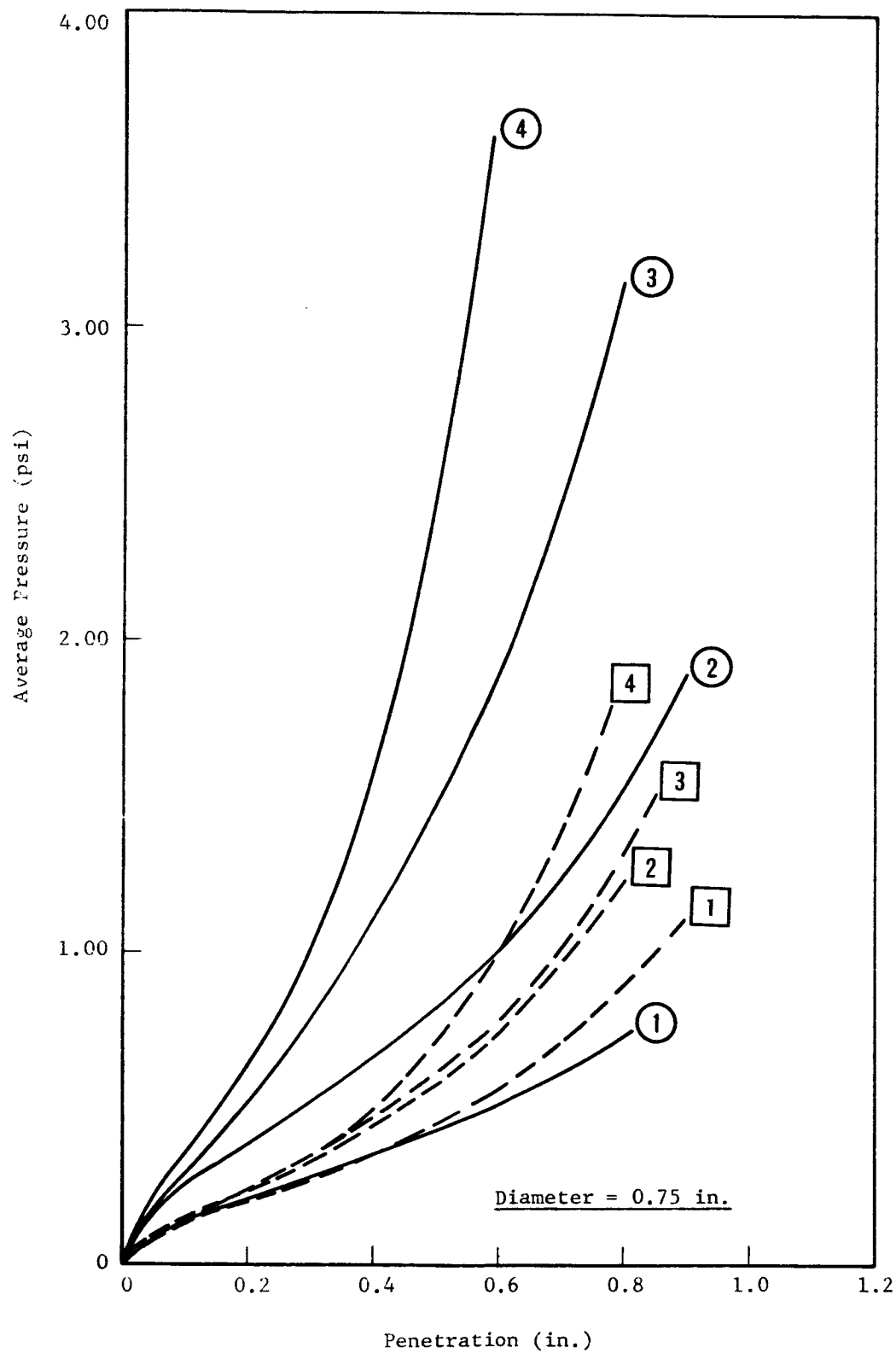


Fig. 79 PENETRATION RESISTANCE FOR VARIOUS DEGREES OF OUTGASSING

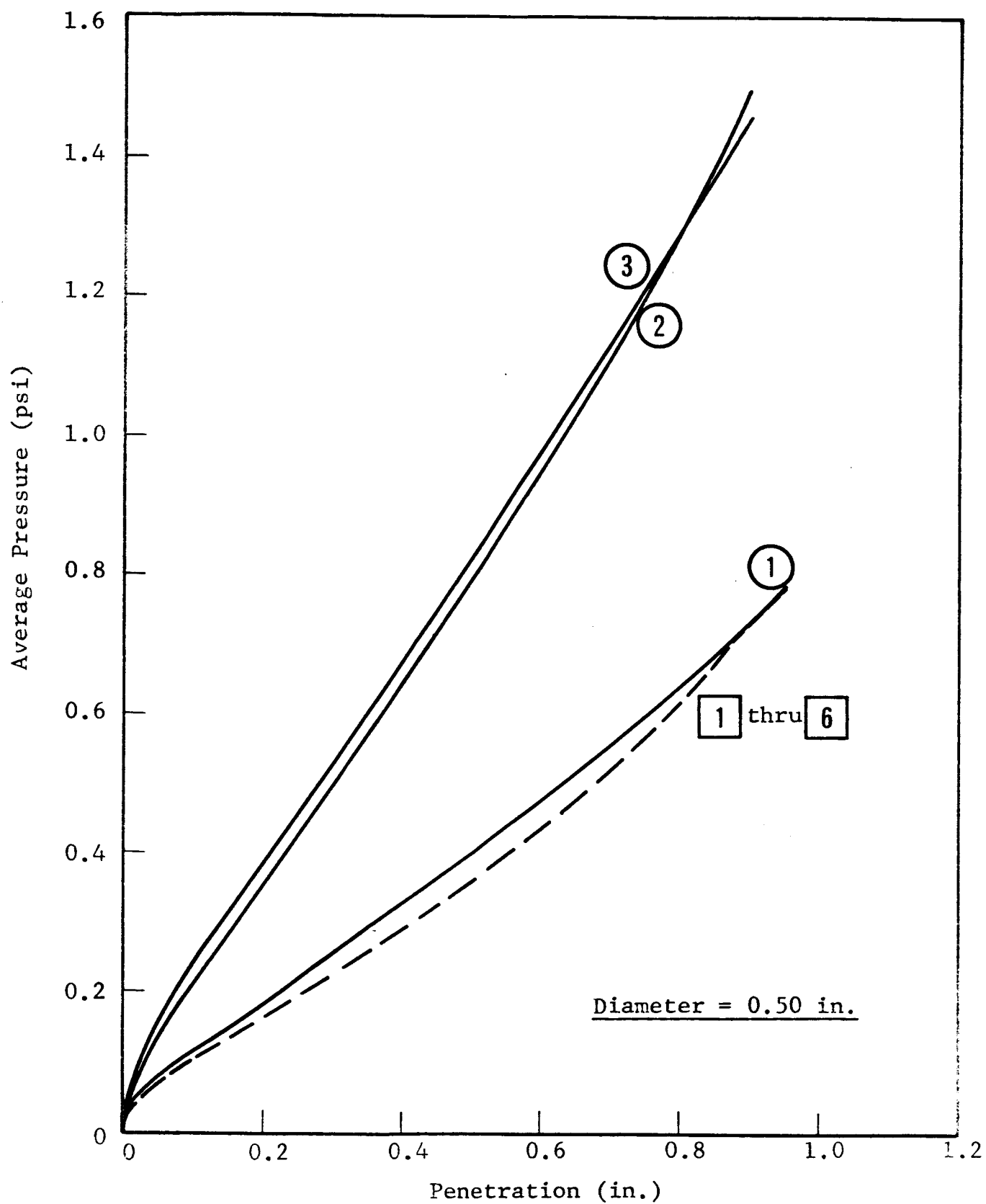


Fig. 80 PENETRATION RESISTANCE FOR VARIOUS DEGREES OF OUTGASSING

in vacuum divided by the average bearing pressure in the atmosphere at the same penetration. In this way the effects of the container could be taken into account for the 0.75 in. penetrometer by using the different curves for atmosphere to compute the strength ratio.

Also, the relative cleanliness of the soil was defined as the quantity of gas, q , (as determined by Eq. (9)) desorbed by the time at which the penetration resistance was measured divided by the total amount of gas initially adsorbed on the soil grains. Thus, in atmosphere the relative cleanliness of the soil is zero whereas the relative cleanliness of an atomically clean surface would be 1.0. This term is somewhat analogous to the coverage of a surface.

The strength ratio at penetrations of 0.20, 0.40 and 0.60 in. are shown as a function of the relative cleanliness in Fig. 81. The total amount of initially adsorbed gas was computed from the data given in Table 2 and was used as the base for the determination of relative cleanliness. The data for the 0.75 in. penetrometer indicates that the strength ratio increased exponentially with relative cleanliness. If curves are drawn connecting the individual points for each particular penetration it is seen that the curves tend to decrease in slope at higher values of cleanliness, but more data are necessary before any definite conclusions can be drawn regarding the actual shape of the curve. The data for the 0.50 in. penetrometer are limited but the same trend is clearly indicated. Nevertheless, it is quite definitely shown that although all experiments were performed at approximately the same vacuum level, the different relative cleanliness at the different times had a very pronounced influence on the penetration resistance.

It can be noted that although the pumpdown extended over a period of ten days, the maximum relative cleanliness attained was only 0.112. Hence, as a measure of the magnitude

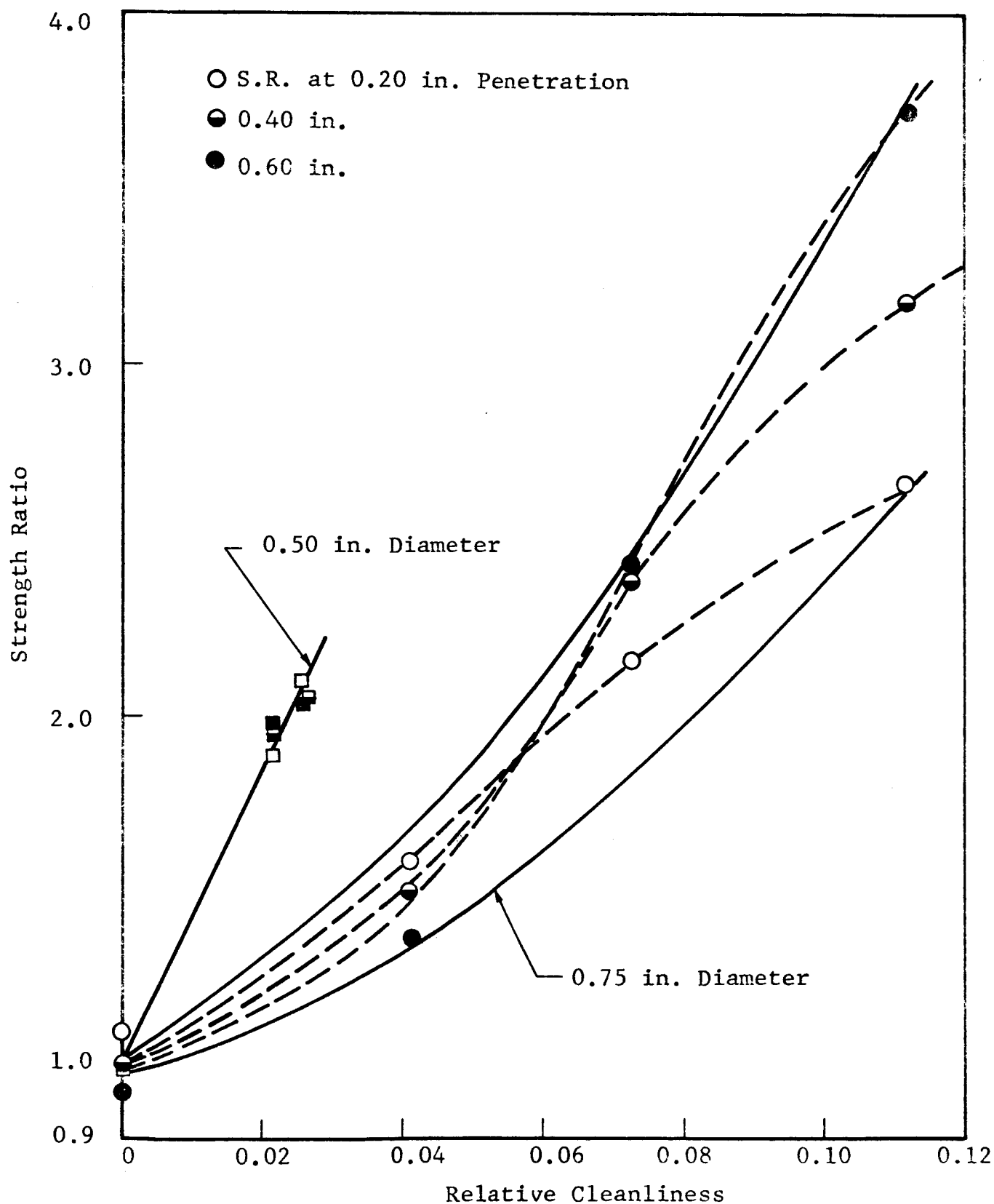


Fig. 81 EFFECT OF RELATIVE CLEANLINESS ON STRENGTH RATIO

of the strength ratio that may be expected to be attained at a relative cleanliness of 1.0, a sample of quartz powder was sintered at a temperature of approximately 1200°C in atmosphere. While this does not necessarily represent the same conditions as a relative cleanliness of 1.0 it does give an indication of the strength of the powder if high bonds exist between the particles. Penetrometer measurements were then performed on the sintered material and the observed penetration resistance is shown in Fig. 82.

The strength ratio was then computed on the basis of the penetration resistance of the loose powder and was plotted in Fig. 83 at a relative cleanliness of 1.0 along with the data for the experiments in vacuum.

It is seen that on a logarithmic plot the points for vacuum appear to fall on straight lines which may be drawn parallel for the two different penetrometers. While considerable uncertainty exists as to the slopes of these lines they would be expected to be parallel if they are influenced by the same types of surface forces. This will be discussed in more detail in Section IX.

While it is possible to draw curves connecting the points obtained in vacuum with those for the sintered material, it can be seen that this is not in actuality the most logically expected extrapolation of the line through the points obtained in vacuum. Also, as was pointed out in Fig. 81 there appears to be a greater tendency for the curves to be concave toward the abscissa rather than the ordinate. Hence, it would be expected that if a sample could be outgassed to attain a relative cleanliness of 1.0 its strength would be considerably lower than that of the sintered material. More data are necessary, however, at values of relative cleanliness between 0.10 and 1.0.

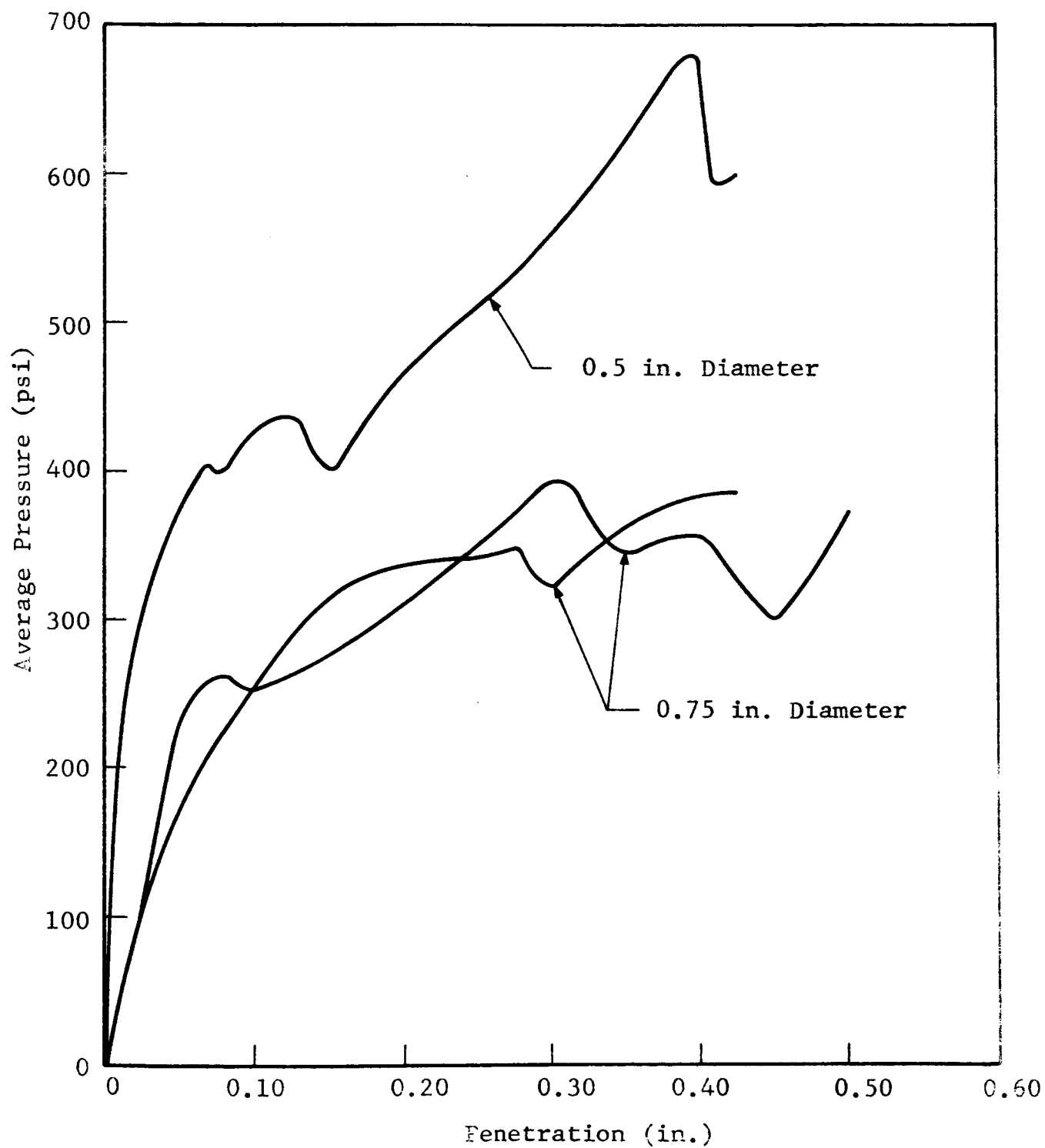


Fig. 82 PENETRATION RESISTANCE OF SINTERED QUARTZ POWDER

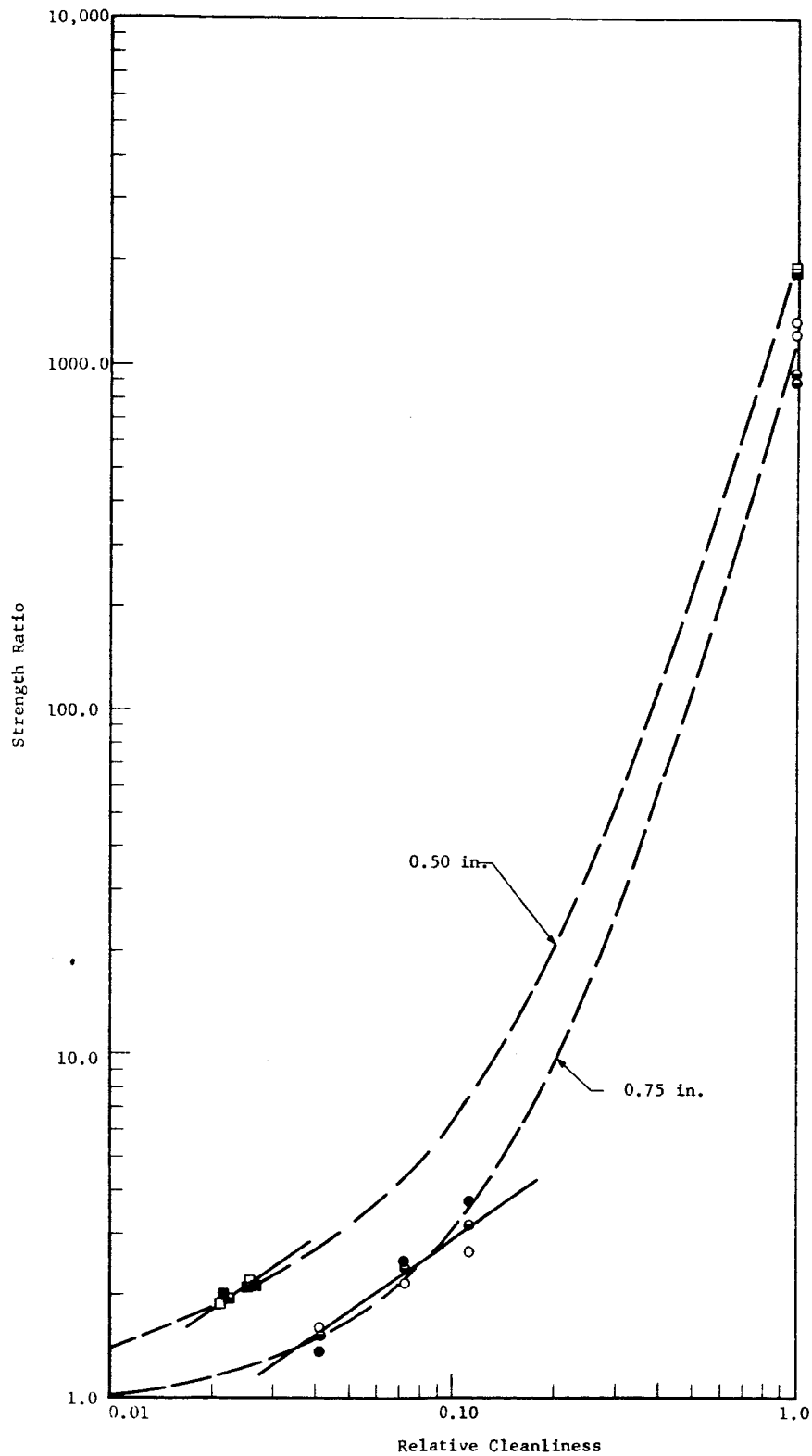


Fig. 83 EFFECT OF RELATIVE CLEANLINESS
ON PENETRATION RESISTANCE

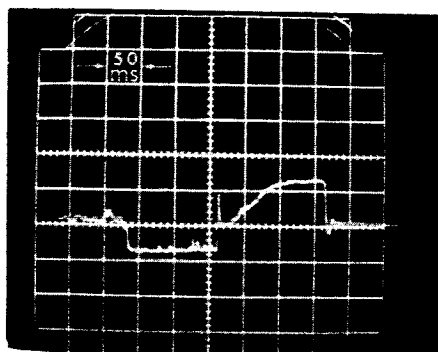
VIII. STUDIES OF SIMULATED MARTIAN SOILS

A limited number of preliminary experiments were performed to investigate the effects of the Martian environmental conditions on the properties of simulated Martian soils. As discussed in Section 2 the material used in these experiments was fine grained limonite with the grain size distribution shown in Fig. 3.

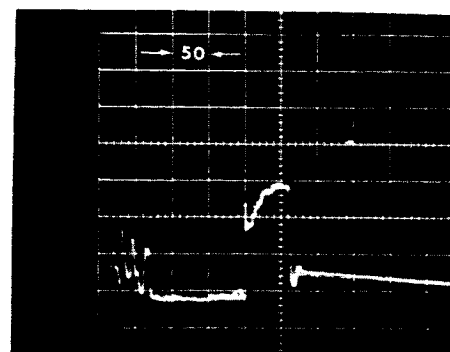
The environmental conditions that were simulated were the composition of the Martian atmosphere and the atmospheric pressure. The principal constituent of the atmosphere is CO_2 ²⁶ with the remainder probably consisting of N_2 and traces of H_2O and inert gasses. Estimates of the atmospheric pressure at the surface vary somewhat but range from approximately 3 to 15mm Hg.

These experiments consisted of dynamic penetration experiments similar to those described in Section 4. The soil sample was placed in a vacuum chamber and pumped down to a pressure of 1mm Hg over a period of approximately 3 hours. A gas mixture consisting of 66 percent CO_2 , 33 percent N_2 and 1 percent Argon was then introduced to raise the pressure to that at which the experiment was to be performed. Experiments were performed at pressures of 3mm and 15mm Hg which are the upper and lower bounds for the range of estimates.

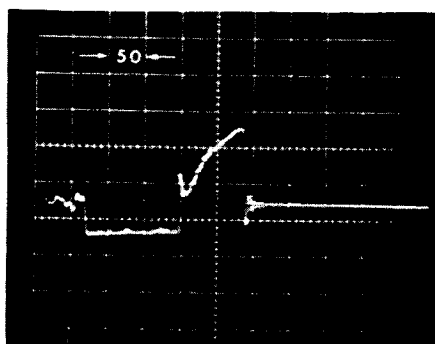
Typical signatures for the loose and dense samples of limonite in atmosphere and the two vacuum levels are shown in Fig. 84. Since only one oscilloscope was used to record the trace both the acceleration and deceleration portions of the record are shown. The similarity of the signatures to those for the lunar soils in atmosphere and rough vacuum can be noted. A sharp initial spike is evident due to the inertia of the soil followed by a more gradual increase in deceleration until the penetrometer came to rest. It can be seen that a reduction in pressure to 15mm Hg caused an increase in the soil strength as was observed for the lunar soils in rough vacuum,



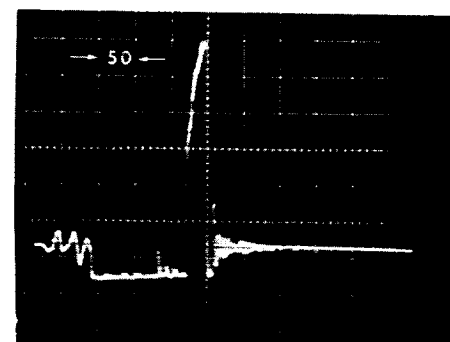
a) Atmosphere, $n = 0.739$



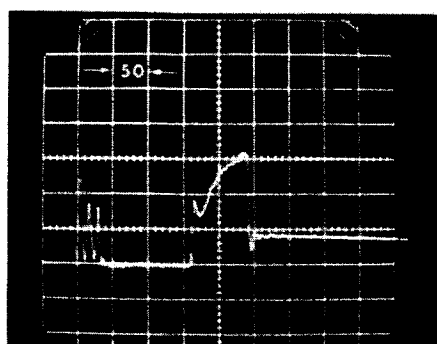
d) Atmosphere, $n = 0.711$



b) 15mm Hg, $n = 0.738$



e) 15mm Hg, $n = 0.708$



c) 3mm Hg, $n = 0.735$



f) 3mm Hg, $n = 0.710$

Loose

Dense

Fig. 84 TYPICAL SIGNATURES IN LIMONITE POWDER

and a further decrease to 3mm Hg resulted in a further increase in strength.

The penetration resistance was determined from the signatures (Eq. (2)) and is shown for loose and dense soil in Fig. 85 and 86. Again the sharp initial spike can be observed for the loose material but in the dense material it occurred only in atmosphere. However, for the dense material in vacuum a point of bifurcation as discussed previously was observed.

The resistance-penetration curves were integrated and the penetration caused by 0.3 in.-lb work were plotted as a function of porosity in Fig. 87. While points are shown for only two porosities at each vacuum level the curves were drawn with some curvature on the basis of the results presented previously.

It is seen that a rather substantial increase in strength occurred due to a decrease in the pressure to 15mm with a further increase in strength at 3mm. Also the curves appear to converge at the lower porosity but the range in porosity is not great enough to clearly demonstrate this.

It is of interest to note that while the difference in curves for atmosphere and vacuum may be attributed somewhat to a reduced strength in atmosphere because of the development of pore air pressures, the difference between the curves in vacuum is not in proportion to the differences in pressure. Also, it is believed that the pore pressures developed at 15mm would be quite small and therefore, would have a negligible effect. In addition, the previously discussed investigation of the generation of clean surfaces showed that very little of the total amount of initially adsorbed gas was desorbed at low vacuum levels. Hence, it is evident that some interparticle surface forces were present and it appears that even relatively small amounts of outgassing, which may have removed only the hygroscopic moisture, were sufficient to cause an increase in these forces.

IIT RESEARCH INSTITUTE

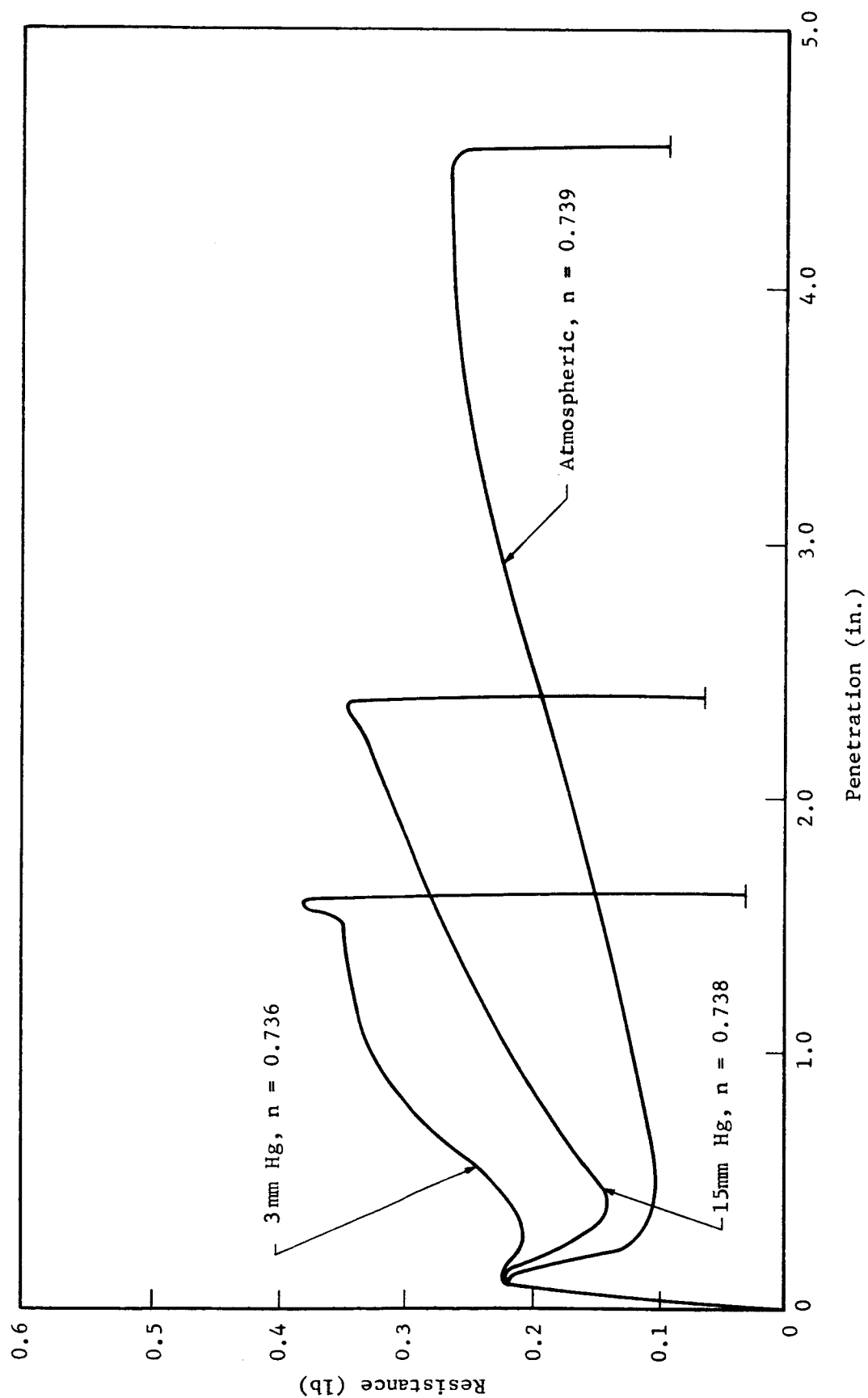


Fig. 85 RESISTANCE AS A FUNCTION OF PENETRATION FOR LOOSE LIMONITE

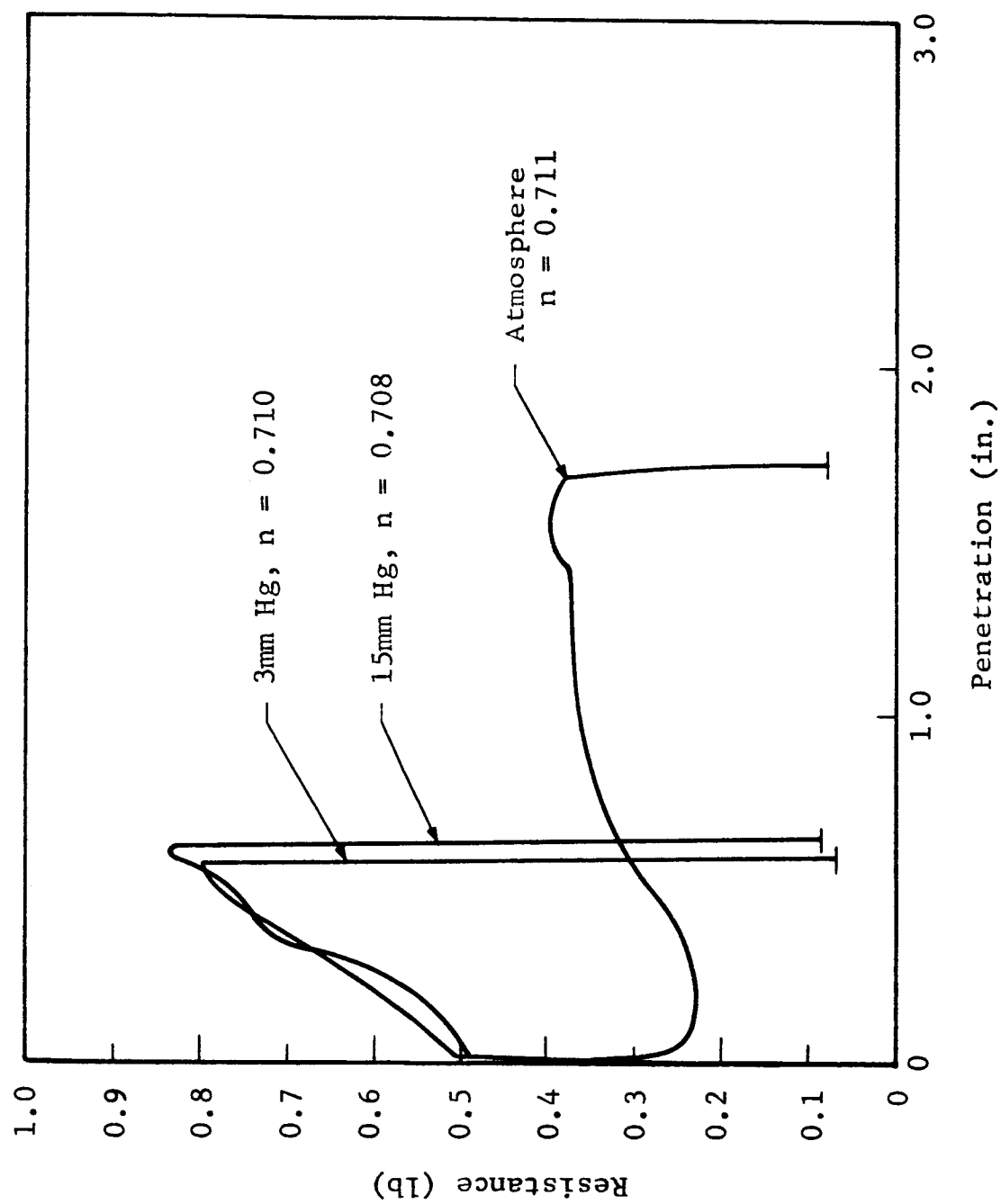


Fig. 86 RESISTANCE AS A FUNCTION OF PENETRATION FOR DENSE LIMONITE

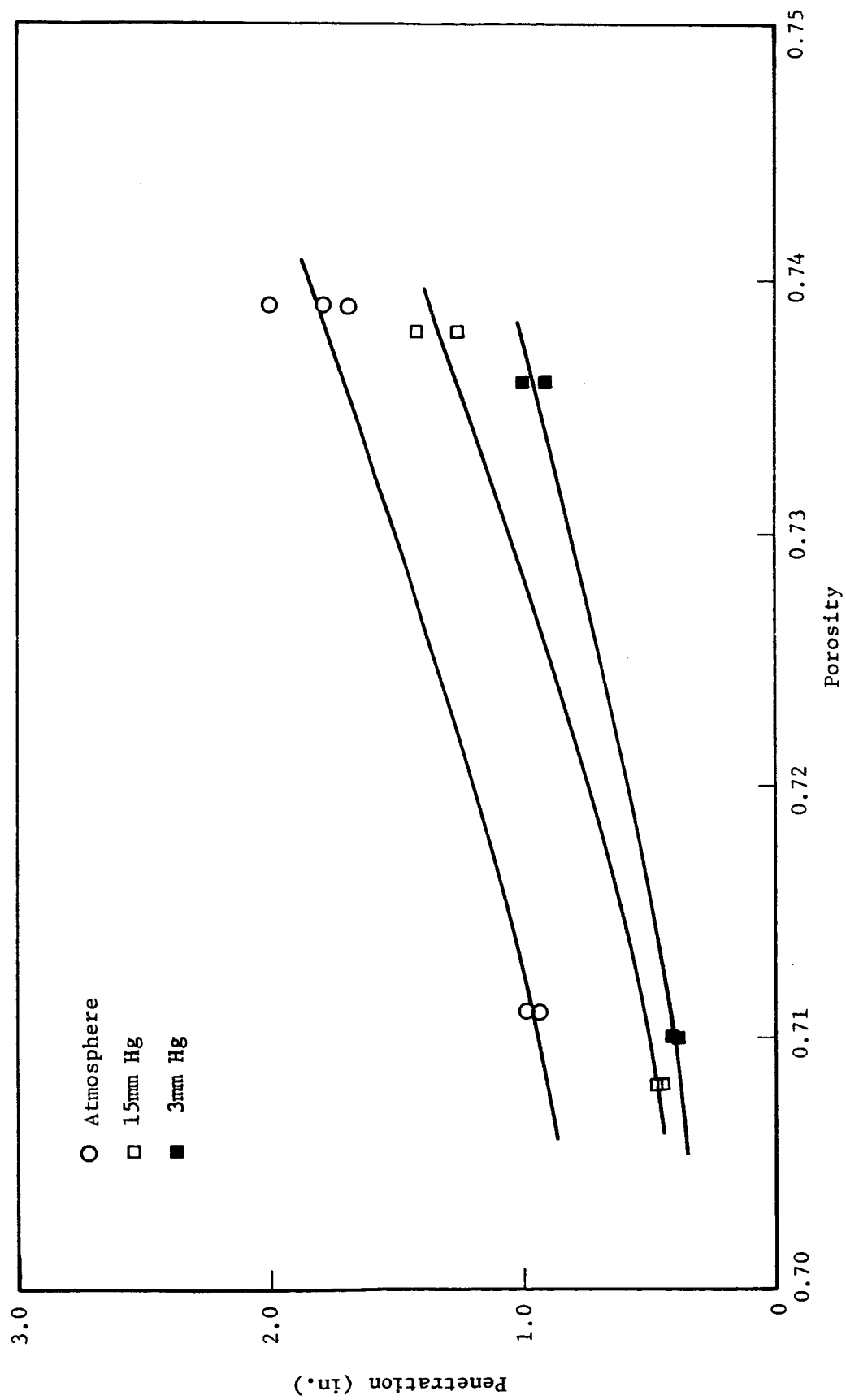


Fig. 87 PENETRATION AT 0.3 IN.-LB WORK VS POROSITY FOR LIMONITE

IX. DISCUSSION OF RESULTS

A. SIMULATED LUNAR SOILS

It is clear that ultra-high vacuum had a pronounced effect on the soil properties but the degree to which the properties were affected depended upon the mineralogical composition of the material. In the direct shear experiments the shear strength of the olivine exhibited almost no change except after considerable outgassing, whereas in the other three materials a rather pronounced change in ultra-high vacuum occurred.

The small initial peak shear stress observed under some conditions at low values of normal stress indicates the development of relatively strong bonds at the asperity contacts. The difference in the nature of this peak for the different materials (Section III) indicates that it is not due entirely to the desorption of gas and may, therefore, be influenced somewhat by differences in grain size and shape. The fact that this peak was more pronounced in some materials than others (e.g. it was not very pronounced in the enstatite) may be due to different contact stresses at the asperities which influenced the magnitude of the bond developed at these points.

While this peak was not observed at the higher normal stresses, it is believed that in these cases the frictional resistance of the soil was greater than at the lower normal stresses and, hence, after the initial bonding had been broken the shear strength was of sufficient magnitude that no strength decrease occurred.

Thus, the maximum cohesion and angle of internal friction may be developed at different values of shear strain, and as a result of this, an increase in shear strength due to the vacuum could appear largely as an increase in the stiffness of the soil rather than an increase in the shear strength parameters. This is of particular importance in penetration

experiments since the penetration resistance of the soil is a function of not only its ultimate or peak shear strength but also the forces required to cause deformations in the soil mass.

In the dynamic penetration experiments it was seen that the penetration caused by a particular amount of work done on the soil was decreased quite significantly in vacuum. While this effect was partly due to the absence of pore air pressures in vacuum, a considerable difference was also observed between the results in rough vacuum and ultra-high vacuum. It is evident, therefore, that the further outgassing of the material resulted in an increase in the shear strength and/or stiffness.

It was noted that the penetration resistance was essentially the same in both very high vacuum and ultra-high vacuum and consequently, it is believed that very little outgassing of the soil occurred between the times at which the experiments were performed. Since it was seen in the desorption studies that very little readsorption will occur on the particle surfaces during cooling in vacuum, it is apparent that the lack of a further increase in strength at ultra-high vacuum was merely due to the fact that desorption from the soil did not continue at the lower temperatures. This also emphasizes the fact that the primary environmental factor influencing the shear strength was not the vacuum level in the surrounding environment but rather the amount of gas remaining on the particle surfaces.

The initial spike in the signatures obtained in dynamic penetration experiments was attributed to the inertia of a small zone of soil accelerated by the penetrometer and hence, the observed increase in this spike in vacuum would indicate that this zone was larger than in atmosphere and/or greater forces were required to accelerate it. From the previously discussed initial peak in the direct shear tests it appears that it is actually due to a combination of both factors.

If some bonds were developed at the asperities the increased interaction between particles would result in a larger zone of soil being influenced initially. Also, since some relative displacement between particles must occur in this zone it is obvious that these bonds would provide a greater resistance of the particles to displacement by the penetrometer.

For the enstatite sand in atmosphere a second maximum deceleration was observed after the initial spike but this was not observed in vacuum. However, a change in the slope of the second half of the spike was observed in vacuum and is believed to have been caused by the second maximum occurring at a lower value of penetration. That is, the peak shear strength was developed at lower values of shear strain as the result of an increase in soil stiffness in the vacuum. While it is not clearly established whether pore air effects were significant in the enstatite sand, an increase in the spike even in rough vacuum indicates a greater amount of interlocking between the soil grains. In atmosphere sufficient pore air pressures were developed to reduce the apparent cohesion due to this interlocking of grains.

The effect of vacuum has been seen, therefore, to be one of increasing the soil strength in all materials, but it is much more pronounced in some materials than in others. The investigations of the nature of the gas desorbed during outgassing of the soil showed the principal constituent of the gas to be water vapor for all materials and, hence, differences in the composition of the adsorbed gas would not account for the difference in vacuum effects. The amount of gas that could be desorbed from the soil was seen to differ for the different materials and for some, this difference was greater than two orders of magnitude. Furthermore, it appears that this gas was not all adsorbed on the surfaces initially but instead, substantial amounts were absorbed in the soil grains. Thus, in the materials from which the greatest

amount of gas was desorbed (enstatite and olivine) it is believed that during outgassing this absorbed gas was removed from within the particle and replaced the gas desorbed from the surfaces. Consequently, even after a considerable amount of outgassing had taken place, the cleanliness of the surfaces in these materials may have been relatively unaffected. It is believed that the quartz and obsidian contained much less absorbed gas and, hence, the same amount of outgassing as for the olivine and enstatite would result in much cleaner surfaces.

In the penetrometer experiments at different values of surface cleanliness it was seen that even small changes in the relative cleanliness had a large effect on the penetration resistance. Of interest in these experiments is the fact that the degree of influence appears to be inversely proportional to the penetrometer diameter. Thus, since the volume of soil which is compressed during penetration is related to the area of the penetrometer and the area of the shear surface is proportional to the circumference it is believed that the shear strength was influenced by relative cleanliness much more than the compressibility.

The increase in shear strength in vacuum was attributed to two factors: 1) an increase in interparticle forces due to the removal of adsorbed gas resulting in a closer proximity of the particle surfaces, and 2) an increase in the coefficient of friction between soil grains, also as a result of the desorption of gas. The individual effects of each of these factors may not be separated but it is believed that the former predominates.

As was discussed in the previous final report² the interparticle forces are believed to have been primarily of the Van der Waals type, and thus, would vary exponentially with the distance of separation between surfaces. Therefore, if the shear strength is a function of the Van der Waals forces and the distance of separation is a function of the relative cleanliness, the results of the penetrometer experiments would be

IIT RESEARCH INSTITUTE

expected to plot as straight lines on a logarithmic plot which they do. It should be noted that a straight line through these points intersects the ordinate for a relative cleanliness of 1.0 at a point much below those determined on the sintered material. However, at closer spacing between the surfaces, forces other than Van der Waals forces, such as electrostatic and hydrogen bonding, may also become effective. Also interaction between adsorbed gas layers on the different particles may occur. Thus, the slope of the straight lines in Fig. 83 could increase significantly at some point between a relative cleanliness of 0.10 and 1.0. Depending on the point at which it begins to change, an increase in slope of even a relatively small amount can be seen to result in a relatively high strength for materials with atomically clean surfaces.

It should be mentioned that in the experiments on the desorption of gas the obsidian was observed to have sintered during the heating process. While this material was heated to the same temperature as the other materials, this particular experiment was continued for a considerably longer period of time than for the quartz and, hence, it is believed that a relative cleanliness of very close to 1.0 was actually attained. The strength of the sintered obsidian was quite high and although the sample was only approximately 1/4 in. in diameter it could not be broken by hand.

Considerably more data are necessary at higher values of relative cleanliness than were attained in the penetrometer experiments to more clearly define the relationships between strength and cleanliness. It appears, however, that the interpretation of data in this manner will provide a reasonable and fairly accurate mechanism to permit extrapolation of data obtained in the laboratory to actual lunar surface conditions.

B. SIMULATED MARTIAN SOILS

In the experiments on limonite it was observed that even low vacuum levels had a pronounced effect on penetration resistance which could not be attributed entirely to pore air pressures. Since the grain size of the material was very small, surface forces were expected to be quite large and were evidenced by the fact that the soil grains had a tendency to cluster in the atmosphere. It appears, therefore, that for this soil, even at a relative cleanliness close to zero, interparticle forces were significant.

The removal of even very small amounts of gas from this soil appears to have resulted in an increase in interparticle forces but the effect of these forces relative to pore air pressures is not clearly indicated and considerably more research is required before the two effects can be separated.

X. CONCLUSIONS

The following conclusions are based primarily on an analysis of the results of the data obtained during this phase of the program in conjunction with data obtained in the previous phases where it pertains.

1. Bonds of fairly high strength are developed at the asperity contacts in soil under ultra-high vacuum but are effective at only relatively low values of shear strain. These bonds increase the stiffness of the soil and cause an increase in its inertial resistance to dynamic penetration.

2. The desorption of gas from the particles allows a closer proximity of the particle surfaces resulting in the development of interparticle forces. These forces influence the strength at all values of shear strain and cause an increase in the shear strength parameters ϕ and c , the magnitude of which depends on the mineralogical composition of the soil.

3. Because of the different values of strain at which the aforementioned asperity bonds and the interparticle forces are most effective the maximum values of ϕ and c are developed at different values of shear strain. Consequently, while in most materials the most pronounced effect of ultra-high vacuum is to increase the shear strength, in others the primary effect may be to increase the stiffness with little or no change in ϕ and/or c .

4. Since both the stiffness and shear strength influence the resistance of soil to dynamic penetration, all materials investigated showed an increase in penetration resistance in ultra-high vacuum. This increase was in addition to an apparent increase (or in some cases a decrease) in rough vacuum due to the absence of pore air pressure.

5. The composition of the adsorbed and/or absorbed gas is approximately the same for all materials and, hence, cannot be considered as being responsible for the dependency of vacuum effects on mineralogical composition.

6. The amount of adsorbed and/or absorbed gas is substantially greater for some materials than others. Basic minerals appear to contain more gas than acidic minerals and the difference may be greater than two orders of magnitude depending on the minerals considered.

7. The static penetration resistance and, hence, the stress-strain and strength characteristics of the soil varies exponentially with the relative cleanliness of the particles. Consequently, the difference in vacuum effects for different materials may be attributed to their differences in amounts of adsorbed and absorbed gas (i.e. after similar pump-down procedures the amount of gas remaining in the different materials may vary).

8. Although the data is somewhat limited, it appears that unless forces stronger than Van der Waals forces are effective at higher values of relative cleanliness than those achieved in the laboratory, the strength of loose fine grained soil with atomically clean particle surfaces will be substantially lower than that of the same material sintered at high temperatures.

9. Even relatively low vacuum levels (3 to 15 torr) appear to cause a significant increase in the interparticle forces in the simulated Martian soil.

10. The method of analyzing the gas desorbed from the soil sample is a promising procedure for the evaluation of relative cleanliness, and the static penetration resistance at small penetrations provides a simple, convenient method to correlate relative soil strength with relative cleanliness.

11. Using the above procedure (item 10) it will be possible to compare the extrapolated curves with the strength of sintered material at various stages of bonding and hence arrive at an estimate of what ultimate strength might be expected in lunar surface deposits due to environmental effects.

BIBLIOGRAPHY

1. Vey, E. and Nelson, J. D., "Studies of Lunar Soil Mechanics", Final Report, IIT Research Institute Project M272-I, Contract NASr-65(02), July, 1963.
2. Vey, E. and Nelson, J. D., "Studies of Lunar Soil Mechanics", Final Report, IIT Research Institute Project M272-II, Contract NASr-65(02), February, 1965.
3. Tolbert, C. W. and Coats, G. T., "Lunar Radiation at 3.2 Millimeters and a Lunar Model", Report No. 7-24, Electrical Engineering Research Laboratory, University of Texas, Austin, Texas, August 15, 1963.
4. Strom, Robert G., "Fault Mechanics of the Lunar Straight Wall and the Nature of the Mare Material", Unpublished preliminary report, Space Sciences Laboratory, University of California, Berkeley, California, January 1963.
5. Sytinskaya, N. N., "Explosions of Meteors as a Factor in the Development of the Lunar Surface", Probl. of Cosmogony, Vol. 2, No. 27, April 1964 (N64-19451).
6. Rosenberg, D. L. and Wehner, G. K., "Darkening of Powdered Basalt by Simulated Solar Wind Bombardment", J. Geophysical Research, Vol. 69, No. 15, August 1, 1964.
7. Hapke, B. W., "Experiments Relating to the Lunar Surface", 2nd Preliminary Report, Center of Radiophysics and Space Research, Cornell University, Ithaca, New York, July 1962.
8. Kopal, Z. and Rackham, T. W., "Excitation of Lunar Luminescence by Solar Flares", Nature, Vol. 201, No. 4916, Jan. 18, 1964.
9. Kopal, Z. and Rackham, T. W., Icarus, Vol. 2, p. 481, 1963.
10. Derham, C. J. and Geake, J. E., "Luminescence of Meteorites", Nature, Vol. 201, No. 4914, January 4, 1964.
11. Anand, S.P.S., Oster, L. and Soria, S., "Excitation of Lunar Luminescence by Solar Protons", Nature, Vol. 202, No. 4937, June 13, 1964.

BIBLIOGRAPHY (Contd.)

12. Beskrovnyy, N. S., "Causes for the Luminescence of Rocks on the Moon", Priroda, Nr. 12, 1962 (FTD-TT-63-508).
13. Runcorn, S. K., "The Interior of the Moon", JPL Tech. Rept. No. 32-529, December 15, 1963.
14. Urey, H. C., "Age of the Moon, Chemical Composition, Geological Aspects, Stress and Cooling History", Conference on Lunar Exploration, Virginia Polytechnic Institute, Blacksburg, Virginia, August 1962.
15. Lowman, P. D. Jr., "The Relation of Tekites to Lunar Igneous Activity", Icarus 2, 35-48, 1963.
16. Baldwin, R. B., "The Nature of the Lunar Surface and Major Structural Features", Conference on Lunar Exploration, Virginia Polytechnic Institute, Blacksburg, Virginia, August 1962.
17. Miyamoto, S., "A Geological Interpretation of the Lunar Surface", Planet Space Sci., Pergamon Press, Vol. 2, 1960.
18. O'Keefe, J. A., "Tektites and Impact Fragments from the Moon", Scientific American, February 1964.
19. Dobar, W. I., Bendix Systems Division, Ann Arbor, Michigan, Discussed in Missiles and Rockets, p. 31, May 10, 1965.
20. Van Diggelen, J., "Photometric Properties of Lunar Crater Floors", Recherches Astronomiques de l'Observatoire d'Utrecht, Vol. XIV, No. 2, 1958.
21. Briggs, M. H. and Reville, J. P., "The Chemistry of Mars, I. The Atmosphere", J. Brit. Ast. Soc., Vol. 17, No. 11, September-October, 1960.
22. Zebal, G. P., "A Preliminary Analysis of the Geology of Mars", Aeronutronic Publication No. U-3065, March 19, 1965.
23. McCarty, J. L. and Carden, H. D., "Impact Characteristics of Various Materials Obtained by an Acceleration-Time History Technique Applicable to Evaluating Remote Targets", NASA-LRC TN D-1269, June 1962.

BIBLIOGRAPHY (Contd.)

24. McCarty, J. L., A. G. Beswick and G. W. Brooks,
"Application of Penetrometers to the Study of Physical
Properties of Lunar and Planetary Surfaces", NASA
TN D-2413, Langley Research Center, August 1964.
25. Hanks, B. R. and McCarty, J. L., "Investigation of the
Use of Penetrometers to Determine the Capability of Dust
Materials to Support Bearing Loads", NASA TN D-3200,
Langley Research Center, January 1966.
26. Davies, W. O., "Spectroscopic Observations of Mars",
Frontier, IIT Research Institute, Winter, 1965.